General Disclaimer

One or more of the Following Statements may affect this Document

- This document has been reproduced from the best copy furnished by the organizational source. It is being released in the interest of making available as much information as possible.

- This document may contain data, which exceeds the sheet parameters. It was furnished in this condition by the organizational source and is the best copy available.

- This document may contain tone-on-tone or color graphs, charts and/or pictures, which have been reproduced in black and white.

- This document is paginated as submitted by the original source.

- Portions of this document are not fully legible due to the historical nature of some of the material. However, it is the best reproduction available from the original submission.

Produced by the NASA Center for Aerospace Information (CASI)

REPORT NO. GDC-DDB70-007
CONTRACT NAS 8-21465

LOW GRAVITY PROPELLANT CONTROL USING CAPILLARY DEVICES IN LARGE SCALE CRYOGENIC VEHICLES

PHASE I FINAL REPORT

GENERAL DYNAMICS
Convair Division

FACILITY FORM 602
N71-10653 (ACCESSION NUMBER)
138 (PAGES)
CR-102900 (NASA CR OR TMX OR AD NUMBER)
G3 (CODE)
28 (CATEGORY)

RECEIVED
NASA STI FACILITY
INPUT BRANCH
OCT 1970

REPORT NO. GDC-DDB70-007

LOW GRAVITY PROPELLANT CONTROL USING CAPILLARY DEVICES IN LARGE SCALE CRYOGENIC VEHICLES

PHASE I FINAL REPORT

August 1970

Prepared Under
Contract NAS8-21465
CONVAIR DIVISION OF GENERAL DYNAMICS
San Diego, California

FOREWORD

This final report for Phase I of NASA/MSFC contract NAS 8-21465, DCN-8-52-10174(IF) and S-1(IF) covers work performed during the period from June 1968 to January 1969. The report was prepared by M. H. Blatt, Project Manager, K. R. Burton, F. Merino, C. K. Perkins and L. E. Siden. The study was performed under the technical direction of Mr. Leon J. Hastings, NASA/MSFC, R-P&VE-PT.

PRECEDING PAGE BLANK NOT FILMED

TABLE OF CONTENTS

		Page
1	INTRODUCTION	1-1
2	TECHNICAL DISCUSSION	2-1
2.1	MISSIONS	2-1
2.1.1	S-IVC Mission Requirements	2-1
2.1.2	Oxygen Tanker Requirements	2-22
2.2	THERMAL ANALYSIS	2-39
2.2.1	S-IVC Thermal Analysis	2-39
2.2.2	LOX Tanker Thermal Analysis	2-46
2.3	PHASE I DESIGN	2-54
2.3.1	Preliminary Design Concept	2-54
2.3.2	LOX Tanker Propellant Transfer Designs	2-71
2.3.3	Heat Exchanger Attachments	2-83
2.4	SYSTEMS COMPARISONS	2-89
2.4.1	S-IVC System Comparisons	2-90
2.4.2	LOX Tanker System Comparisons	2-97
3	REFERENCES	3-1
APPENDIX A	S-IVC STRESS CALCULATIONS	A-1
APPENDIX B	LOX TANKER STRESS CALCULATIONS	B-1

PRECEDING PAGE BLANK NOT FILMED

LIST OF FIGURES

Figure		Page
2-1	S-IVC Restart Configuration	2-1
2-2	Capillary Device for Small Quantity of Liquid	2-3
2-3	Head Retention	2-4
2-4	Venting	2-4
2-5	Liquid Spillage During Thrusting	2-5
2-6	Comparison of Liquid Retention Using Screen Capillary Forces and Screen Gas Flow Losses	2-6
2-7	Liquid Hydrogen Retention by Screen Capillary Forces and Screen Flow Losses	2-9
2-8	Start Basket Refill Following S-IVC Restart	2-12
2-9	Liquid Head Difference at S-IVC Burnout	2-14
2-10	S-IVC Start Basket Configuration	2-15
2-11	Start Basket Volume (Based on a 1/3 Annulus)	2-16
2-12	Fluid Simulation of S-IVC Liquid Hydrogen Tank Settling	2-19
2-13	Fluid Simulation of S-IVC Liquid Hydrogen Tank Settling	2-20
2-14	Fluid Simulation of S-IVC Liquid Hydrogen Tank Settling	2-21
2-15	Large Liquid Volume Capillary Device	2-22
2-16	Flow From a Liquid Collector	2-23
2-17	Channels Tapered to Eject Vapor	2-24
2-18	Top of Enclosure Tapered to Eject Vapor	2-24
2-19	Oxidizer Tank Liquid Residual Versus Angle, θ	2-27
2-20	Retriever Channel Surface Area Versus Angle, θ	2-28
2-21	Liquid Settled at Tank Equator Due to Lateral Acceleration	2-29
2-22	Flow Distribution Effect of Connector Channel	2-30

Figure		Page
2-23	LOX Transfer Flow Model	2-31
2-24	LOX Tanker Pool Residuals Vs Transfer Rate	2-35
2-25	Total LOX Tanker Liquid Residuals Vs Channel Geometry and LOX Flow Rate	2-36
2-26	Effect of Retriever Channel Screen Diameter and Channel Depth on Allowable LOX Transfer Rate	2-37
2-27	Typical Screen Support	2-40
2-28	Thermal Model for Boiling at Screen Support	2-40
2-29	Thermodynamic Vent Device	2-42
2-30	Schematic of S-IVC Heat Exchanger Vent System	2-42
2-31	Thermodynamic Performance of Figure 2-30 Configuration	2-45
2-32	Schematic of Alternate S-IVC Heat Exchanger Vent System	2-46
2-33	LOX Tanker Cooling With Cooling Channels Inside the Collector Channels	2-47
2-34	LOX Tanker Cooling With Coolant Channels Outside the Tank Wall	2-47
2-35	O_2 Tanker Vent Flow Rate Required for Constant Tank Pressure	4-29
2-36	Vapor Formation in Bench Test Specimen	2-51
2-37	Screen Retention-Evaporation Test Apparatus	2-53
2-38	Weight Estimates/Fuel Reservoir, 60 Ft^3	2-57
2-39	Weight Estimate/Fuel Reservoir, 60 Ft^3	2-58
2-40	Fuel Reservoir Sized for 40.0 Inch Dia Tank Access Opening (Approx. 60 Ft^3 Vol)	2-59
2-41	Weight Estimate/Fuel Reservoir, 1970 Ft^3	2-60
2-42	Weight Estimate/Fuel Reservoir, 1015 Ft^3	2-61
2-43	Weight Estimate/Fuel Reservoir, 500 Ft^3	2-62
2-44	Weight Estimate/Fuel Reservoir, 180 Ft^3	2-63

Figure		Page
2-45	Fuel Reservoir Annular Reservoir	2-64
2-46	Fuel Reservoir Weights Versus Volume	2-65
2-47	Weight Estimate/Oxidizer Reservoir/S-IVC Tank	2-68
2-48	S-IVC Oxidizer Assembly	2-69
2-49	Oxidizer Start Reservoir Concept/S-IVC Tank	2-70
2-50	Oxidizer Collector System	2-73
2-51	Weight Estimate/Oxidizer Reservoir	2-74
2-52	Weight Estimate/Oxidizer Retrieving Channels	2-75
2-53	Weight Estimate/Oxidizer Retrieving Channels	2-76
2-54	Weight Estimate/Oxidizer Collector System	2-77
2-55	Oxidizer Collector System/Full Liner Concept	2-78
2-56	Alternate Gore Panel Construction and Interconnecting Arrangements	2-79
2-57	Fuel Reservoir Heat Exchanger Installation, Case 1	2-84
2-58	Fuel Reservoir Heat Exchanger Installation, Case 2	2-85
2-59	Fuel Reservoir Heat Exchanger Installation, Case 3	2-86
2-60	Heat Exchanger Installation, Case 4	2-87
2-61	S-IVC Screen System Weights	2-91
2-62	Equivalent Hardware Weight Comparison for S-IVC Mission Restart	2-95

PRECEDING PAGE BLANK NOT FILMED

LIST OF TABLES

Table		Page
2-1	S-IVC Mission Ground Rules	2-2
2-2	Liquid Oxygen Tanker Ground Rules	2-24
2-3	S-IVC Mission, DEP Weights	2-93
2-4	S-IVC Restart Systems LH_2 Tank - Relative Reliability	2-96
2-5	S-IVC Restart Systems LH_2 - Relative Cost	2-97
2-6	LO_2 Tanker Weight Comparisons	2-99
2-7	Relative Reliability of LOX Tanker Transfer Systems	2-100
2-8	Relative Cost of LOX Tanker Transfer Systems	2-101

PRECEDING PAGE BLANK NOT FILMED

SUMMARY

This report covers work performed at Convair during the first phase of the study "Low Gravity Propellant Control Using Capillary Devices in Large Scale Cryogenic Vehicles." The report contains a discussion of the missions of interest, problem areas investigated, methods of solving these problems with corresponding results, preliminary capillary containment system design concepts which were considered and comparisons of promising capillary devices with other means of propellant control.

The missions considered were an S-IVC LH_2 and LO_2 tank restart in orbit and a propellant transfer mission using a LOX tanker to fill an S-IIB.

Using capillary devices in cryogenic vehicles introduces heat transfer and thermodynamic constraints which must be complied with in order to prevent excessive vapor from forming in the capillary device prior to and during expulsion.

Initially fluid analysis of both missions was performed to develop capillary device designs which would satisfy mission acceleration and flow conditions. This investigation included pressure drop, retention, settling, spilling, vapor ingestion, refilling, and venting analyses.

The configurations, based primarily on fluid considerations, were then thermally analyzed. Prevention of vapor formation was attempted both passively and actively. An active thermodynamic vent system cooling system was used for both missions in order to control tank pressure, destratify propellants and cool the capillary devices and feedlines for the preliminary design configurations.

Bench tests were run to evaluate the retention capability of capillary barriers when subjected to evaporation. The tests indicated that liquid wetting around vapor bubbles formed prevented drying out of screens. Wicking screens were found to provide better retentive properties than non-wicking screens.

Preliminary designs of capillary devices were developed for the S-IVC and LOX tanker missions based on the fluid and thermal analysis performed during Phase I. The most promising designs were then compared with other means of propellant control including bladders, dielectrophoresis, and linear acceleration on the basis of cost, reliability, weight and manufacturing feasibility. Capillary devices for large scale cryogenic vehicles compared favorably with the other systems.

1

INTRODUCTION

In orbiting spacecraft containing subcritical storage vessels, periods of orbital drag and disturbing accelerations may position liquid away from the tank outlet. Prior to engine restart or propellant transfer it is necessary to have liquid positioned over the outlet in order to effectively accomplish fluid transfer.

Acquisition devices for controlling propellants prior to transfer come under two categories, partial orientation devices that control only a small percentage of the tank contents and total orientation devices that attempt to control all the propellant in the tank. For the present study partial acquisition devices are required for the S-IVC restart mission and total acquisition is required for the LO_2 tanker mission.

Spacecraft low gravity restarts have primarily been accomplished in the past through the use of linear acceleration to provide settling thrust with which to collect fluid over the outlet. This well proven technique introduces weight penalties and operational constraints compared to more advanced methods of acquisition. These methods include positive displacement devices such as bladders, bellows and diaphragms, dielectrophoretic devices and capillary devices.

Capillary devices are particularly attractive because they are lightweight, passive and introduce minimal operational constraints. These devices, while successfully applied to non-cryogenic propellant acquisition, have not been adequately studied for cryogenic fluid applications. Using cryogenic fluids, however, introduces thermodynamic and heat transfer problems which greatly affect capillary control system design.

The purpose of this contract is to ascertain the feasibility of using capillary devices such as screens and/or perforated plates, for propellant control in large scale cryogenic vehicles.

The first phase of the two-phase program defined the thermodynamic and heat transfer problems associated with the use of capillary devices, derived methods for solving these problems and selected promising propellant control schemes. This was predominately an analytical study with some low cost bench testing required to verify basic concepts. Based on the general results of the initial analytical and experimental effort, designs were developed for an S-IVC LH_2 and LO_2 tank restart mission and an S-IIB LOX tanker propellant transfer mission. Promising capillary control designs were compared with other means of propellant control in order to ascertain the feasibility of using capillary devices for propellant control in large-scale cryogenic vehicles.

During the second phase of the study, Phase I results were used as a base for an experimental/analytical program which examined the various problems in detail and develop design solutions. Techniques developed in Phase I were refined and expanded. A series of bench tests were run with noncryogenic fluids to provide information with which to correlate analytical models and develop empirical relationships where analytical models were not applicable. Second phase results have been presented in the form of a design handbook containing useful fluid, thermal and structural information, and a report covering analytical, experimental and design studies performed for the missions of interest.

This report is one of four volumes of the final report. The other volumes are the Design Handbook, Phase II Final Report and Related IRAD Studies.

2

TECHNICAL DISCUSSION

Ground rules for the missions to be considered during Phase I of the program were selected based on discussions with the contract monitor at MSFC. The ground rules for the S-IVC mission were obtained from DAC-57997, "Feasibility of Modifying the S-IVB Stage as an Injection Stage for Manned Planetary Flyby Missions," NAS8-18032, and the ground rules for the LOX tanker mission were obtained from LMSC-A74810-II, "Orbital Tanker Design Data Study," NAS8-11326, T1-51-67-21, "Orbital Refueling and Checkout Study," NAS10-4606, and SID-67-275-3, "Feasibility of Modifying the S-II Stage as an Injection Stage for Manned Planetary Flyby Missions," Volume 3, NAS8-18031.

2.1 MISSIONS

2.1.1 S-IVC MISSION REQUIREMENTS. Three S-IVC vehicles and a spacecraft will be boosted into orbit using the Saturn V vehicle. The S-IVC's and the spacecraft will be assembled in a 100 × 263.5 n.m. orbit and the first S-IVC will be completely burned along with 25% of the second S-IVC in order to circularize the orbit. The mission being considered is the restart of the $S\text{-}IVC_2$ from this 263.5 n.m. circular orbit with the vehicle configuration shown in Figure 2-1 and the ground rules in Table 2-1.

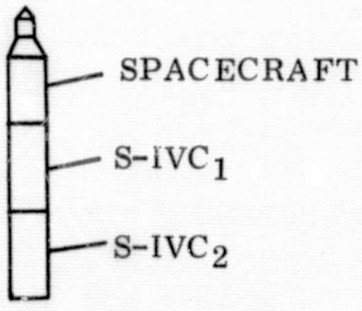


Figure 2-1. S-IVC Restart Configuration

Table 2-1. S-IVC Mission Ground Rules

Configuration:	S-IVB LH_2 Tank J2S Engines No Recirculation System S-IVB Pressurization System
Orbital Environment:	263.5 n.mi. Circular Orbit 10^{-6} g Drag Acceleration Total Orbital Heating = 2140 Btu/hr Forward Dome and Joint Area = 200 Btu/hr Cylinder Wall = 170 Btu/hr Aft Dome and Joint Area = 470 Btu/hr Common Bulkhead = 1300 Btu/hr
Vehicle Conditions:	60% Liquid Hydrogen Level Thermodynamic Vent Separator (1-2 psi Band) 30 Day Mission Duration 25 psia Tank Pressure
Orbital Restart:	Idle Mode Operation LH_2 Flow Rate = 2.8 lb/sec Vehicle Acceleration = 8.23×10^{-3} g's Main Engine Operation LH_2 Flow Rate = 74.4 lb/sec Vehicle Acceleration = 0.337 g's

It is required in this study to select a means of maintaining the liquid hydrogen tank in a state of readiness without resorting to ullage thrustors during the 30-day orbit duration. The techniques to be employed are a thermodynamic vent device for maintaining tank pressure control, and a capillary device for propellant control.

A review of the mission requirements reveals that there are two areas of concern. The first is maintaining satisfactory propellant control during the 30-day orbital period preceding engine start. The second is to assure 100 percent liquid feed from the propellant tank during engine start.

The maintenance of satisfactory propellant control during orbit is chiefly a thermal control or thermal protection problem. That is, it is necessary to protect a portion of the tank propellants against any adverse effects due to tank heating or venting. It is of course necessary to achieve propellant control against the accelerations of attitude control or aerodynamic drag. However, only when the variable of heating and liquid evaporation is introduced does it become difficult to design a satisfactory capillary device.

Two methods of propellant control are under consideration in this study: the control of a just enough liquid to guarantee restart, and the control of a substantial quantity of the tank propellants. Controlling small quantities of liquid is advantageous because of the relative ease of fabrication and, more important, maintaining thermal protection during coast. The advantage of controlling large quantities of liquid is that engine restart problems may be easier to solve, if thermal protection problems can be overcome.

Fluid Analysis

If a small quantity of liquid is to be held in readiness for an engine restart, the containment device (start basket) must necessarily be located at the tank outlet. The device currently under consideration is sketched below. Details of this device are contained in Section 2.3.

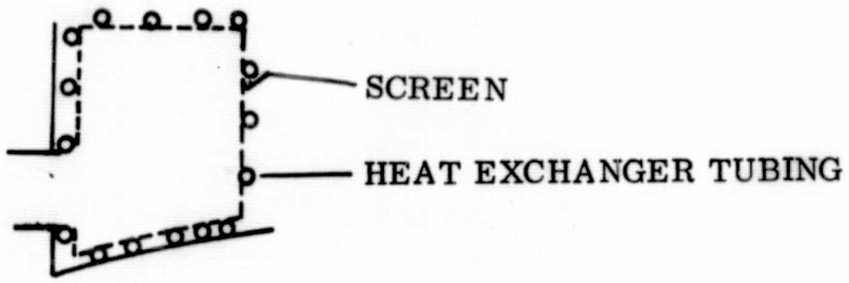


Figure 2-2. Capillary Device for Small Quantity of Liquid

Liquid containment at 10^{-4} g's to 10^{-6} g's can be accomplished with a capillary device constructed of coarse screen or perforated plate. Figure 2-3 shows that rather large screen mesh or perforated plates with large openings will retain sufficient head of liquid against 10^{-4} g's.

It is the restart sequence which dictates screen mesh selection, however, requiring a fine micron screen of the order of 15 microns bubble point in order to contain the fluid at .337 g's. The advantage of this capillary device (start basket) configuration, utilizing a thermodynamic vent system for cooling, is that it should be possible to keep the contained liquid in a subcooled state at all times.

An advantage of the subcooled liquid state is that evaporation during tank venting will be held to a minimum or even eliminated by proper design of a thermal control system.

Liquid head that can be contained by surface tension pressure is equal to the same head of trapped vapor. It is clear, therefore, that vapor generation within a capillary system must be eliminated if entrapment is to be avoided. One source of vapor generation is due to tank pressure blowdown below liquid vapor pressure. An analysis was conducted to determine whether liquid boiling due to tank blowdown would be

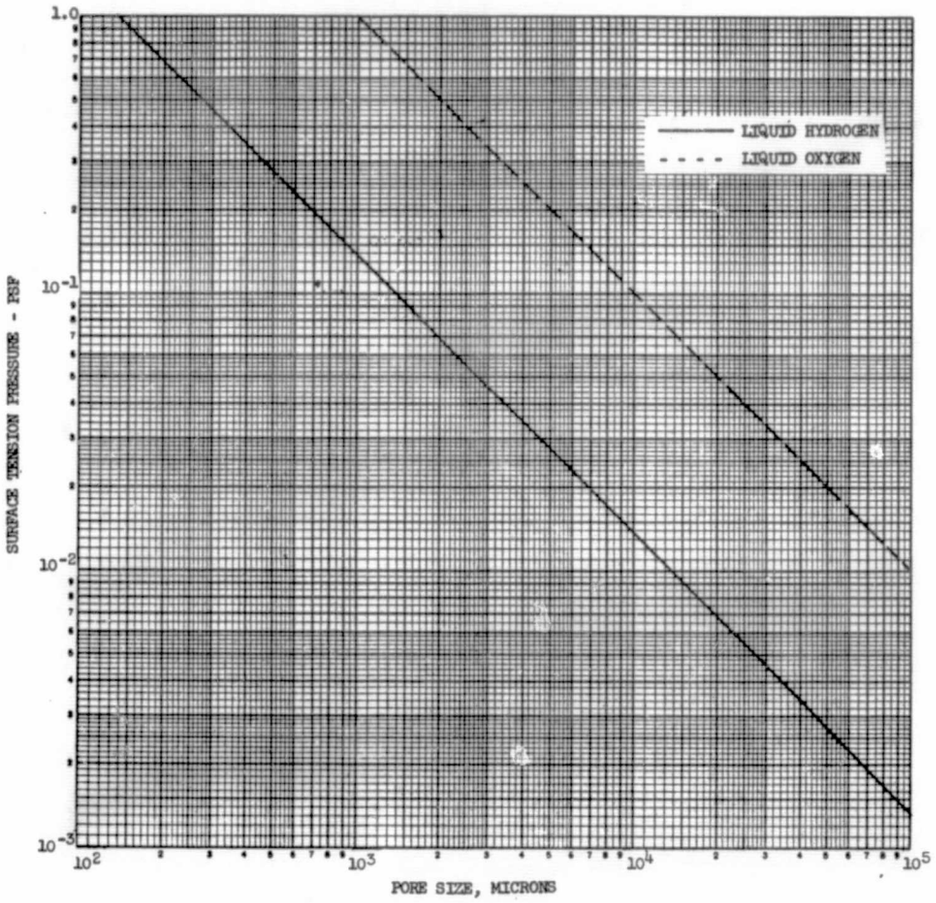


Figure 2-3. Head Retention

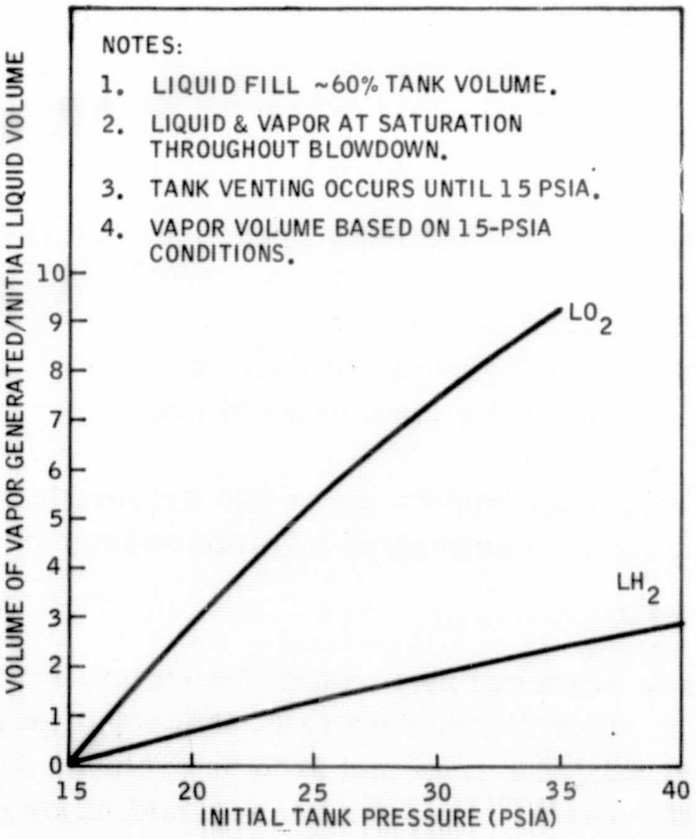


Figure 2-4. Venting

appreciable. The systems considered were a liquid oxygen and liquid hydrogen tank with the liquid/vapor phases in thermodynamic equilibrium prior to and during tank venting. The results presented in Figure 2-4 show that even a two psi drop in liquid vapor pressure will generate substantial vapor within a liquid. It is thus evident that care must be exercised if venting (other than constant pressure venting) is required in a tank containing a capillary device. With a thermodynamic separator system for venting, tank pressure excursions should be minimized sufficiently to avoid this problem.

There are alternate approaches to an engine start sequence. First, the engine idle mode can be utilized for feedline chilldown until such time as the hot vapor is expelled and the engine primed for restart. Using a dual thrust approach such as this will create problems with spilling from the capillary because the vapor volume in the feedline is insufficient to settle the propellants. This is explained in ensuing paragraphs. A more acceptable approach is to maintain the feedline in a state of readiness during coast engine, so that start can be effected immediately upon receiving the start signal.

Start basket sizing depends directly on the time to settle propellants. That is, sufficient propellant must be contained so that the tank contents will be settled and replenishment begun before liquid depletion occurs. Propellant settling times for this mission are currently under study. Initially a volume of 60 ft^3 was assumed for the preliminary start basket design. This volume is equivalent to approximately 3.5 seconds of main engine operation. A volume of 200 ft^3 was later adopted as most representative based on settling considerations discussed on page 2-18.

Should the idle mode be employed to prime the main engine pump prior to restart, it would be desirable to maintain liquid in the basket during this period. The problem with devising a system to contain liquid during the 8×10^{-3} g idle mode is illustrated below.

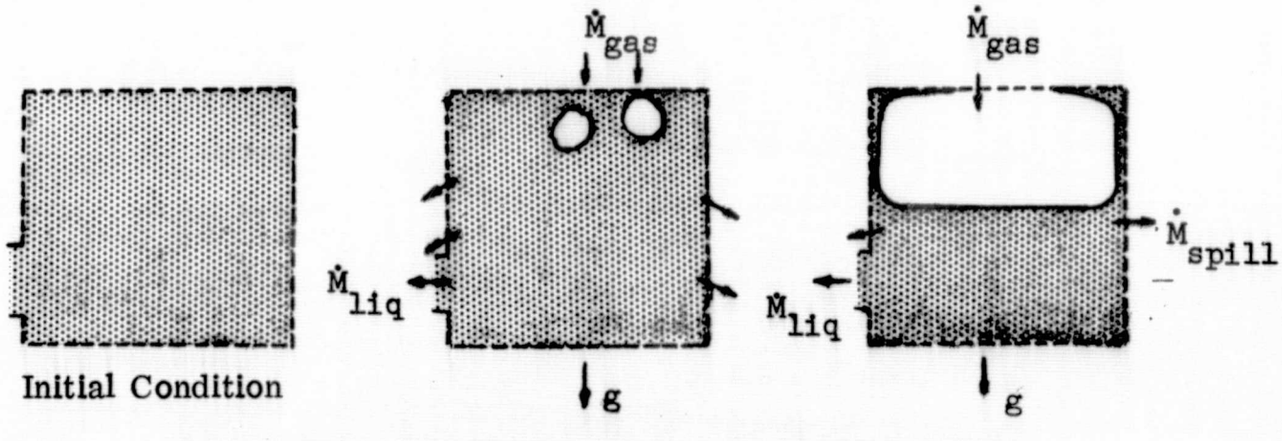
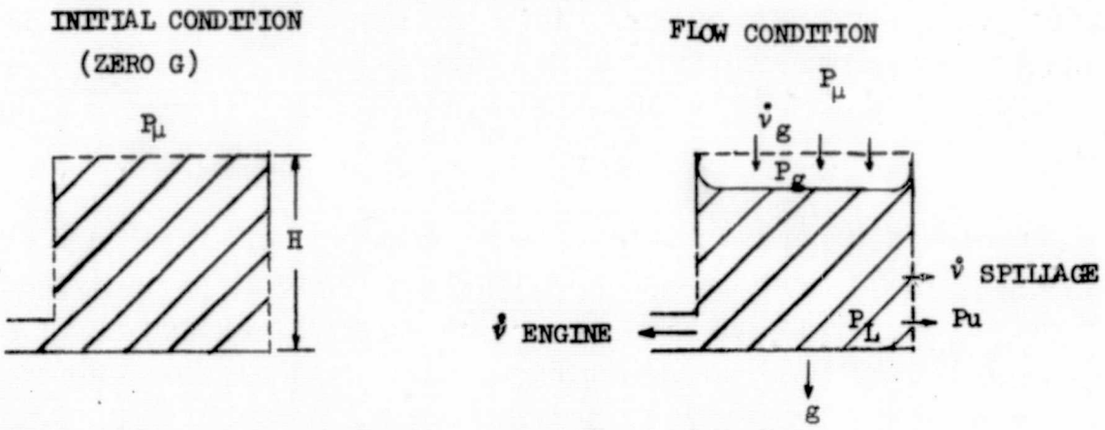


Figure 2-5. Liquid Spillage During Thrusting

As liquid withdrawal commences vapor will begin to penetrate the basket from the surrounding vapor environment. This penetration will tend to neutralize the screen

SCREEN CAPILLARY FORCES

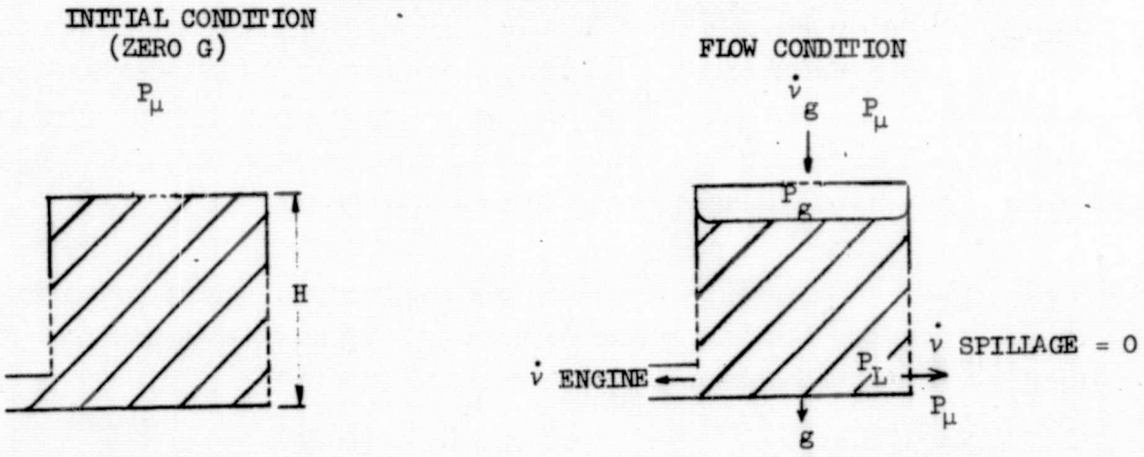


$P_g \approx P_\mu$, $P_L = P_g + \rho\,(g/g_c)\,H$, $P_L = P_\mu + \rho\,(g/g_c)\,H$

therefore $P_L > P_\mu$.

When $P_L > P_\mu$ liquid spillage will occur

SCREEN GAS FLOW LOSSES



$P_\mu - P_g = \Delta P_g$, $P_L = P_g + \rho\,(g/g_c)\,H$, $P_L = (P_\mu - \Delta P_g) + \rho\,(g/g_c)\,H$

when $P_L = P_\mu$ then $\Delta P_g = \rho\,(g/g_c)\,H$ and $\dot{v}$ spillage = 0

where P_μ = tank ullage pressure

P_g = start basket gas pressure

P_L = local liquid pressure

H = liquid head

g = vehicle acceleration

$\dot{v}_{ENGINE}$ = volumetric flow rate to engine

$\dot{v}_{SPILLAGE}$ = volumetric spill rate from basket

$\dot{v}_g$ = volumetric gas flow rate into basket $[=(\dot{v}_{ENGINE} + \dot{v}_{SPILLAGE})]$

ΔP_g = gas flow pressure loss across screen

Figure 2-6. Comparison of Liquid Retention Using Screen Capillary Forces and Screen Gas Flow Losses

surface tension pressure because of vapor communication across the screen. Thus, the liquid head created by the idle mode acceleration will not be restrained by surface tension and liquid will spill out of the basket.

There are two approaches for minimizing or eliminating liquid spill. The screen area about the cylindrical portion of the start basket can be decreased to reduce liquid spillage. Or, the screen area at the top of the cylinder can be decreased so that the pressure loss due to vapor flow across the screen will be greater than the liquid head pressure. Liquid spillage would not occur for this condition.

Designing of a start basket for engine restart requirements, however, must take into account the orbital coast requirements as well as the main engine burnout requirements. Conflicting design requirements exist for engine restart and engine burnout condition. The former necessitates minimum flow area in order to reduce liquid spillage. The latter requires considerable flow area to minimize burnout liquid residuals.

The first task in defining a screened start basket (capillary device) for the S-IVC mission was to determine a means of liquid containment under conditions of 74.4 lb/sec engine flow and 0.337 g's. It was evident that capillary forces would be inadequate under these conditions. Thus, it was decided to rely on the pressure loss of vapor entering the basket to retain liquid. Referring to the sketches of Figure 2-6 it is seen that liquid spillage will occur once vapor penetrates a basket, if a negligible gas flow loss occurs. But, if the flow area for vapor penetration is substantially reduced, then the flow loss will exceed liquid head pressure and prevent liquid spillage. From Figure 2-6 liquid spillage is zero when

$$\Delta P_g = \rho_L (g/g_c) H \qquad (1)$$

where

ρ_L = liquid density, 4.35 lb/ft^3

g/g_c = vehicle gravity field, .337 g's

H = liquid head

ΔP_g = gas flow pressure loss across screen, psf

$$\Delta P_g = \frac{\rho_g v^2}{2g_c} C_s \quad \text{(for Reynolds Number > 300)}$$

C_s = screen pressure drop coefficient, 22*

*C_s = 22 is based on GDC experimental data conducted on a 200 × 600 dutch twill weave.

$v = \dot{\nu}_g / A_T$, ft/sec

$\dot{\nu}_g$ = volumetric gas flow rate across screen, ft^3/sec

A_T = total screen flow area, ft^2

ρ_g = GH_2 density

Introducing the expression for ΔP_g into equation 1 gives the following relationship with H and A_T

$$H (A_T)^2 = \frac{C_s}{(2g_c)(g/g_c)} (\rho_g / \rho_L) \dot{\nu}_g^2 = .035 \dot{\nu}_g^2 \quad (2)$$

Under engine flow conditions of $\dot{\nu}_g = 17.1 ft^3/sec$,

$$H (A_T)^2 = 10.5 \quad (2a)$$

Equation 2a is plotted in Figure 2-7 giving liquid head retained versus total screen flow area. Figure 2-7 also illustrates the great advantage provided by screen flow loss in retaining liquid head when compared to the surface tension capability of a fine weave screen.

It is noted here that penetration of vapor through screened areas other than that designated for vapor flow may be unavoidable. Referring to the sketch on p. 2-10, a small screen area, A_T, may result in a high pressure drop and cause vapor penetration through the bottom of the screened basket. For example, let H = 6 ft, $A_T = 0.8 ft^2$, $g/g_c = .337$ and $d_\mu = 34\mu$.

From Figure 2-7:

$H_g = f(\Delta P_g) = 16$ ft and $H_\sigma = f(\Delta P_\sigma) = 1.4$ ft

Therefore, $\Delta P_g > \Delta P_\sigma + \rho_L (g/g_c) H$ (vapor penetration occurs).

But, if $A_T = 1.02 ft^2$, $H_g = f(\Delta Pg) = 7.4$ ft and

$\Delta P_\sigma = \Delta P_\sigma + \rho_L (g/g_c) H$ (no vapor penetration)

For $\dot{\nu} > 0$, $P_\mu - P_L > \Delta P_\sigma$ (3a)

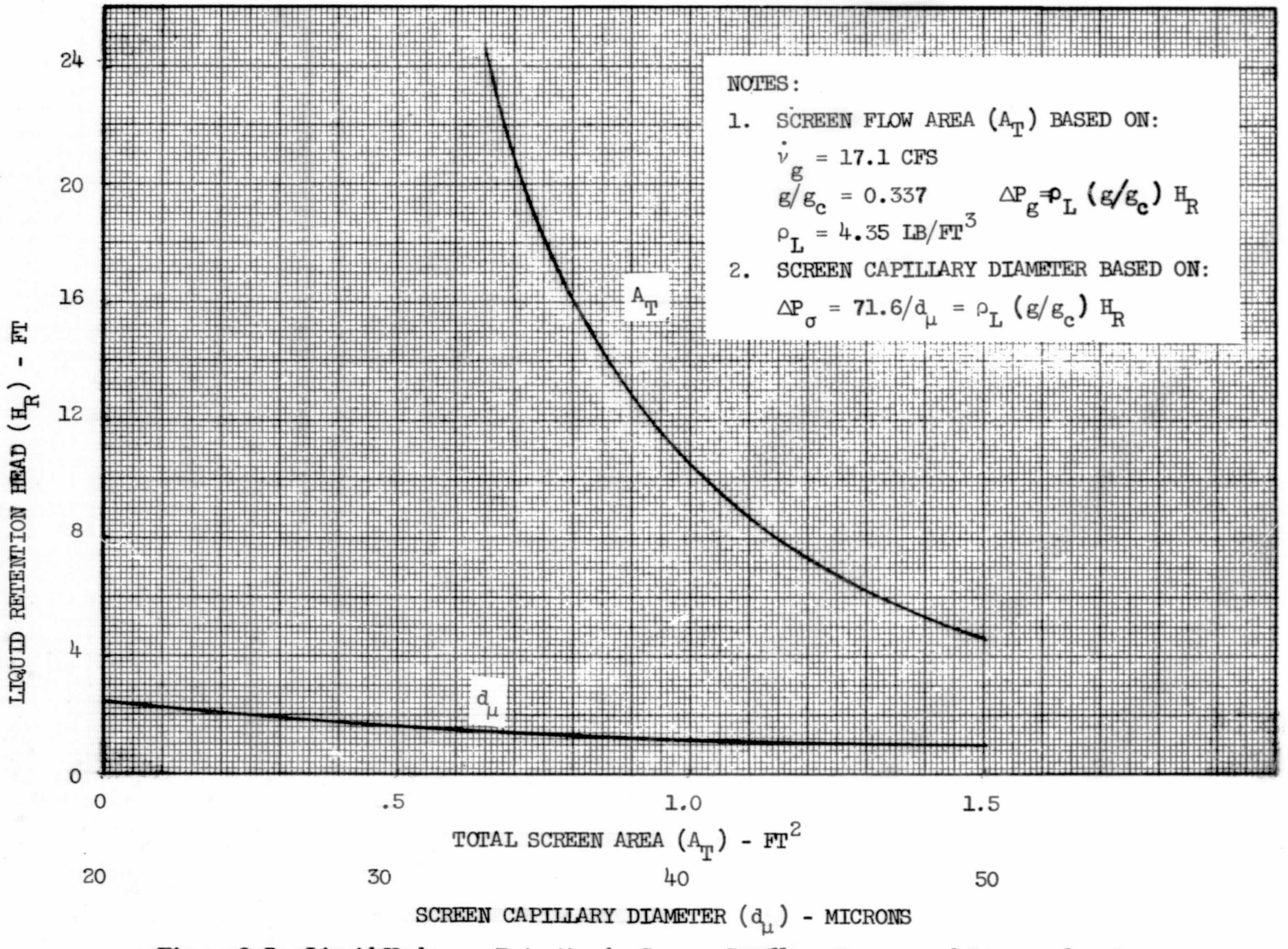
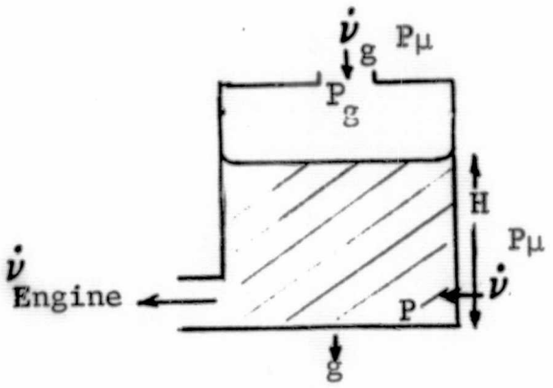


Figure 2-7. Liquid Hydrogen Retention by Screen Capillary Forces and Screen Flow Losses



but $P_L = \rho_L g/g_c\, H + P_g$ (3b)

$P_g = P_\mu - \Delta P_g$, (3c)

and $P_\mu - P_L = \Delta P_g - \rho_L g/g_c\, H$ (3d)

$\Delta P_g - \rho_L g/g_c\, H > \Delta P_\sigma$ or, $\Delta P_g > \Delta P_\sigma + \rho_L g/g_c H$ (3)

where ΔP_σ = surface tension pressure of screen

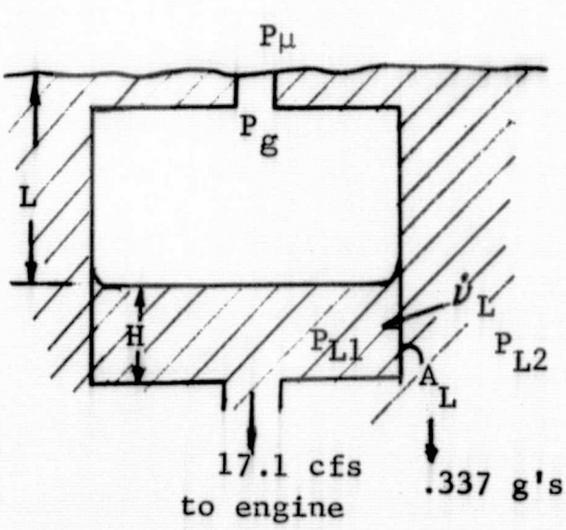
$$= \frac{71.6}{d_\mu} \text{ psf (for liquid hydrogen)}$$

where d_μ is the bubble point of the screen.

It is seen from the example that a screen area, A_T, can be selected to minimize spilling and vapor ingestion by making $\Delta P_g > \rho g/g_c\, H$ and $\Delta P_g < \Delta P_\sigma + \rho(g/g_c)H$. Since H is changing, however, this balance cannot be sustained. The best approach is to let ΔP_g equal $\rho_L(g/g_c)H$ initially and use ΔP_σ to minimize vapor ingestion. If the idle mode is used, g will describe two discrete values making it more difficult, unless ΔP_σ is very large to resist vapor ingestion and/or spilling during restart.

Start Basket Refill

During initial engine firing period liquid will be supplied from the start basket until tank propellants are bottomed. Once the propellants are bottomed and engine flow demand is supplied from outside, the start basket conditions will be as sketched below: (1) a high percentage of vapor volume will exist within the basket, (2) the basket will be immersed in liquid, and (3) liquid flow through the screen will occur where liquid communication exists (a conservative condition).



$$P_{L2} - P_{L1} = C_s \frac{\rho}{2g_c} \left(\frac{\dot{\nu}_L}{A_L}\right)^2 \quad (4a)$$

$P_\mu - P_g = \Delta Pg = f(A_T)$ (4b)

$P_{L1} = P_g + \rho_L(g/g_c)\, H$ (4c)

$P_{L2} = P_\mu + \rho_L(g/g_c)\,(H + L)$ (4d)

$P_{L2} - P_{L1} = (P_\mu - P_g) + \rho_L(g/g_c)\, L$ (4e)

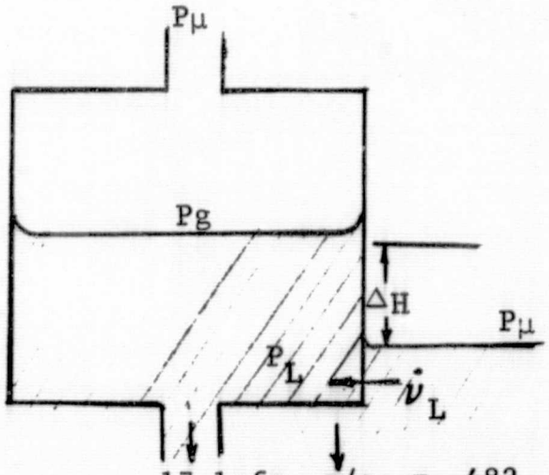
Combining (4a), (4e), and (4b) results in $\Delta P_g + \rho_L (g/g_c) L = C_s \frac{\rho}{2g_c} \left(\frac{\dot{\nu} L}{A_L}\right)^2$ (4)

ΔP_g must be properly evaluated before solving equation (4). During liquid expulsion from the screen P_g is determined by the selection of A_T. However, once the start basket is immersed in the tank propellant, liquid will penetrate everywhere until $P_g = P_T$. Consequently, equation (4) becomes $\Delta P_\sigma = \rho (g/g_c)\ L = C_s \frac{\rho}{2g_c} \left(\frac{\dot{\nu} L}{A_L}\right)^2$ (5)

This equation is solved for $\dot{\nu}_L$ by varying L and A_L; the results are given in Figure .

Figure 2-8 shows that start basket refill will occur for a wetted screen area, A_L, of 6 to 9 ft^2. A wetted screen area less than 6 ft^2 will cause the basket to empty, as refill will be less than the engine flow demand. Such a condition is intolerable because vapor will be carried to the engine when the basket is empty of liquid. Thus, it is desirable to provide as much wetted screen area as possible.

The time required to achieve basket refill was not determined because the engine firing duration is adequate to guarantee refill. A liquid head difference will exist, however, between the basket level and tank liquid level. This head difference is maximized when surface tension pressure prevents gas flow across the standpipe. This condition requires equality between liquid flow into and out of the capillary device. The following sketch and the accompanying equations illustrate that the basket level will lag the tank liquid level:



$$P_\mu - P_g = \Delta P_\sigma \quad (6a)$$

$$Pg = P_L - \rho (g/g_c)\ \Delta H \quad (6b)$$

$$P_\mu - P_L = \Delta P_L \quad (6c)$$

$$\Delta P_L = C_s \frac{\rho_L}{2g_c} \left(\frac{\dot{\nu}_L}{A_L}\right)^2 \quad (6d)$$

Combining (6b), (6c) and (6d),

$$P_g = P_\mu - \rho_L (g/g_c)\ \Delta H - C_s \frac{\rho_L}{2g_c} \left(\frac{\dot{\nu}_L}{A_L}\right)^2 \quad (6e)$$

Finally $\Delta P_\sigma = \rho_L (g/g_c) \Delta H + C_s \frac{\rho_L}{2g_c} \left(\frac{\dot{\nu}_L}{A_L}\right)^2$ (6)

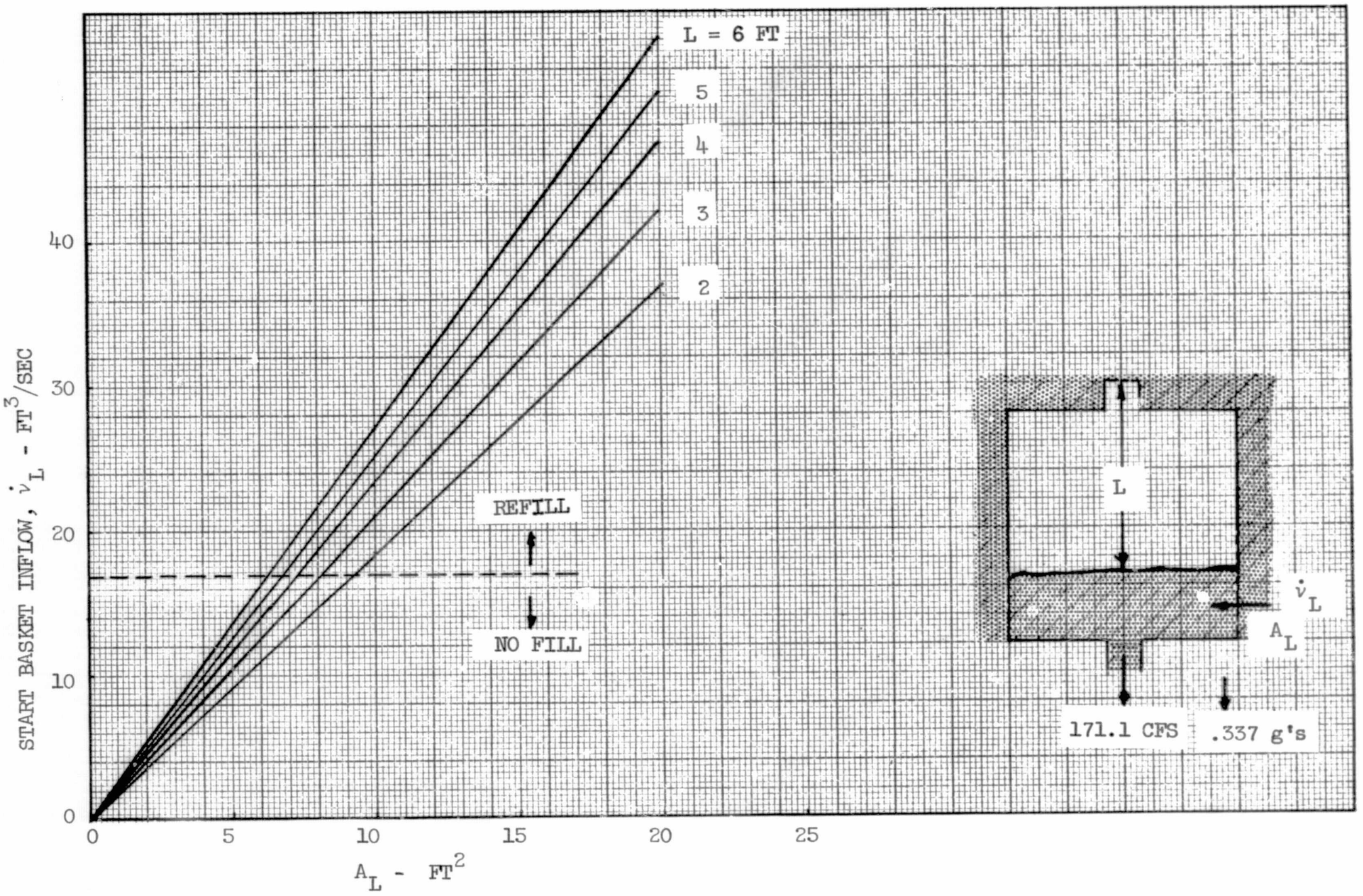


Figure 2-8. Start Basket Refill Following S-IVC Restart

Equation (6) has been solved for Cs = 22.0 (which is the 200 × 600 dutch twill weave screen) and assuming a range of capillary diameters for the screened standpipe on top of the start basket. The results are given in Figure 2-9. One can conclude that a minimum screen flow area is preferrable because it creates a reduced liquid head difference between start basket and tank liquid levels. The maximum head difference (ΔH) will occur for large flow areas where surface tension pressure effects are not diminished by ΔP_L. The ΔH can be a maximum of approximately 1.1 ft.

Selection of Start Basket

Using the data contained in Figures 2-6 through 2-9, a start basket configuration was selected which will satisfy engine start requirements and minimize burnout residuals. The configuration is given in Figure 2-10. The start basket configuration is for a 120° section, but the angle can be varied to satisfy liquid volume requirements as this information is made available. All screened areas of the start basket, including the standpipes, are constructed of 200 × 600 mesh dutch twill weave having an average capillary diameter of 36.7μ. (The calculations also assume that the bubble point of the screen is 36.7μ. The bubble point determined from testing for the screen was found to be 19.05μ.)

A major portion of the start basket is constructed of solid material. In fact, the only opening at the forward end of the start basket is the screened lid (1.42 ft^2) of a standpipe. This flow area will produce a pressure loss due to vapor inflow that will retain 8.4 feet of LH_2 head during the engine restart (see Figure 2-7). The physical head of liquid within the start basket is a maximum of 5.19 feet and a liquid retention by the screened standpipe will be 1.3 ft. Consequently, some vapor will penetrate through the screened areas A_{L1} and A_{L2}. This vapor will not flow to the main engine however, because of the screened deflector, internal to the start basket, that surrounds the tank outlet and prevents overboard vapor flow. The standpipe height of 4.5 inches was provided to minimize trapped vapor during pre-flight tanking. Considerably less vapor volume is trapped if the vapor head is contained within the standpipe. The standpipe attached to the internal screen basket was also installed to minimize trapped vapor within the internal screen during tanking. Its screened area is not critical and need not exceed a few square inches.

According to Figures 2-8 and 2-9 it appears that the optimum liquid screen area A_L will be 20 to 25 ft^2. This range would guarantee a rapid basket refill following propellant settling and result in a liquid head difference of approximately 0.3 ft at S-IVC burnout. These curves, however, do not take into account the increase in tank residual due to the flow restriction of the screen. It is possible that these effects may overcome the slight reduction in start basket residuals that occur by reducing ΔH. Furthermore, although 36.7 ft^2 of screen area (A_{L2}) is available for liquid flow, the small flow area provided by the channel between tank wall and screen will effectively

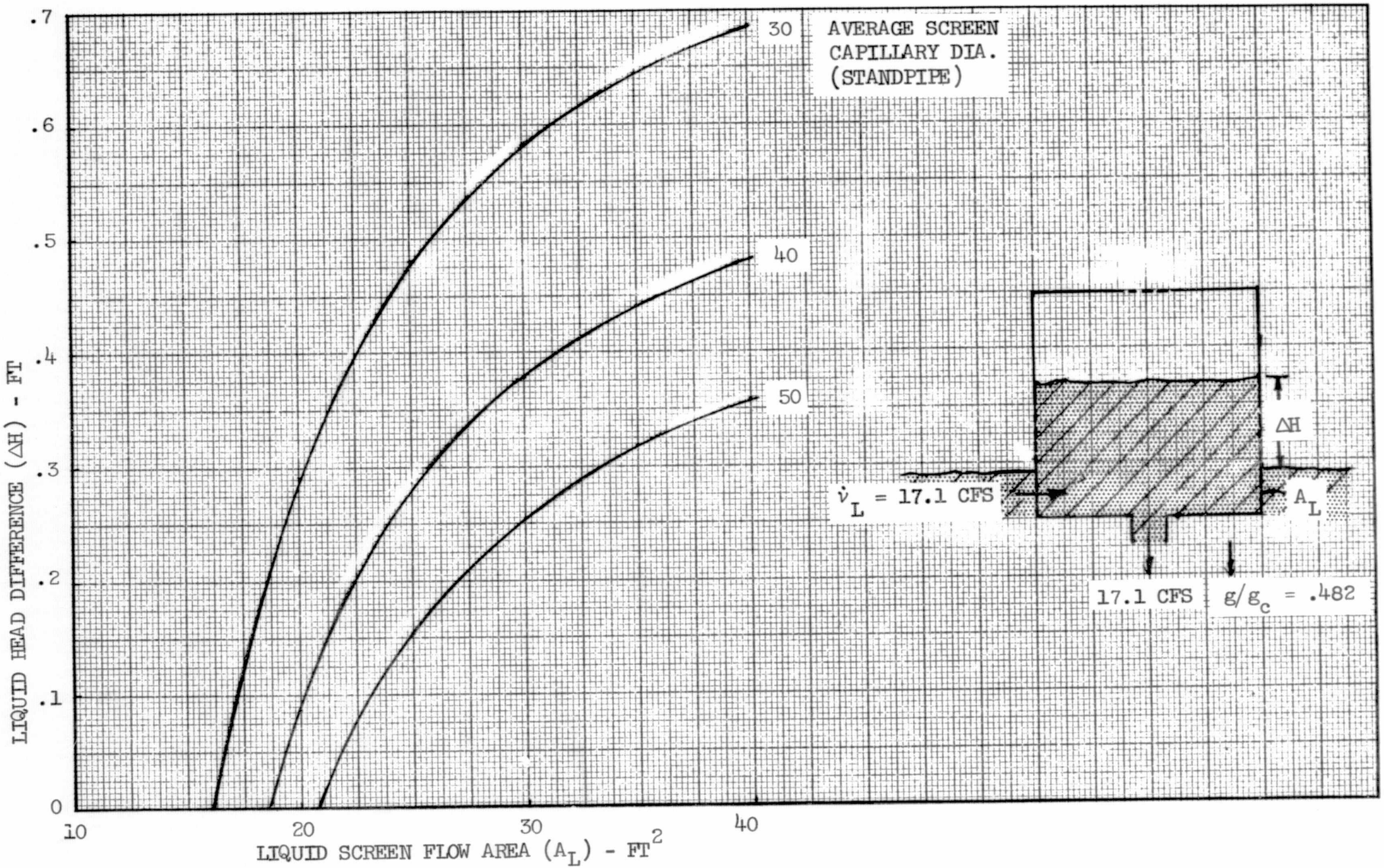


Figure 2-9. Liquid Head Difference at S-IVC Burnout

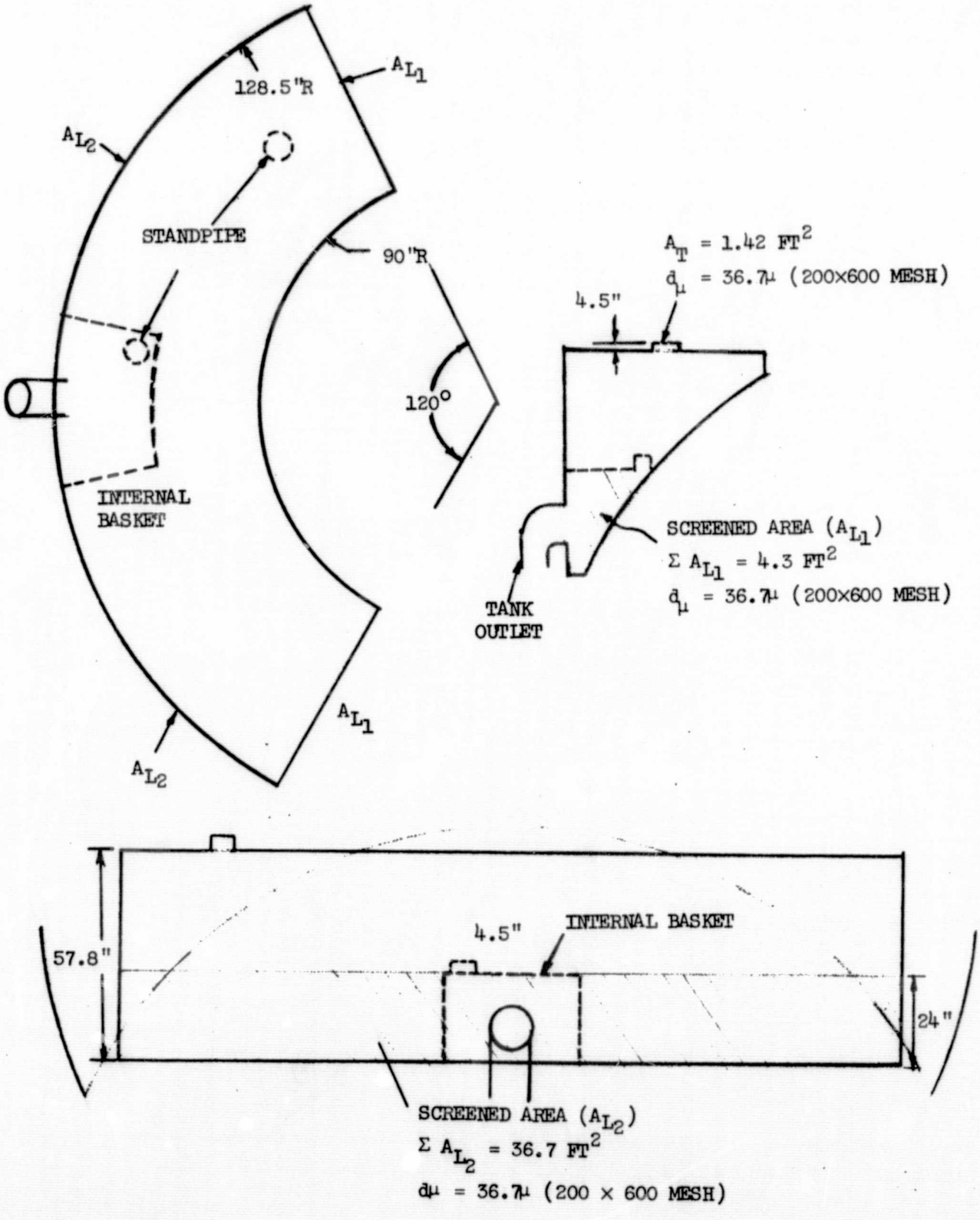


Figure 2-10. S-IVC Start Basket Configuration

Figure 2-11. Start Basket Volume (Based on a 1/3 Annulus)

REPRODUCIBILITY OF THE ORIGINAL PAGE IS POOR.

reduce A_{L_2} because of the channel pressure loss. Thus, $A_{L2} = 36.7$ ft^2 and $A_{L1} = 4.3$ ft^2 were selected as the screen area for liquid inflow.

The start basket volume as a function of height is given in Figure 2-11 for a 1/3 annulus (i.e., a 120° section). The total contained volume is 208 ft^3; 158 ft^3 of which was assumed to be usable. The unusable volume is contained within the bottom 24 inches of the screen. It is assumed that if liquid refill does not begin before 158 ft^3 of liquid is expelled from the basket, vapor will be carried to the engine. The usable liquid volume provides 9.2 seconds of liquid flow at steady state engine firing. If more or less time is required to bottom propellants before basket refill commences, then the basket volume can be altered by varying the 120° annulus section.

The unusable basket residual was determined in part from information obtained from MSFC on S-IVB residuals. MSFC reported that LH_2 residuals of 216 ft^3 would occur 0.35 g's and 80 lb/sec engine flowrate. For a 1/3 section of tank these residuals would be 72 ft^3. One can expect, however, that the presence of a fine mesh screen over the tank outlet will delay suction dip and reduce residuals. Certainly a baffle placed over the outlet which is designed to delay suction dip would reduce LH_2 residuals below 72 ft^3, An unusable liquid residual of 50 ft^3 was selected as reasonable for the start basket during engine restart.

The work conducted to date on the start basket has demonstrated that the system will perform satisfactorily for an S-IVC engine restart. Performance curves have not as yet been obtained for the system. This will require that the basket configuration, screen parameters, restart environment and a propellant settling description be programmed for a parametric evaluation. During the next quarter a computer program will be established to predict start basket performance for engine restart, on an experimental test program will be considered as a means of obtaining these performance details. As stated above, a fine mesh screen or baffle plate over the tank outlet will delay suction dip. But, the start basket screen area will provide resistance to flow into the basket. This resistance will increase residuals outside the basket. This will be studied in more detail in Phase II.

Capillary containment system design for restart devices is strongly influenced by the settling flow pattern and settling time within the propellant tank. Predicting the fluid flow during settling requires a method which describes free surface motion in a liquid for complex tank geometries.

The Convair (MAC) Marker and Cell program, a numerical technique for solving the momentum, energy and continuity equations for a viscous, incompressible fluid, was used to study these field flow problems.

S-IVC settling was investigated for the all-liquid flow case. The configuration which was evaluated is shown in Figure 2-12 with S-IVB-type slosh baffles. Since these baffles may not be included in the S-IVC, the problem discussed here was rerun in

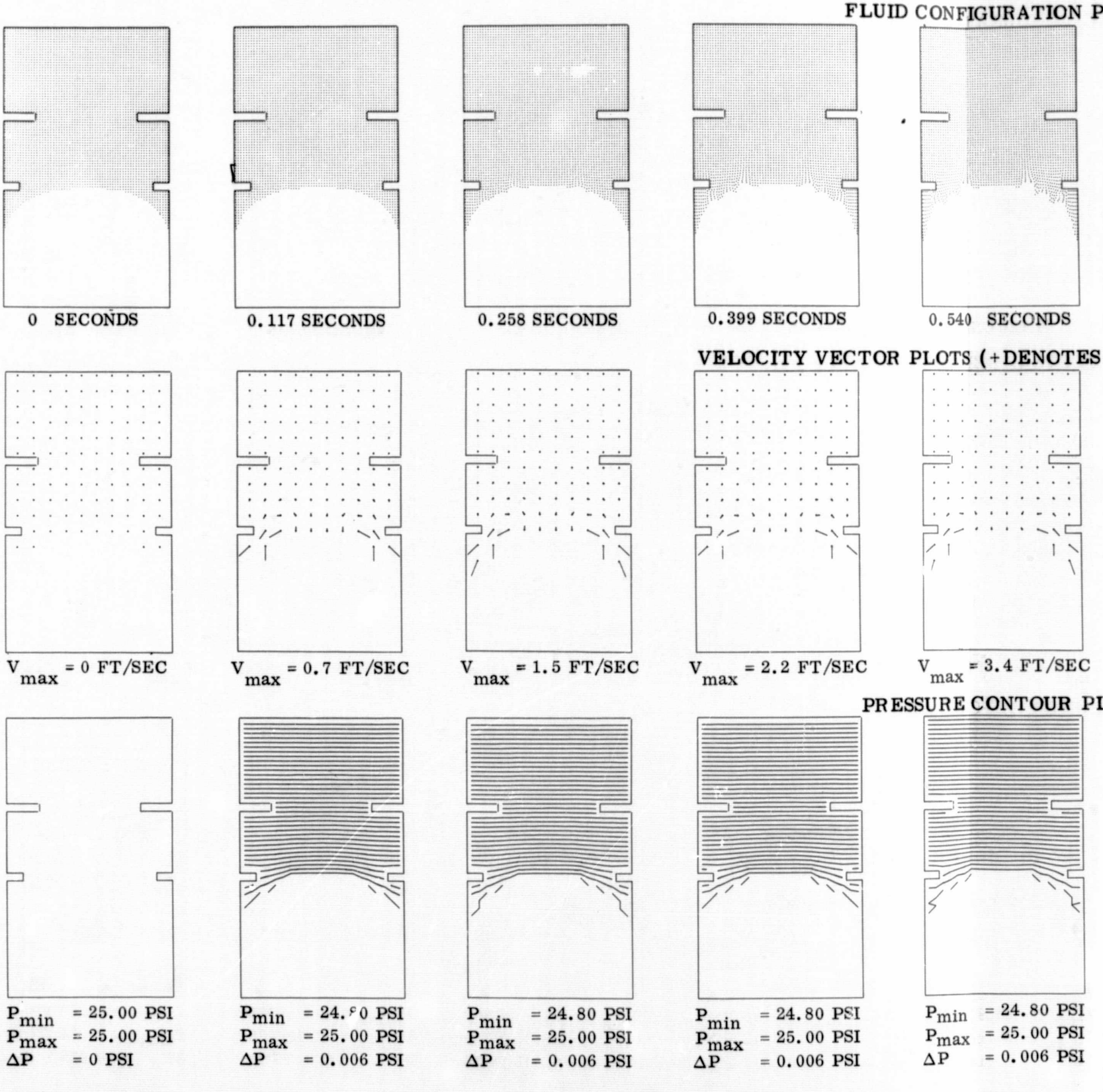
Phase II with the baffles removed. The configuration of the free surface, assuming a 60% full tank experiencing a 10^{-6} drag acceleration, was obtained using Figure 4.3a of Reference 13. These curves represent a numerical solution of the differential equation representing an axi-symmetric meniscus statis equilibrium condition. A contact angle of zero and a Bond number of 3.3 were used to obtain the surface height as a function of radius.

Figures 2-12, 2-13, and 2-14 show the output of the program for the high thrust case with a .337 g settling acceleration. The fluid configuration plots are shown on top with the corresponding time, directly below are the velocity vector plots with maximum velocity and the pressure contour plots with the maximum and minimum static pressure and the pressure difference between contour lines. The output shows the fluid near the wall reaching the aft bulkhead first with the central portion of the fluid striking later. Additional running of the model was used to extend the firing time out to 3.07 seconds. A movie was made of this problem and a copy was sent to the contract monitor. The additional running of the model indicated that considerable recirculation occurs after impingement of the fluid on the aft bulkhead.

Comparing MAC model settling runs and results of a computer program based on information obtained from drop tower tests (References 1 and 2) indicates agreement that impingement on the aft bulkhead should occur after 1.27 seconds. According to the empirical correlations, which were established at lower Bond and Weber numbers, the fluid collection should occur at a fairly rapid rate and the top of the start basket should be covered in 3.5 seconds. The MAC model indicates that considerable recirculation and geysering occur after impingement causing the fluid collection process to be severely disturbed. Based on the MAC model runs, a reorientation time of 10 seconds should be approximately correct; however, considerable uncertainty is present in this estimate. The conclusion was that the established empirical correlations do not hold for the high Bond and Weber numbers being considered.

Should it become necessary to control large quantities of liquid to assure a satisfactory engine start based on settling and spilling requirements, the problem area would shift from engine start to the orbital coast condition. The containment device would be a shell constructed of screen or perforated plate that would follow the contours of the aft end of the hydrogen tank. Structural design details of such a device are given in Section 2.3, Figure 2-44. A simplified sketch is given below. The liquid contained in a 200 ft^3 device of this type would more than suffice for an engine restart.

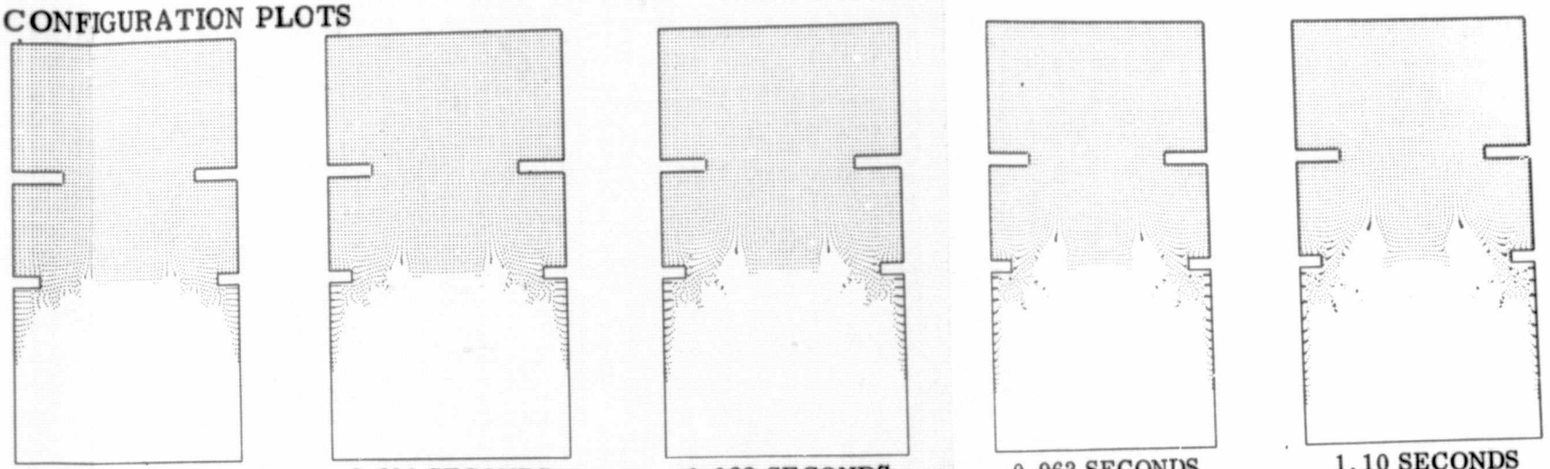
Thermal control of the contained liquid would be more difficult than for the start basket because of size alone. There would be many more penetration heat leaks to contend with. Furthermore, the heat flux through the common bulkhead constitutes the bulk of the fuel tank heat leak, which in turn must be prevented from heating the contained liquid. Another factor is that subcooling this larger volume of liquid requires considerably more cooling capacity than for cooling the start basket volume.



FOLDOUT FRAME

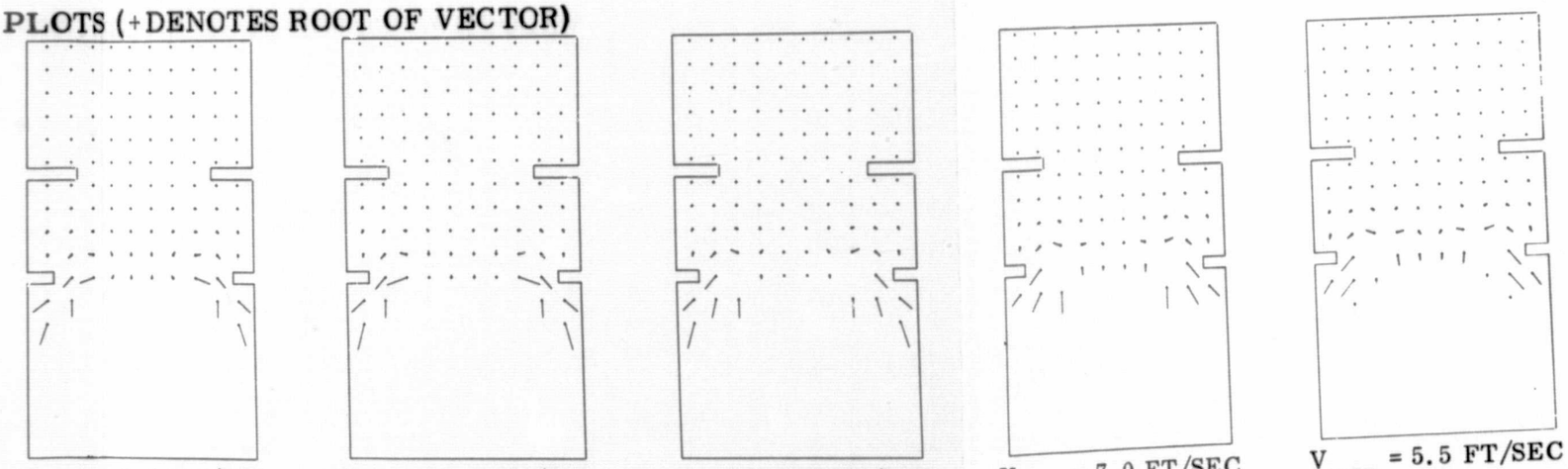
Figure 2-12. Fluid Simulation of S-IVC

ID CONFIGURATION PLOTS



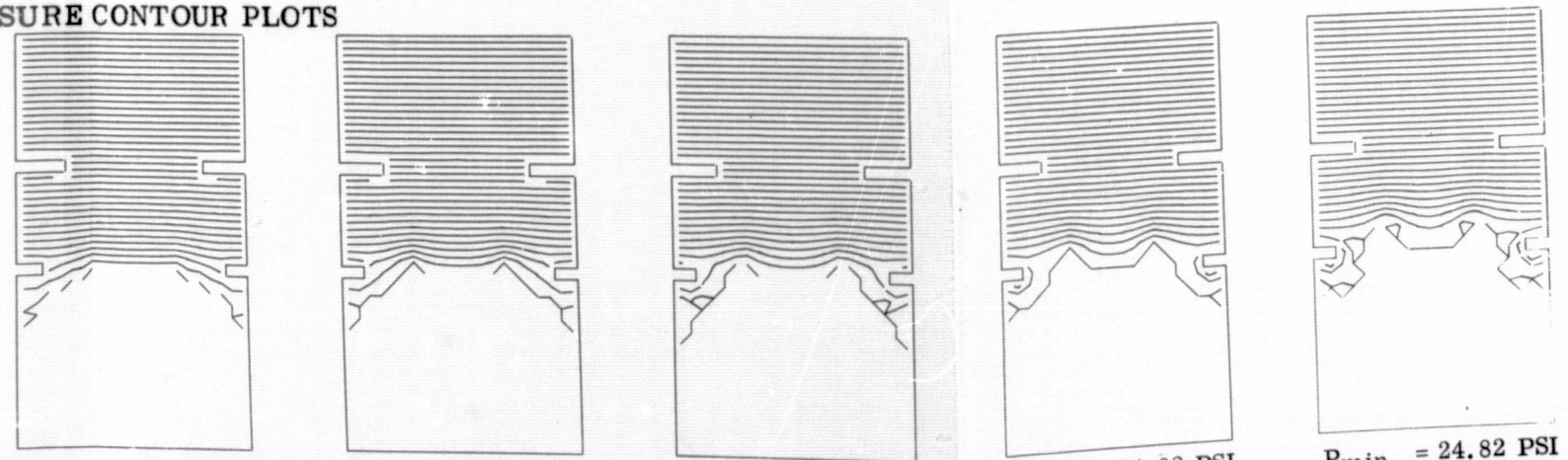
0.540 SECONDS | 0.681 SECONDS | 0.822 SECONDS | 0.963 SECONDS | 1.10 SECONDS

R PLOTS (+DENOTES ROOT OF VECTOR)



V_{max} = 3.4 FT/SEC | V_{max} = 4.5 FT/SEC | V_{max} = 5.4 FT/SEC | V_{max} = 7.0 FT/SEC | V_{max} = 5.5 FT/SEC

ESSURE CONTOUR PLOTS



P_{min} = 24.80 PSI
P_{max} = 25.00 PSI
ΔP = 0.006 PSI

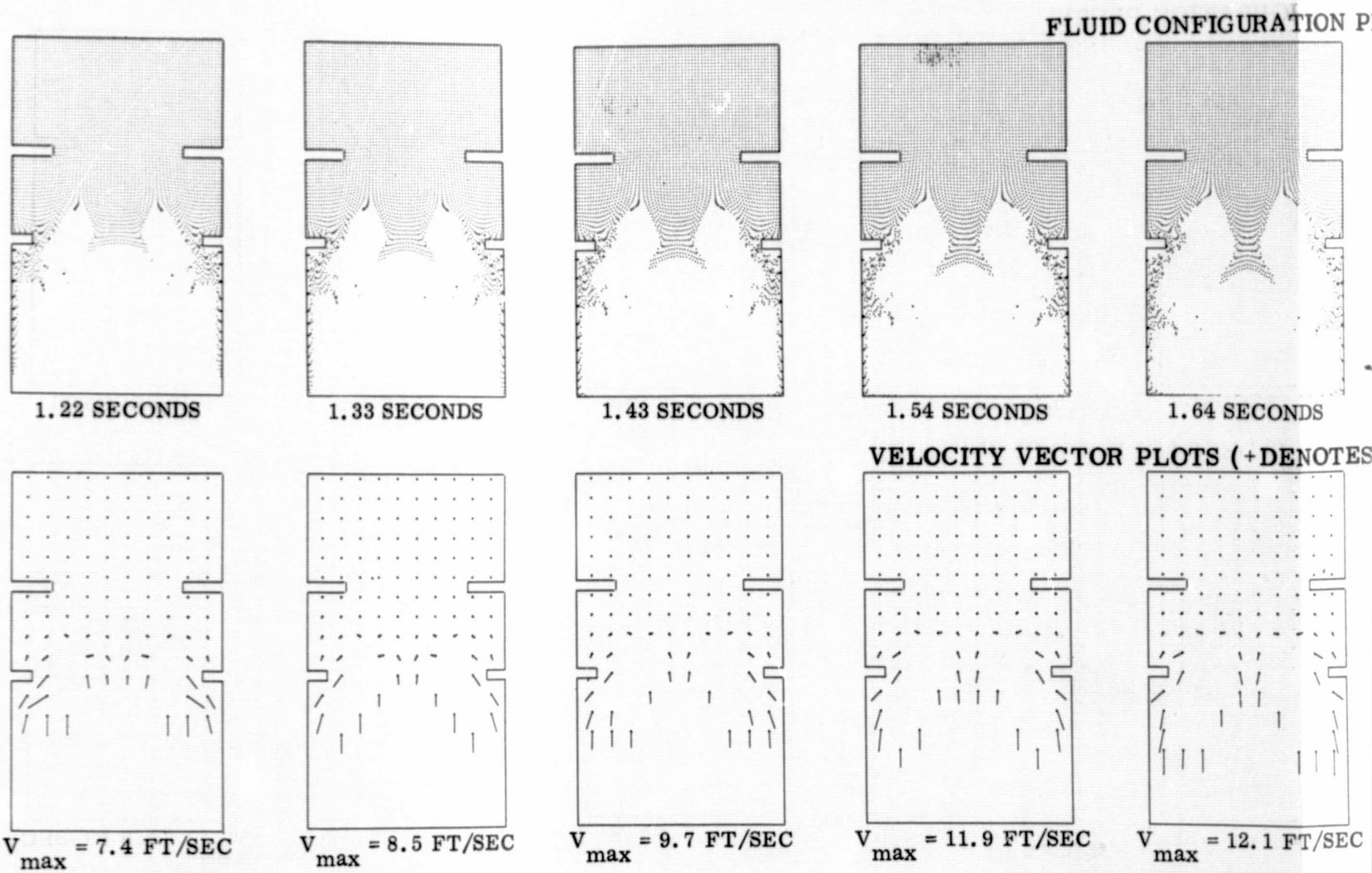
P_{min} = 24.81 PSI
P_{max} = 25.00 PSI
ΔP = 0.006 PSI

P_{min} = 24.81 PSI
P_{max} = 25.00 PSI
ΔP = 0.006 PSI

P_{min} = 24.82 PSI
P_{max} = 25.00 PSI
ΔP = 0.006 PSI

P_{min} = 24.82 PSI
P_{max} = 25.00 PSI
ΔP = 0.006 PSI

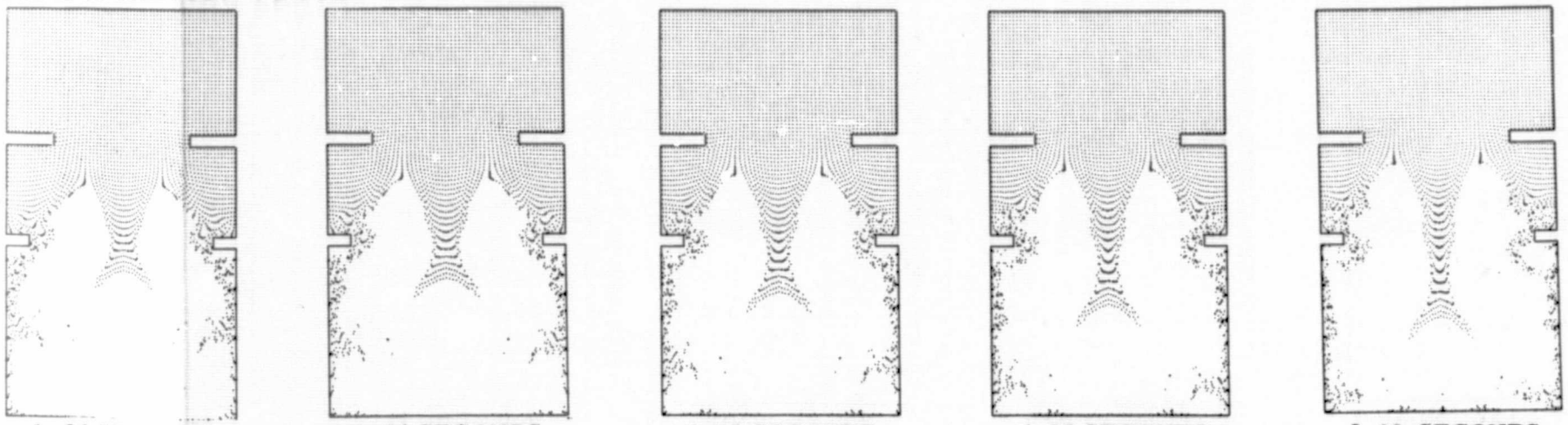
FOLDOUT FRAME 2



FOLDOUT FRAME

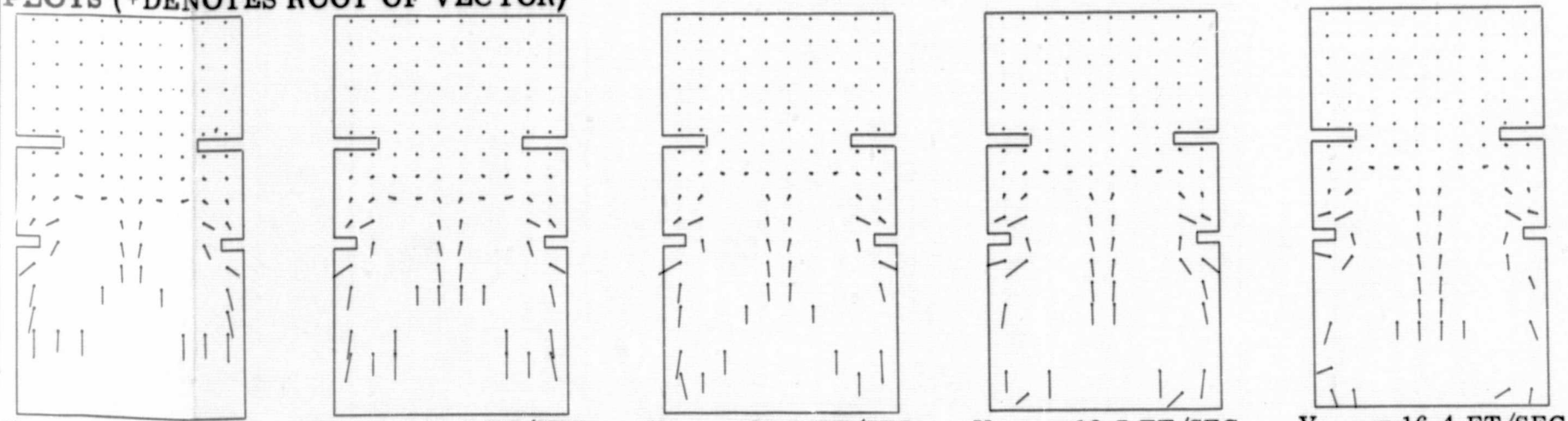
Figure 2-13. Fluid Simulation of S-IV

CONFIGURATION PLOTS



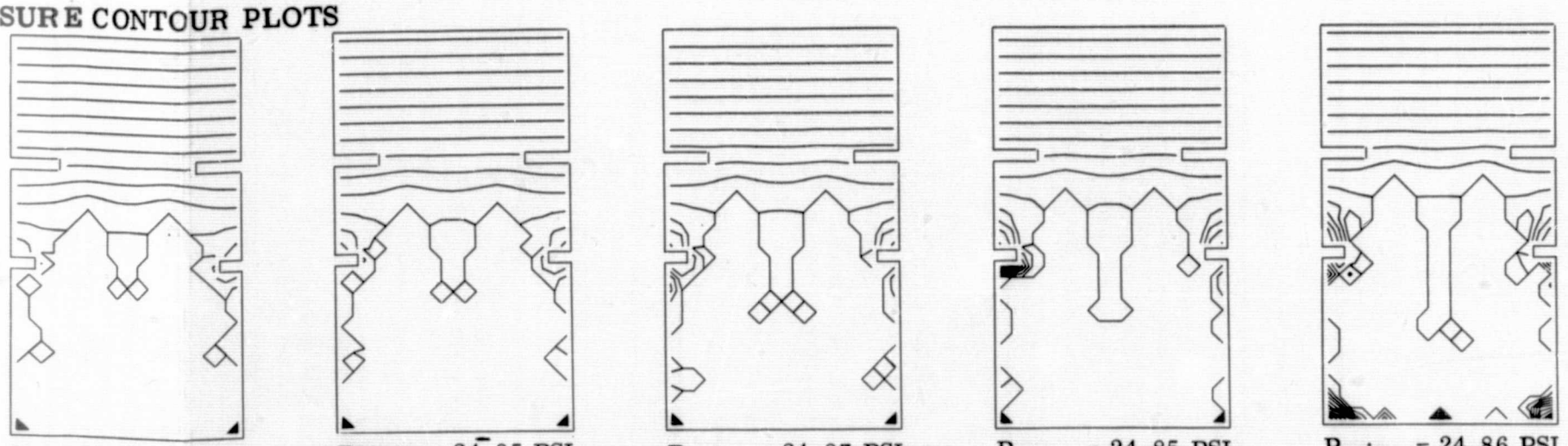
1.64 SECONDS | 1.74 SECONDS | 1.86 SECONDS | 1.97 SECONDS | 2.08 SECONDS

PLOTS (+DENOTES ROOT OF VECTOR)



V_{max} = 12.1 FT/SEC | V_{max} = 14.0 FT/SEC | V_{max} = 20.8 FT/SEC | V_{max} = 16.7 FT/SEC | V_{max} = 16.4 FT/SEC

SSURE CONTOUR PLOTS



P_{min} = 24.85 PSI
P_{max} = 25.10 PSI
ΔP = 0.015 PSI

P_{min} = 24.85 PSI
P_{max} = 25.13 PSI
ΔP = 0.015 PSI

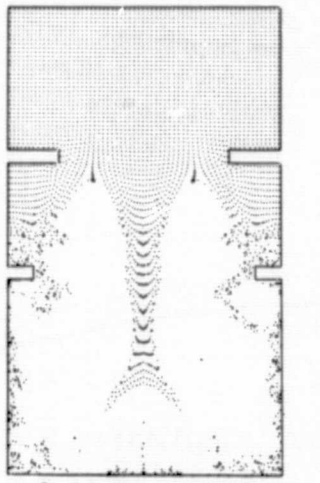
P_{min} = 24.87 PSI
P_{max} = 25.15 PSI
ΔP = 0.015 PSI

P_{min} = 24.85 PSI
P_{max} = 25.12 PSI
ΔP = 0.015 PSI

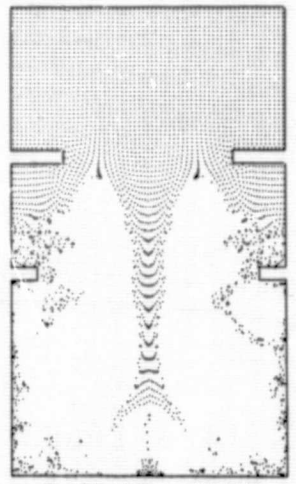
P_{min} = 24.86 PSI
P_{max} = 25.24 PSI
ΔP = 0.015 PSI

FOLDOUT FRAME

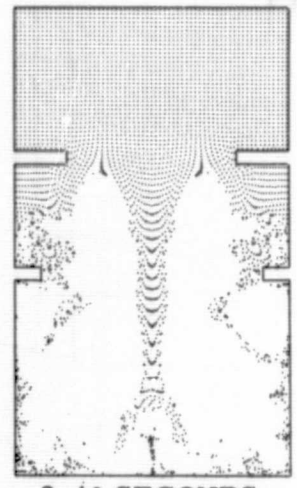
FLUID CONFIGURATION PLOTS



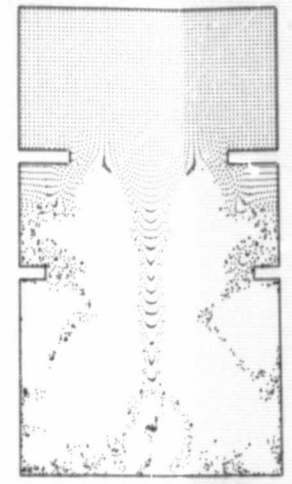
2.19 SECONDS



2.29 SECONDS



2.40 SECONDS

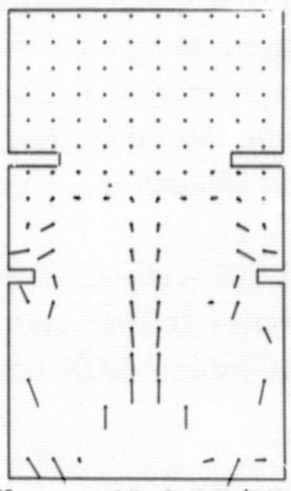


2.50 SECONDS

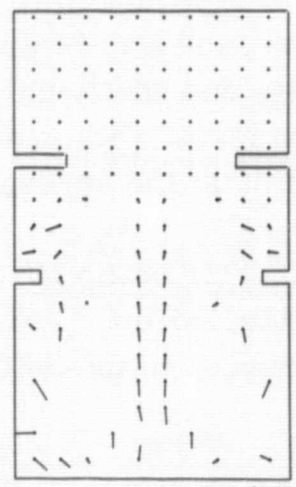


2.61 S

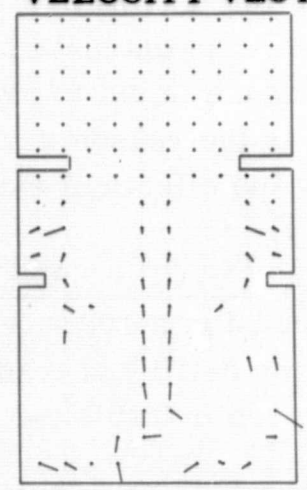
VELOCITY VECTOR PLOTS (+DENOTES ROOT OF



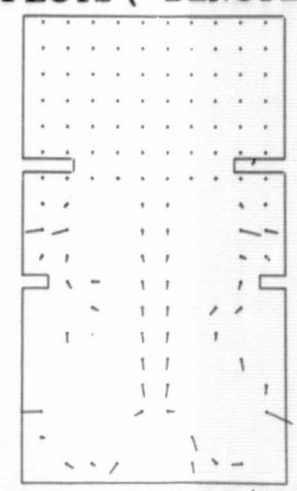
V_{max} = 17.3 FT/SEC



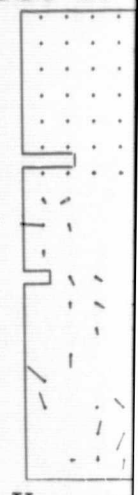
V_{max} = 21.8 FT/SEC



V_{max} = 33.4 FT/SEC

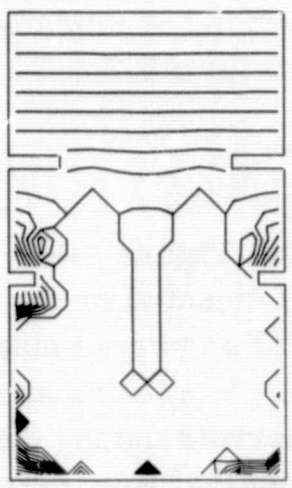


V_{max} = 37.2 FT/SEC

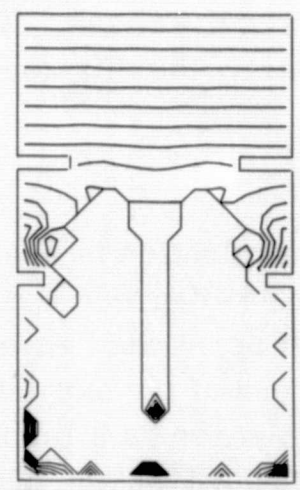


V_{max} =

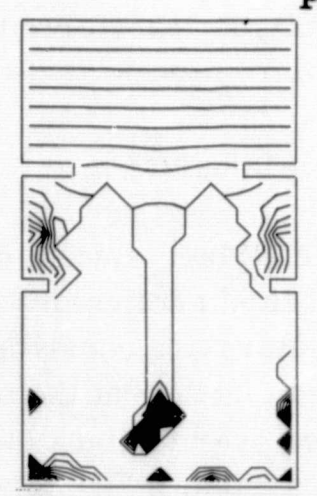
PRESSURE CONTOUR PLOTS



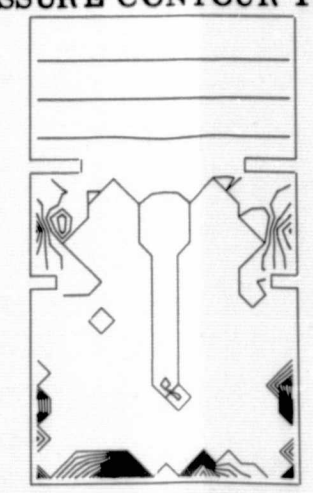
P_{min} = 24.88 PSI
P_{max} = 25.15 PSI
ΔP = 0.015 PSI



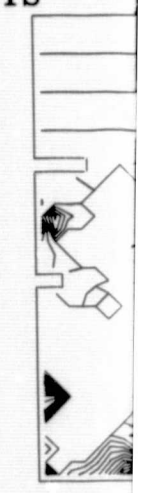
P_{min} = 24.88 PSI
P_{max} = 25.18 PSI
ΔP = 0.015 PSI



P_{min} = 24.81 PSI
P_{max} = 25.24 PSI
ΔP = 0.015 PSI



P_{min} = 24.91 PSI
P_{max} = 25.05 PSI
ΔP = 0.030 PSI

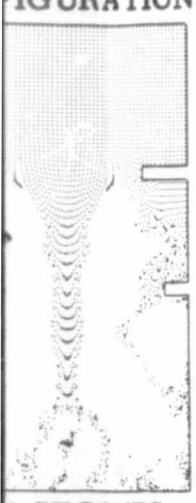


P_{min}
P_{max}
ΔP

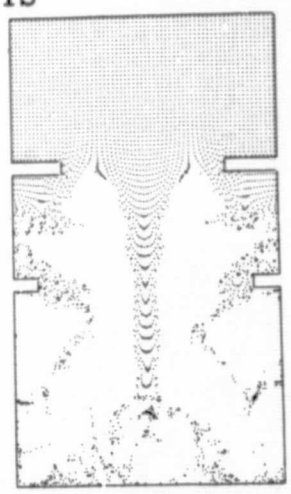
FOLDOUT FRAME

Figure 2-14. Fluid Simulation of S-IVC Liquid Hy

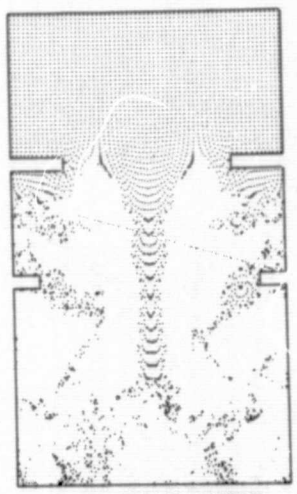
FIGURATION PLOTS



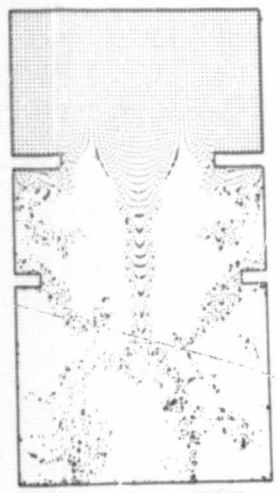
0 SECONDS



2.61 SECONDS

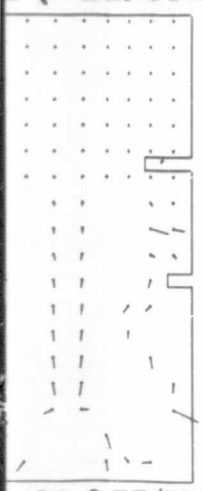


2.71 SECONDS

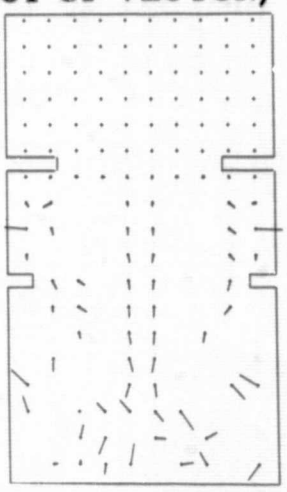


2.83 SECONDS

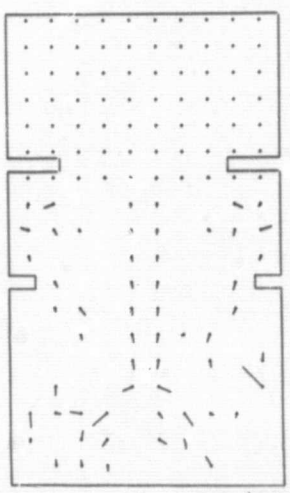
S (+DENOTES ROOT OF VECTOR)



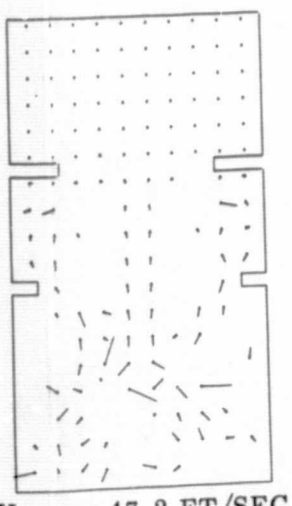
= 37.2 FT/SEC



V_{max} = 25.2 FT/SEC



V_{max} = 48.0 FT/SEC

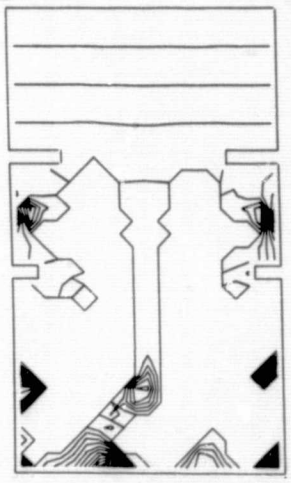


V_{max} = 47.2 FT/SEC

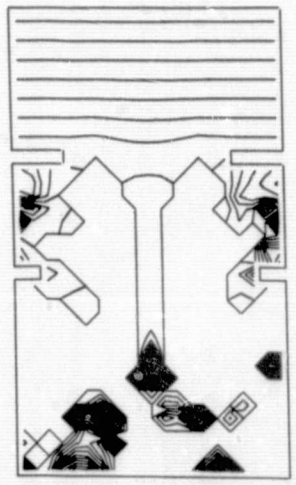
CONTOUR PLOTS



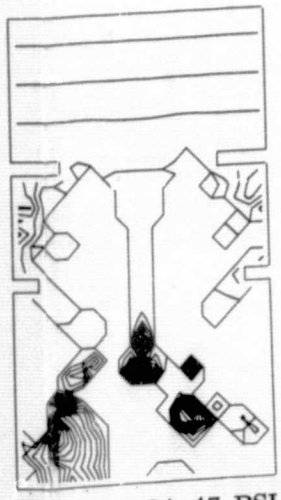
= 24.91 PSI
= 25.05 PSI
= 0.030 PSI



P_{min} = 24.82 PSI
P_{max} = 25.05 PSI
ΔP = 0.030 PSI



P_{min} = 24.88 PSI
P_{max} = 25.27 PSI
ΔP = 0.015 PSI



P_{min} = 24.47 PSI
P_{max} = 25.35 PSI
ΔP = 0.030 PSI

FOLDOUT FRAME

2

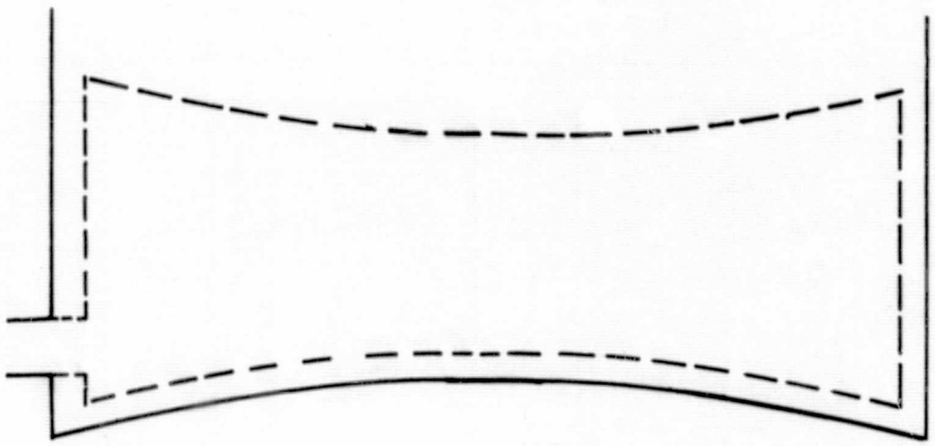


Figure 2-15. Large Liquid Volume Capillary Device

A concern with propellant heating is not only that internal evaporation will force liquid out of the device, but that the capillary device liquid retentive capability may be impaired. As discussed earlier, the way in which vapor forms on the capillary device may cause liquid to drain out, and additional vapor to enter, in an acceleration field. This is the reason that bench tests, with room temperature fluids, were conducted to study the effects of evaporation at the screen-liquid interface.

2.1.2 OXYGEN TANKER REQUIREMENTS. An S-IIB with an empty LOX tank is to be placed in a 100 × 263.5 n.mi. orbit. A LOX tanker in this same orbit is to dock with the S-IIB and transfer oxygen to the S-IIB LOX tank. LOX tanker ground rules are given in Table 2-2.

The oxygen tanker is designed to orbit in space with a full tank of LO_2 for a period up to 163 days. This orbit duration is followed by a propellant transfer period where the LO_2 is transferred to a receiver tank. The purpose of this study is to design a capillary system that can satisfy the mission requirements.

Fluid Analysis

One capillary system under evaluation is sketched in Figure 2-50. It is comprised of eight liquid collectors spaced 45 degrees apart and mounted on the tank surface. The collectors are constructed of perforated sheet metal or screen material and are manifolded together at the outlet end of the oxygen tank. A cylindrical shell/screen is placed over the tank outlet to serve as a liquid reservoir during the transfer period. This system is designed to take advantage of the fact that liquid should maintain continuous contact with the tank wall in a low gravity environment.

It is essential that some portion of the collectors be immersed in liquid at all times in order for the system to function. Should the collectors uncover during propellant transfer, vapor will be ingested, and the transfer operation jeopardized. The sketch below illustrates how a liquid collector operates. The sketch on the left shows that as long as a portion of the collector is immersed, liquid flow will exist during



Figure 2-16. Flow From a Liquid Collector

propellant transfer. As long as the liquid flow area is great enough so that the liquid pressure drop does not exceed the surface tension pressure drop of the screen, vapor will not penetrate the collector.

The tank contents can be almost completely transferred to the receiver tank before the liquid collectors uncover. During the early period of propellant transfer it is evident that the collectors will be immersed. The decelerating effect (10^{-6} g's) of aerodynamic drag will cause the propellants to remain positioned against the tank. Should the acceleration vector change direction, liquid flow will occur to reposition the liquid bulk. The low Bond number will assure that liquid will be along the tank wall as liquid is repositioned. As a safeguard against liquid collector uncovery, the purpose of the cylindrical reservoir is to provide liquid for propellant transfer in the event that the collectors momentarily uncover.

The liquid collection system design will of course be strongly influenced by the flow rate and vehicle acceleration considerations during propellant transfer. A tentative system sizing was selected for the purpose of assessing design techniques. The liquid collectors were 16 inches wide by 2 inches high; they cover about 12 percent of the tank surface area. The liquid reservoir dimensions were selected as 5 ft diameter by 5 ft high, which will provide liquid for 180 seconds during transfer. This configuration represents only a first cut at the preliminary design. Heating consdierations prompt a low collector surface area while collection considerations would warrant a high surface area in order to assure liquid is present in the collection device. Analyses of designs allowing for these competing criteria will provide an optimum collector configuration.

The 163-day period preceding propellant transfer will see the nearly full LO_2 tanker exposed to a 10^{-6} g environment. A thermodynamic vent system will be used for tank venting. The full tank condition excludes the possibility that liquid collectors will uncover. The system design must preclude, however, any adverse effect due to tank heating and venting. Basically, the goal is a system design that will prevent vapor accumulation in the collectors and reservoir. If this goal is achieved, the system will perform satisfactorily for tank venting and be in readiness for propellant transfer.

Adequate thermal protection of the liquid collector is crucial to system performance.

For assurance, the initial approach taken was to select a design that would reject the accumulation of vapor during coast. Several collector configurations with this capability are sketched below. Tapered surfaces were utilized to eject bubbles into the tank.

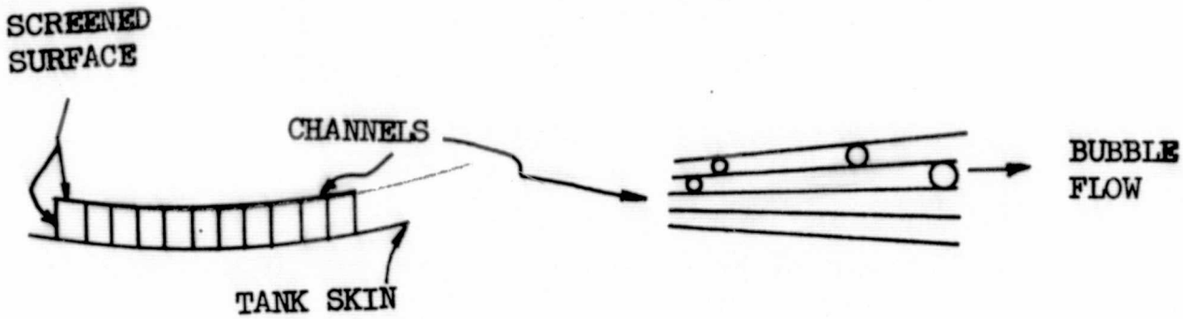


Figure 2-17. Channels Tapered to Eject Vapor

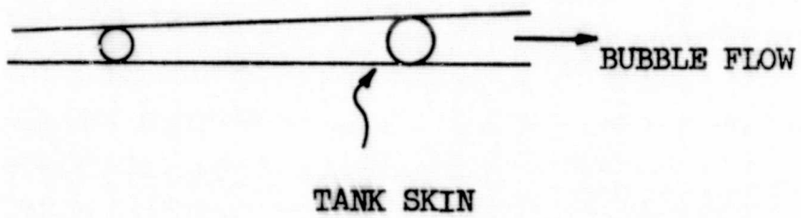


Figure 2-18. Top of Enclosure Tapered to Eject Vapor

The thermodynamic vent system was designed to operate with liquid at the inlet of the heat exchanger. The liquid collectors were tapped to provide this liquid to the system. Furthermore, the oxygen ventage will chill critical areas of the capillary system to intercept heat leaks and assure a vapor-free condition at the tank outlet and within the liquid reservoir.

Table 2-2. Liquid Oxygen Tanker Groundrules

Configuration:	LMSC Tanker for S-IIB Receiver (218" Dia. Sphere)
Orbital Environment:	100 × 263 n. mi. Transfer Orbit 10^{-6} drag acceleration 10^{-3} disturbances possible Total orbital heating is equivalent to 8050 lb boiloff in 163 days

Table 2.2. Liquid Oxygen Tanker Groundrules (contd)

Vehicle Conditions:	163 Day Mission Duration 15 psia tank pressure Thermodynamic Vent Separator 95% Initial Liquid Oxygen Level
Orbital Propellant Transfer	Transfer Flow Rate = $\frac{200,000 \text{ lb}}{90 \text{ minutes}}$

A second cut at the LO_2 tanker capillary device is sketched in Figure 2-53 with selected dimensions given. The screened device is comprise of eight retriever channels equally spaced (circumferentially about the tank) and a connector channel around the tank equator which connects with the LOX tanker. The channels are constructed of a dutch twill weave (an average pore size of 22.8 microns) and have a cross-sectional flow area of 1.4 × 14.0 inches. These channels shall be contoured to maintain an approximate 0.25 inch gap with the tanker sphere. Low conductivity supports, specially designed to provide a high resistance path, are used to maintain spacing of the retriever channels with tank wall and to minimize heat leaks to the channel contents.

It is noted that the retriever channels are not tapered nor are the forward ends of each channel open, as previously indicated. It was originally believed that a proper taper to the channels would make it possible to eject all internally generated vapor. Although it is possible to assure vapor bubble ejection in this manner, it was deemed necessary to enclose the channels with fine mesh screen. Total enclosure is necessary to delay ullage vapor penetration that would occur early during the LOX transfer period if the channels remained open. Total enclosure, however, will preclude the possibility of ejecting any bubbles generated within the channels. Consequently, tapered channel passages will serve no functional purpose. Thus, it now becomes important to find some means of holding net heat input to the retriever channels to an acceptable level. Means of holding this heat flux to acceptable levels are explained in Section 2.2.

Another major departure from the previous design is the introduction of a channel around the tank equator for the purpose of connecting the eight retriever channels. This change will reduce flow losses by permitting liquid flow through all retriever channels (this allows a reduction in channels dimensions). As a result, liquid residuals can be held to a minimum.

The screen cylinder that is located over the tank outlet will function as a liquid reservoir. That is, should the occasion arise during LOX transfer where liquid is not available to retriever channels then liquid would automatically drain from the cylinder rather than permit vapor to penetrate the channel screens. There will be additional details presented later on the screen cylinder and how it complements the overall system performance.

Propellant Flow Analysis

A transfer flow analysis was conducted to optimize the flow channel dimensions and select screen mesh characteristics that would minimize the unusable propellants (residual). Because the system flow losses, and therefore liquid residuals, will be influenced by the liquid orientation near the termination of LOX transfer, the analysis was based on a maximum pressure loss orientation. This orientation condition assumes that a lateral acceleration exists to locate the LOX along the equator of the tank. It is seen from Figures 2-19 and 2-20 that this orientation (curve 8a) will result in the minimum retriever channel screen area wetted per unit volume of LOX remaining as compared to liquid settled at the forward end of tank (curve 8c). Because screen flow pressure losses increase as screen flow area is reduced, residuals will be greater for the condition of minimum wetted screen area.

It is evident from Figure 2-21a that a substantial quantity of liquid can remain "bottomed" at the tank equator while wetting only one of the eight retriever channels. This condition would cause liquid transfer through one channel only, with a resultant increase in flow losses and residuals. It was, therefore, decided to introduce a channel about the tank equator which would connect with the eight retriever channels and provide communication with each. This configuration (Figure 2-22) will enable flow through all eight retriever channels rather than through a single channel, thereby greatly reducing frictional channel flow losses. Furthermore the total screen wetted area (Figure 2-20, curve b) is increased which also reduces screen flow losses.

It is noted in Figure 2-21b that a liquid distribution can be selected that can have a relatively large liquid residual without wetting the channel surfaces. However, the capillary rise provided by the gap between the tank and channels will create additional wetted area. Thus, it was considered realistic to select this liquid distribution model to evaluate wetted screen and liquid residuals.

The flow model established for the LOX transfer analysis is based on the sketch of Figure 2-23. It is noted that

$$P_g - P_L = \Delta P \text{ screen} + \Delta P \text{ friction} + \rho(g/g_c)\, L + \frac{V_L^2}{2g_c} \qquad (7)$$

In order to arrive at this flow model it was first necessary to determine an equivalence between flow through the eight channels and flow through a single channel. This equivalence was based on the frictional pressure loss created by flow through the channel. That is, the volumetric flow rate, $\dot{\vartheta}_e$, through a single channel was determined that would result in the same frictional pressure loss as having the total flow rate $\dot{\vartheta}_t$, distributed over the eight channels. The equivalent flow rate was found to be $\dot{\vartheta}_e \approx 0.29\, \dot{\vartheta}_t$. LOX transfer will continue until vapor penetrates the screened channels. Penetration will occur at the point along the channel where the local liquid static pressure has been sufficiently reduced below ullage pressure that the screen

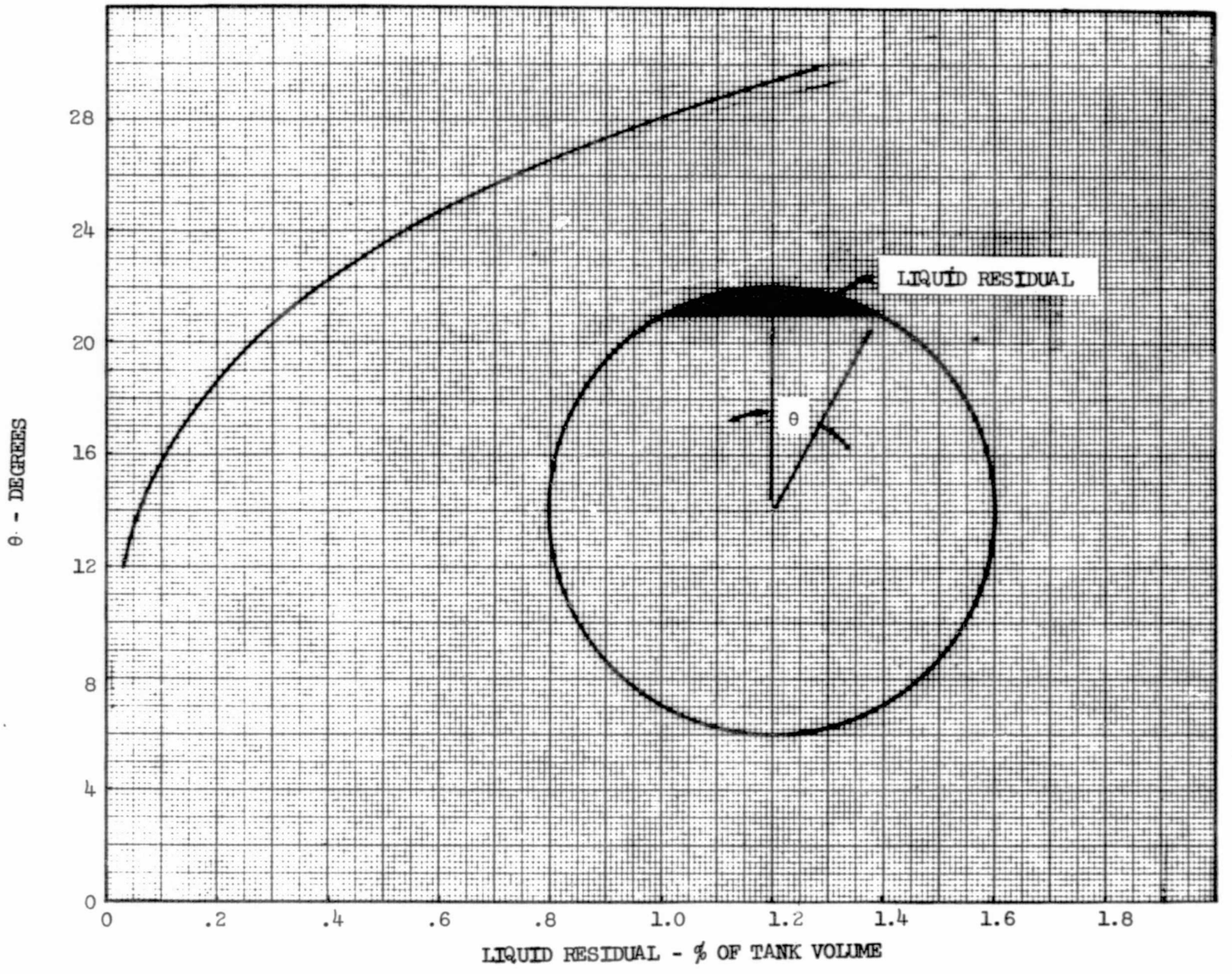


Figure 2-19. Oxidizer Tank Liquid Residual Versus Angle, θ

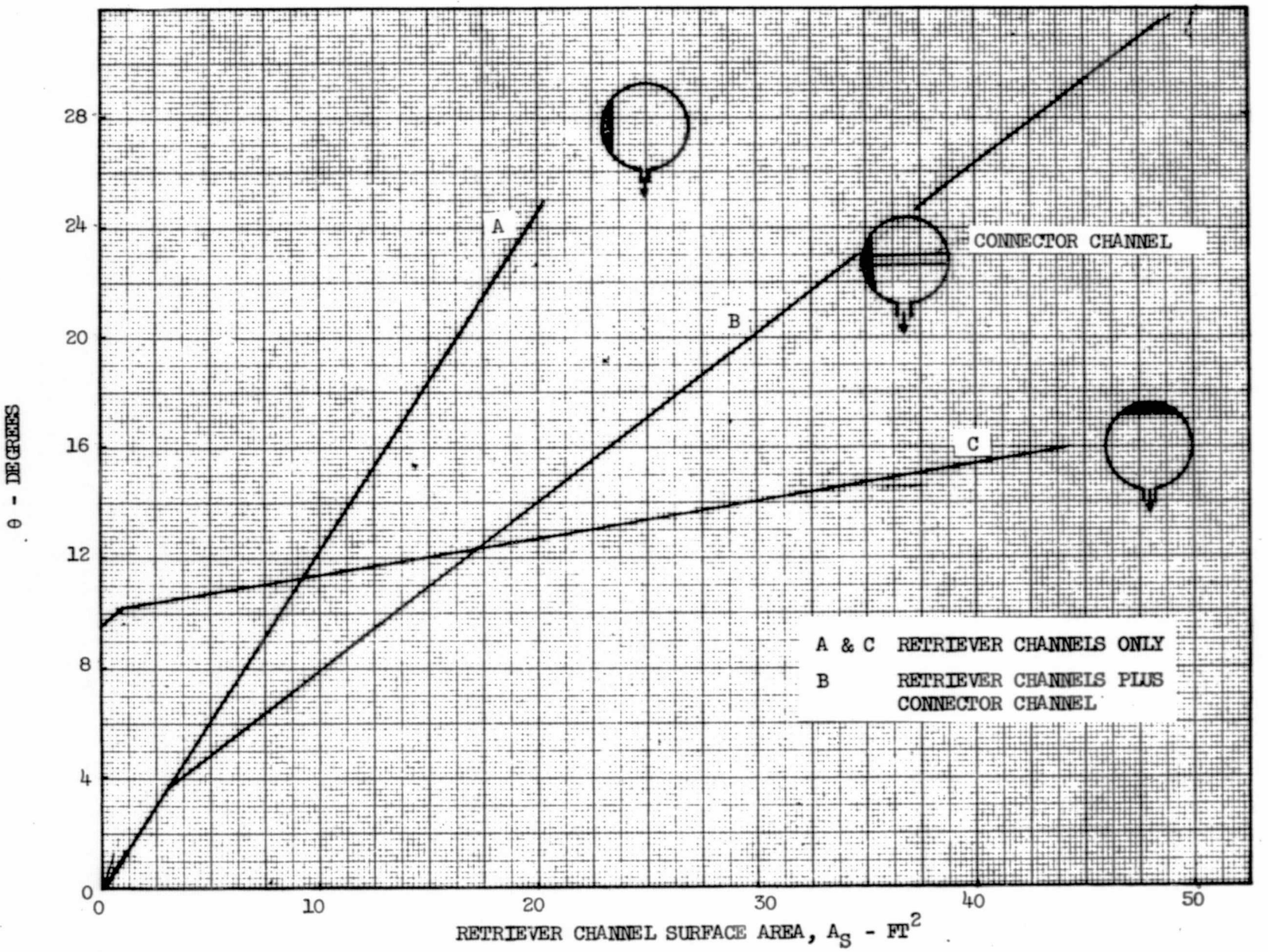
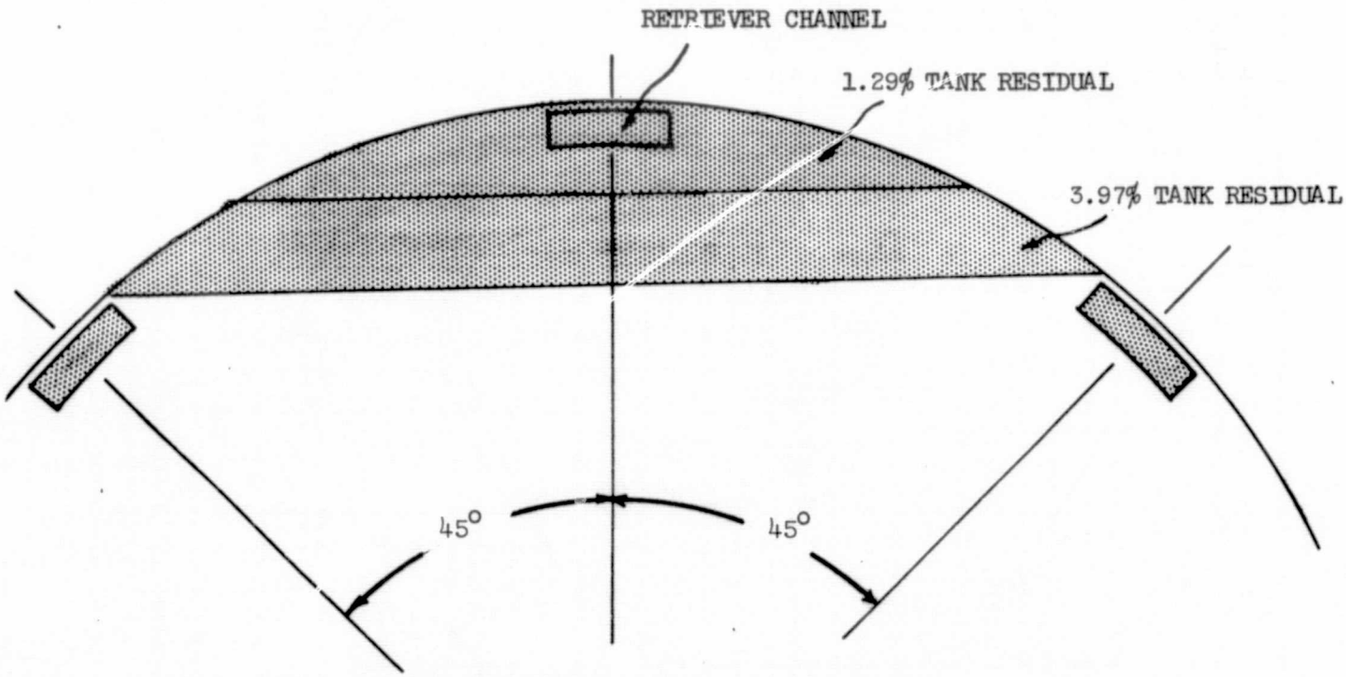
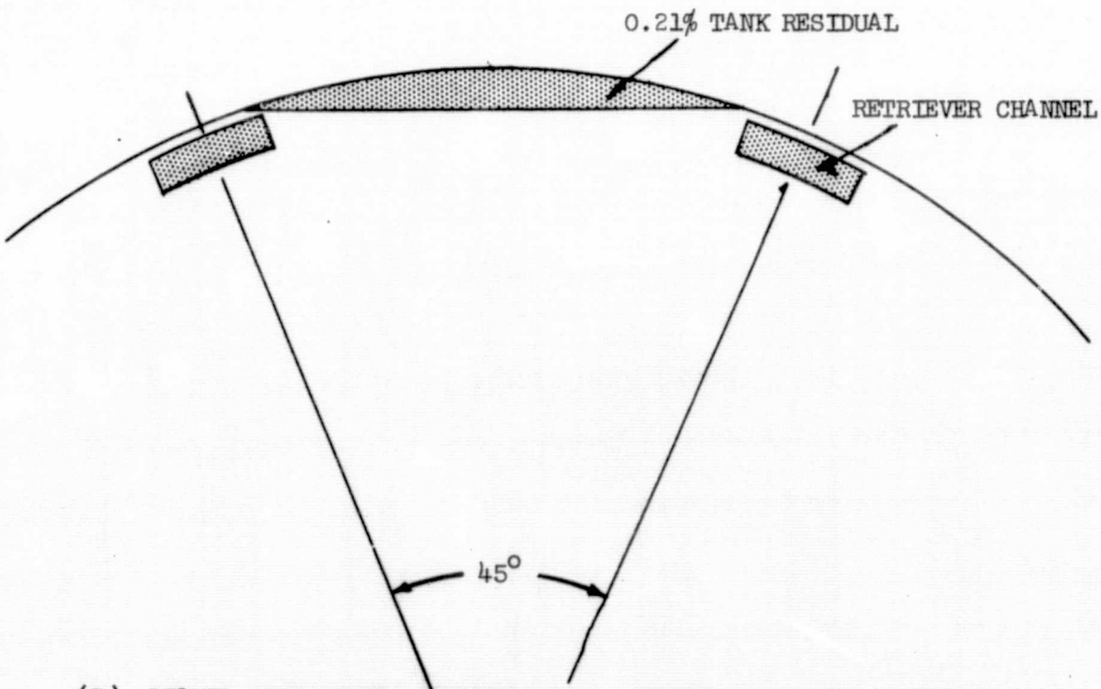


Figure 2-20. Retriever Channel Surface Area Versus Angle, θ



(A) LIQUID DISTRIBUTED SYMMETRICALLY ABOUT A RETRIEVER CHANNEL



(B) LIQUID DISTRIBUTED SYMMETRICALLY BETWEEN RETRIEVER CHANNELS

Figure 2-21. Liquid Settled at Tank Equator Due to Lateral Acceleration

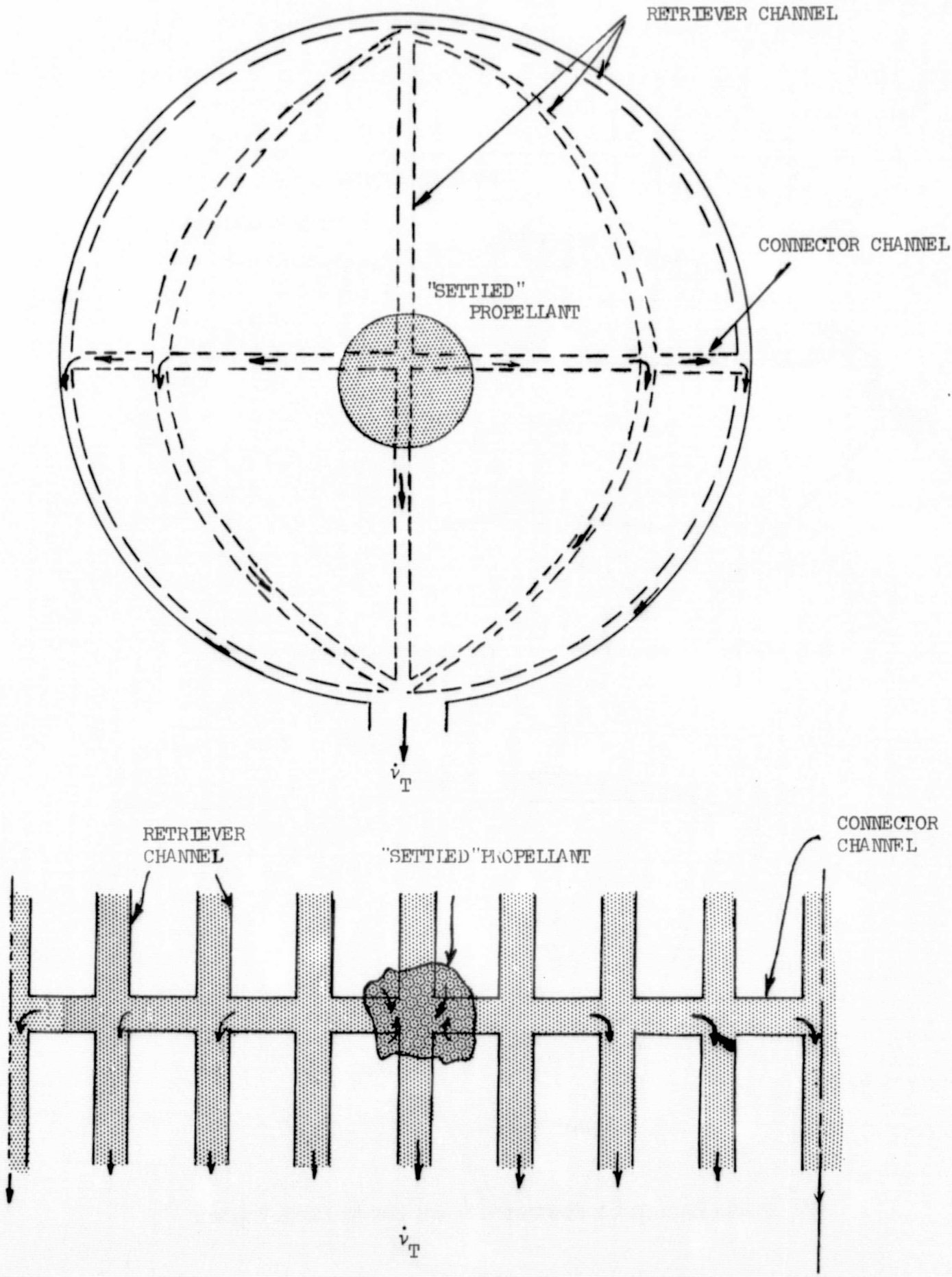


Figure 2-22. Flow Distribution Effect of Connector Channel

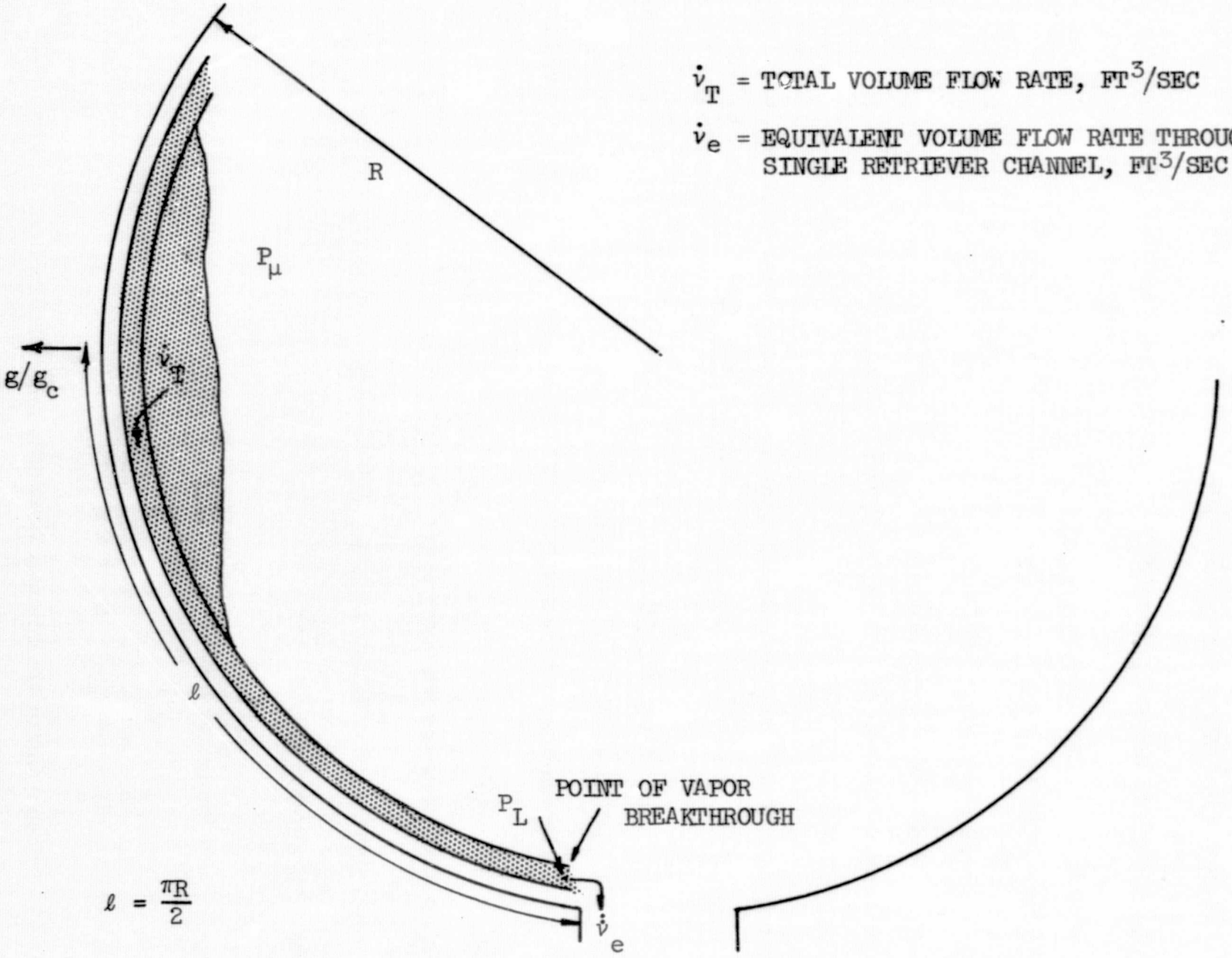


Figure 2-23. LOX Transfer Flow Model

surface tension + pressure (ΔP_σ) is overcome. Thus, whenever $P_g - P_L \geq \Delta P_\sigma$ vapor penetration will occur. It is evident from Figure 2-23 that the penetration will occur at the point where liquid enters the sump region of the tank, since this is the region of minimum liquid local static pressure. Therefore, it can be stated that liquid residuals are defined by the condition of $\Delta P_\sigma \leq \Delta P$ screen + $\Delta P_{friction}$ + $\rho \frac{V_L^2}{2g} + \rho(g/g_c)\, L$ or $\Delta P_\sigma - \rho(g/g_c)\, L \equiv \Delta P\Phi \leq \Delta P$ screen + $\Delta P_{friction}$ + ΔP channel (8)

where ΔP_σ = (surface tension pressure) = ΔP_σ = 561/34.2 psf (for LOX) (conservative)

σ = LOX surface tension, 13 dyne/cm

$\rho(g/g_c)L$ = gravity head pressure, psf

ρ = liquid density, 71 lb/ft^2

(g/g_c) = acceleration field, g's

$L = R$ = physical head of LOX above reference plane, 9.17 ft

R = tanker radius ft

ΔP screen = pressure loss due to liquid flow across screen into channel, psf

$= .5 \times 10^7 \mu \frac{t \dot{\vartheta}}{\bar{d}_\mu^2 A_s}$ (for laminar flow only, Reference 3)

μ = LOX viscosity, 0.2 cp

t = screen thickness, 0.0057 inches*

$\dot{\vartheta}_s$ = LOX volumetric flowrate through screen, cfs

$\bar{d}_\mu$ = average capillary diameter, 22.8$^*_\mu$

A_s = total wetted screen area, ft^2

φ = screen porosity (void volume/total volume), 0.346*

therefore ΔP screen = $31.7 \frac{\dot{\vartheta}_s}{A_s}$

$\Delta P_{friction}$ = frictional loss in the channel from entrance to sump, psf

$$= \frac{f\ell}{d_c} \rho \frac{V_c^2}{2g_c} = \frac{f\ell}{d_c} \frac{\rho}{2g} \left(\frac{\vartheta_c}{A_c}\right)^2$$

f = friction factor (function of Reynolds number) 0.04

$\ell = \frac{\pi R}{2}$ = length of channel, 14.4 ft

*These are measured properties of a 200 × 1400 mesh dutch twill weave sample provided by KRESSILK CORP.

$$d_c = 4 R_h = 4 \left(\frac{\text{wetted area}}{\text{wetted perimeter}}\right) = 4 A_f/(a+3b)$$

(note: R_h includes effect of two stiffeners within channel)

A_c = channel flow area, a b, ft^2

a = channel width, ft

b = channel height, ft

$\dot{\vartheta}_c$ = volumetric flow rate in channel, ft^3/sec

V_c = liquid velocity in channel, ft/sec

$$q \text{ channel} = \rho \frac{V_c^2}{2g} = \frac{\rho}{2g} \left(\frac{\dot{\vartheta}c}{A_c}\right)^2$$

Combing the above terms results in:

$$\Delta P\Phi \equiv \frac{561}{34.2} - 651 \, g/g_c = 16.4 - 651 \, g/g_c$$

$$\Delta P\Phi \leq 31.7 \frac{\dot{\vartheta}s}{A_s} + .48 \frac{(a+b)}{a\,b} \left(\frac{\dot{\vartheta}c}{A\,c}\right)^2 + 1.1 \left(\frac{\dot{\vartheta}c}{A_c}\right)^2$$

Remembering that $\dot{\vartheta}_S$ = total volume flow rate, $\dot{\vartheta}_T$, and $\dot{\vartheta}_c$ = equivalent flow rate through a single channel, $\vartheta_e = .29 \, \vartheta_T$, then

$$\Delta P\Phi \leq 31.7 \frac{\dot{\vartheta}T}{A_s} + \left[.48 \frac{(a+b)}{a\,b} + 1.1\right] (.084) \left(\frac{\dot{\vartheta}T}{A_c}\right)^2 \qquad (9)$$

Although LOX transfer will occur in a near zero gravity environment, it was assumed that a relatively large lateral acceleration of $g/g_c = 10^{-3}$ would be imposed near the termination of transfer. System design for this environment would assure conservatism and provide confidence that an unexpected acceleration of this magnitude, or lower, would not adversely affect performance. Finally, the inception of vapor penetration is defined as:

$$\Delta P\Phi = 16.4 - .65 = 15.75 = 31.7 \left(\frac{\dot{\vartheta}T}{A_s}\right) + \left[.48 \frac{(a+b)}{a\,b} + 1.1\right] (.084) \left(\frac{\dot{\vartheta}T}{A_c}\right)^2$$

where $g/g_c = 10^{-3}$ has been introduced.

Use of this expression provides A_s, and therefore liquid residuals outside the channels, as a function of $\dot{\vartheta}_T$ and A_c. Figure 2-24 provides these pool residuals, Δm_p, for a range of $\dot{\vartheta}_T$ and A_c. Because Δm_p is a function of flow channel depth and width and not flow area alone, these variables are included in Figure 2-25.

It should be mentioned that A_s, the total screen area, represents the total surface area of the retriever and collector channels. The actual surface area available for the passage of flow is less than A_s because approximately 40% of the sides (depth) and bottom (width) of the channels is solid for structural requirements. Only the top (or the inside width) of the channels is completely open to flow.

Total tank mass residuals include not only pool residuals, but liquid trapped within the channel, Δm_c. That is, the liquid contained within the retriever channels and connector channel is unusable because once vapor penetrates the channels under a near zero gravity environment flow must be terminated in order to prevent vapor flow to the receiver tank. The channel residuals, Δm_c, are of course a function of geometry only. These residuals are indicated by the dashed curves of Figure 2-25. The solid lines represent the total liquid residual, $\Delta m_c + \Delta m_p$; which are based on a 14 inch wide channel only. Care must be taken not to select a marginal system because small changes in dimensions could greatly increase pool residuals. For example, as channel depth is reduced from 1.5 to 1.4 inches for a fixed flow rate of 53 lb/sec there is a substantial increase in total residuals.

Although a channel geometry of 1.4" × 14.0" was selected as the design point and weighed out (Section 2.2), Figure 2-25 shows that the channel depth should be approximately 1.5 inches rather than 1.4 inches. This choice would result in a minimum residual of 2720 lb at 53 lb/sec. If it is required to transfer LOX at 60 lb/sec, then a minimum total residual of 2960 lb would occur for a channel depth of 1.61 inches. Since a reduce channel flow area will also reduce Δm_c, it would seem that this would provide a more optimum channel selection. Figure 2-26, however, illustrates that the LOX transfer flow rate would greatly be reduced. Thus, transfer flow rate and, therefore, the time to complete propellant transfer would be sacrificed for a further reduction in propellant residual.

It is estimated that liquid residual can be reduced to an absolute minimum of approximately 1800 lb. This will require an average screen rating of 10 μ, which is a practical lower limit on screen capability. The increased surface tension pressure capability will permit use of a channel cross-section selection of 1.0" × 14.0". To

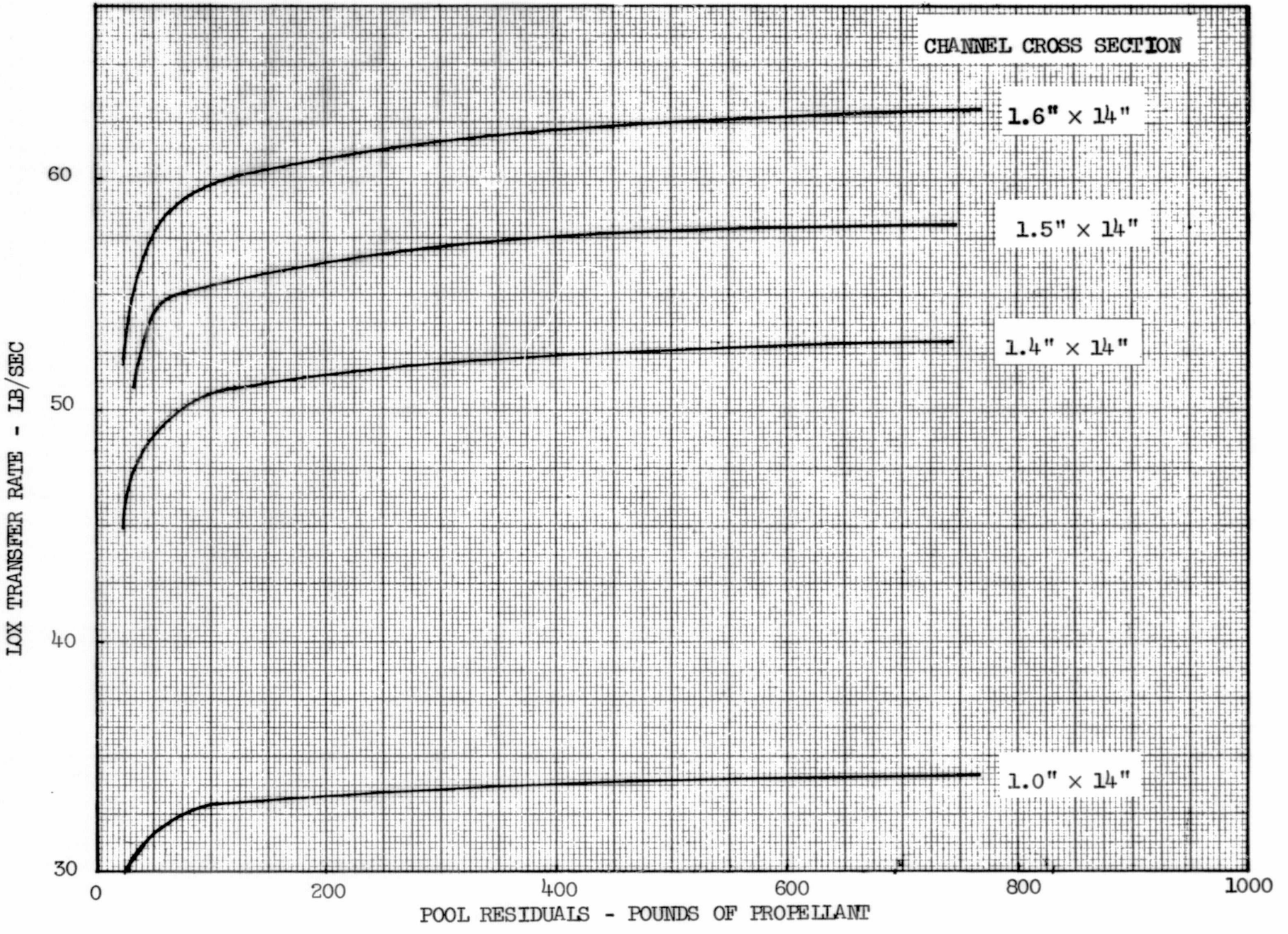


Figure 2-24. LOX Tanker Pool Residuals Versus Transfer Rate

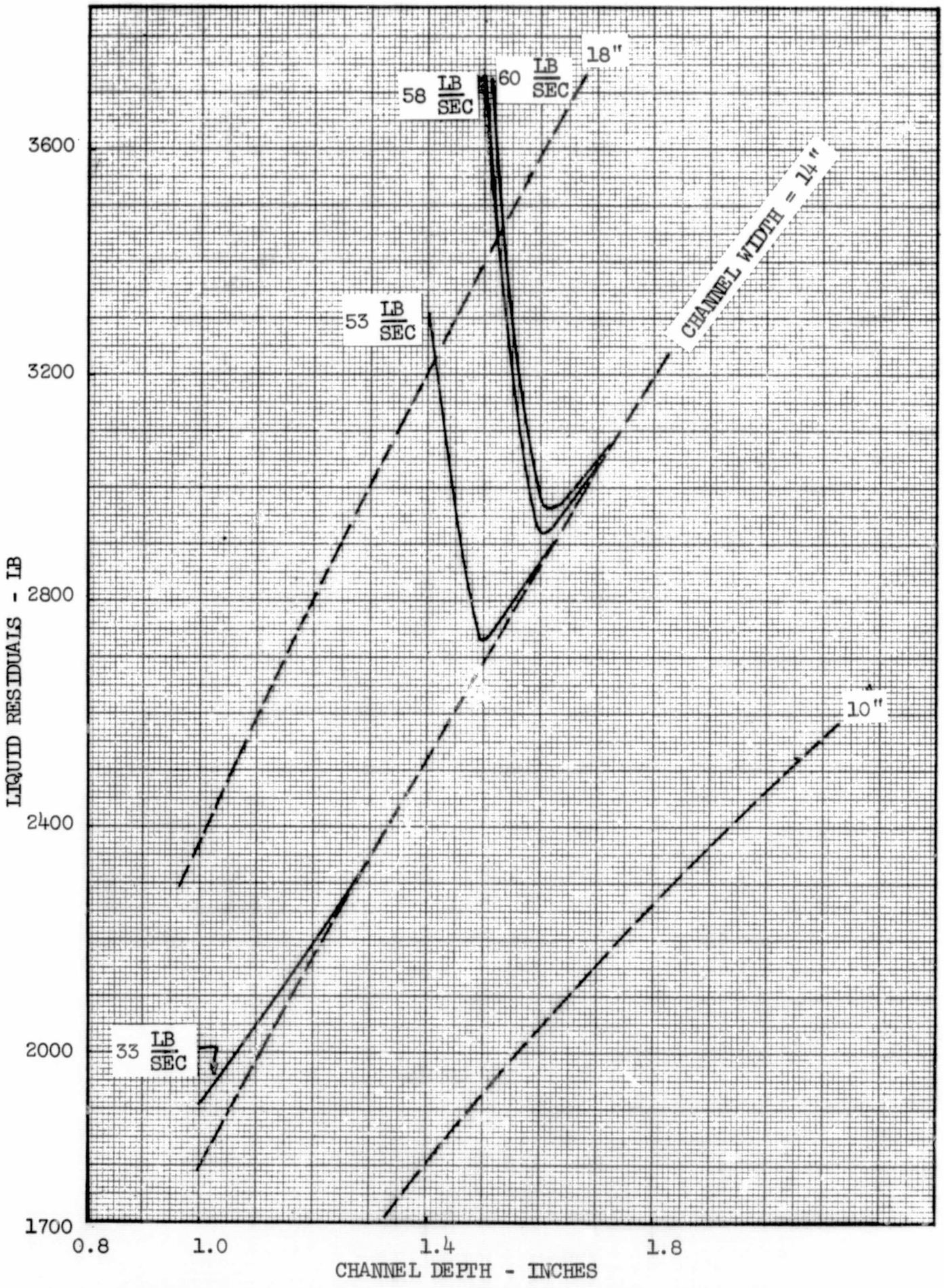


Figure 2-25. Total LOX Tanker Liquid Residuals Versus Channel Geometry and LOX Flow Rate

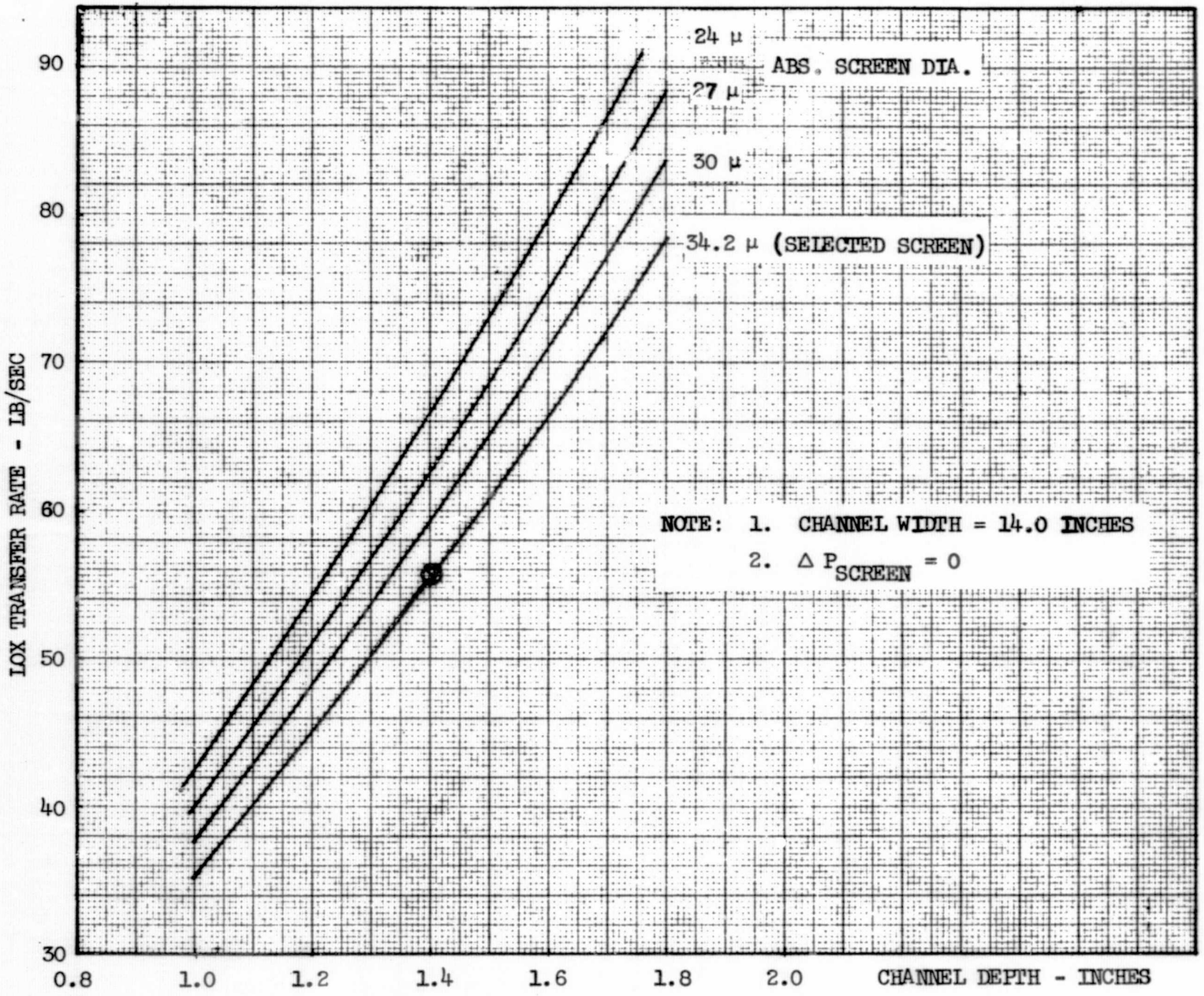


Figure 2-26. Effect of Retriever Channel Screen Diameter and Channel Depth on Allowable LOX Transfer Rate

further reduce liquid residuals will require a means of scavenging liquid prior to termination of propellant transfer. Lockheed, Reference 2, has studied this technique and found that liquid residuals can be reduced from approximately 2750 lb to 33 lb.

Propellant scavenging is accomplished by accelerating the LOX tanker prior to the termination of LOX transfer. A positive acceleration will bottom the propellants over the tank outlet. This condition will decrease the pool residual below those values reported in Figure 2-24, because of a reduction in channel flow path for the draining liquid. More important, the positive acceleration will permit a majority of the liquid to drain from within the flow channels before vapor is transferred to the receiver tank. Under these conditions vapor will penetrate the channels at the forward end of the tank and not be entrained in the liquid. An acceleration level of 10^{-4} to 10^{-3} g's will be required to insure efficient scavenging.

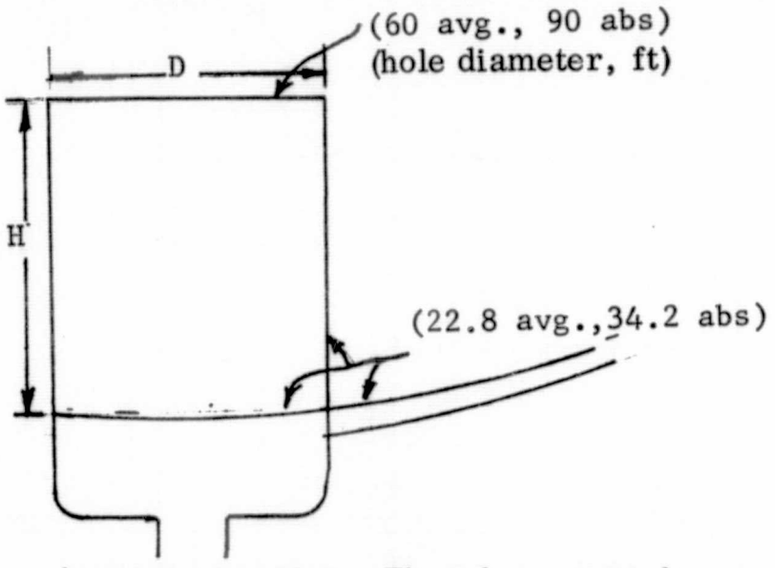
System Philosophy

The principle guideline for the design of a surface tension device was that heat transfer effects should be minimized. This was the overriding concern because (1) it is generally accepted that a screened device can be successfully applied to room temperature fluids, and (2) the major differences between a device for room temperature fluids versus one for cryogens are the heat transfer aspects that must be overcome. Consequently, it was believed that a device consisting of individual flow channels would present fewer heat transfer problems than would a spherical screened shell within the LOX tanker. The reason for this assertion is that all heat input to a tank containing a spherical screen will be absorbed by liquid between the screen and tank surface. Thus, the total heat input to the tank represents a potential threat to the satisfactory performance of a screened device. By designing a device of individual flow channels, however, it is possible to substantially reduce heat input to the contained fluid. A detailed heat transfer analysis of this system is given in Section 2.2.

The retriever channel device does have a shortcoming relative to the screened liner concept. It does not provide the absolute guarantee that liquid communication will be maintained across the channel screens. Because the screened liner completely encapsulates the tank contents, liquid contact with the liner is guaranteed, unless it is temporarily suspended in the ullage as a result of a perturbation. The retriever channels, on the other hand, cover 28.6% of the tank surface (for a 14-inch wide channel). Consequently, it might be possible to postulate a situation where liquid contact with the channel screens would be broken. Such an occurrance would be temporary and would not be expected to affect propellant transfer.

The cylindrical reservoir over the tank outlet has been selected as a means of minimizing premature vapor ingestion into the channels. The 4 ft. dia. by 5 ft. high reservoir will have available approximately 63 ft^3 of liquid for propellant transfer in

the event that the retriever channels break communications with the tank propellants. It is hoped that the liquid reserve will supply propellants until communications with the retriever channels is again established. The reservoir operation is as follows:



1. While tank propellants remain in contact with the channel screen or reservoir screen an uninterrupted flow of liquid will exist.
2. If the tank propellants become temporarily suspended in the ullage, vapor will penetrate the screen as LOX transfer continues.
3. The sketch shows that the top screen of the reservoir has the largest pore size. Therefore, initial vapor penetration will occur through the cylinder as liquid drains overboard.
4. Approximately 75 seconds of propellant transfer at 60 lb/sec is available from the reservoir. The entire volume of liquid can be expelled once vapor penetrates, or it can be apportioned by installing horizontal screens across the reservoir at the desired volumes (liquid expulsion will only terminate at a horizontal screen if communication has been re-established between propellants and the retriever channels).

2.2 THERMAL ANALYSIS

To successfully separate the liquid and vapor phases of a cryogenic propellant with a surface tension screen device, it is necessary to assure that boiling takes place only in the volume which has been reserved for vapor. This can be attempted by passively or actively cooling the volume where pure liquid is desired. Initial attempts were made to passively cool the capillary devices using low conductive supports and the latent heat of the liquid outside the capillary device. A thorough investigation of this problem led to the conclusion that, since nucleate boiling can occur at very low ΔT's, vapor formation within the capillary devices could not be completely assured unless an active cooling system was employed. Active cooling was explored using the cooling capacity of a thermodynamic vent system to prevent vapor formation. The feasibility of this type of cooling system was established with preliminary calculations for both the S-IVC and LO_2 tanker applications.

2.2.1 S-IVC THERMAL ANALYSIS. The S-IVC capillary restart device was initially supported at the tank wall by several pins designed to prevent boiling at the screen (Figure 2-27). Investigation of the phenomenon of vapor formation near the pins has revealed the importance of accurately establishing the nucleate boiling incipient point.

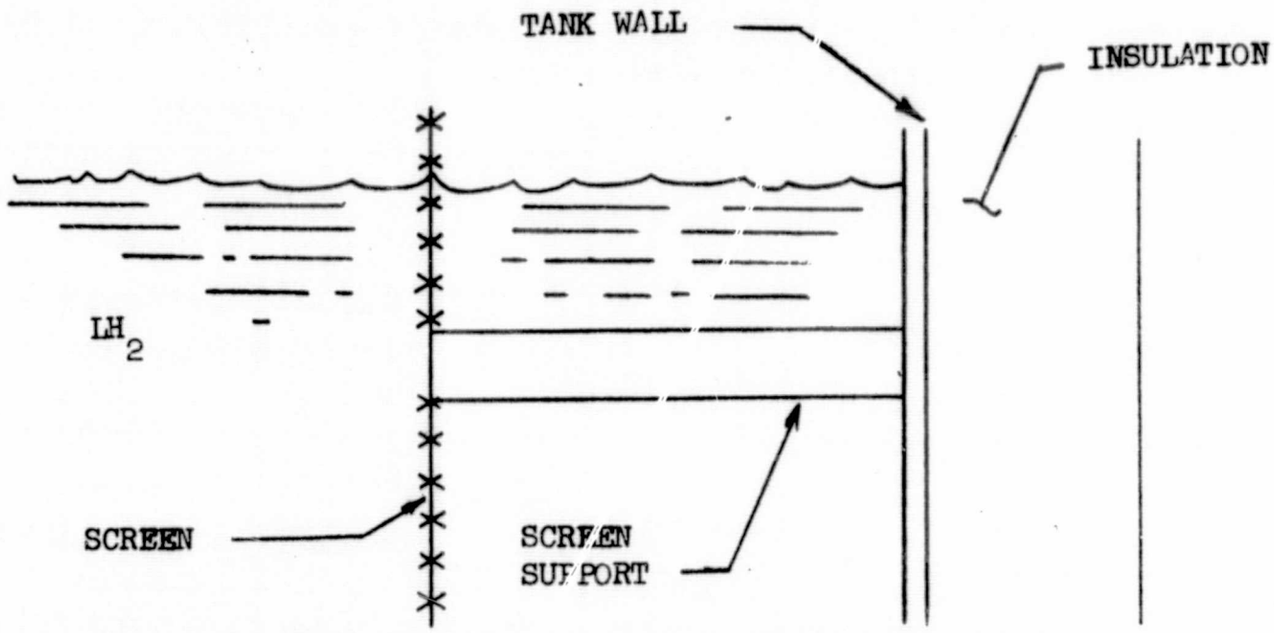


Figure 2-27. Typical Screen Support

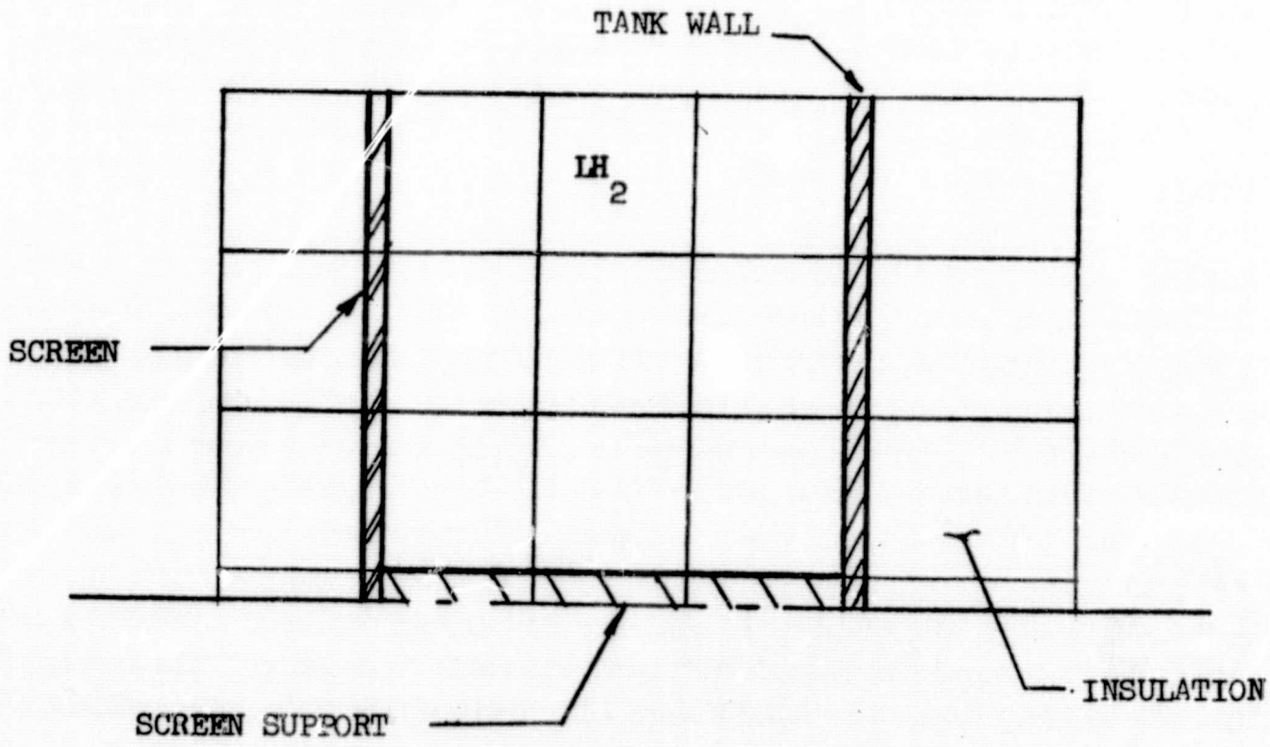


Figure 2-28. Thermal Model for Boiling at Screen Support

For S-IVC orbital heat input, the heat flux available for boiling is on the order of 0.1 Btu/hr-ft^2 at the cylindrical tank walls. This corresponds to a wall superheat of about 0.04°R. Experimentally determined nucleate boiling incipient points for hydrogen at 1 g appear to range from 0.01°R to 2.5°R superheat.

Two concepts of the relationship between the gravity field and incipient point are:

1. Nucleate boiling begins when free convectional heat flux at a given ΔT is no longer greater than boiling heat flux at the same ΔT.
2. The initiation of boiling is not a function of gravity.

If the incipient point is not a function of gravity, then very likely no vapor will form at the wall or at the screen. Heat will be carried away by free convection and vaporization will occur at the vapor-liquid interface.

If the incipient point decreases with gravity, then possibly with the assistance of artificial nucleation sites, vapor may form at the tank wall and pin surfaces. The screens, however, are likely to harbor nucleation sites which will cause vapor to also form at the wall.

If vapor forms at the tank wall and pin surfaces so that these areas are blanketed, increased heat will flow through the pin and since the area of the pin face is small, heat flux may be sufficient to cause boiling. Maintenance of wetted walls and pin surfaces therefore, is desirable to reduce the probability of boiling at the screen. Lengthening the pins to reduce heat flux at the pin face is one method of overcoming the drying out of wall surfaces.

Work continued on pin design to keep the ΔT at the screen below the incipient point until the conclusion was finally reached that even the very low ΔT's which might occur could cause boiling at the screen surface. It was thus decided to utilize the cooling capacity of a thermodynamic vent system to prevent vapor formation within the capillary device.

Several configurations have been considered, each of which contains: a throttling device to lower the temperature of the vent fluid, a heat exchanger to transfer heat from the tank fluid and start basket to the vent fluid, and a mixer to improve hot side heat transfer and provide sufficient liquid circulation to cool the ullage. The venting process is represented by the T-S diagram shown below.

The thermodynamic vent device inlet will be designed to always be in liquid. This is required since gas at the inlet will severely reduce the cooling capacity of the vent fluid to the point where all the heat incident on the start basket cannot be

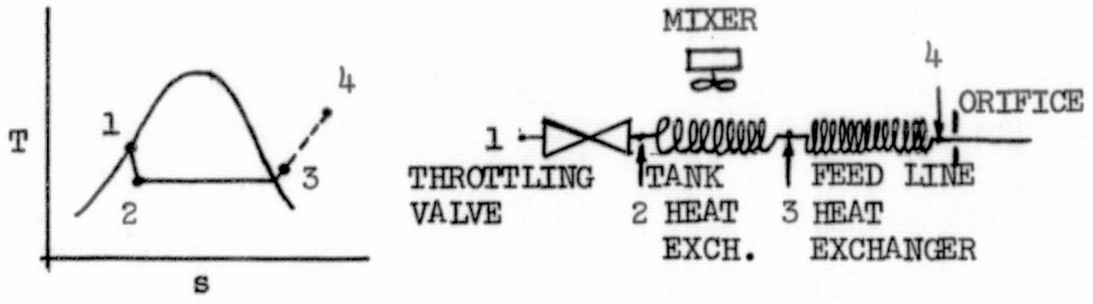


Figure 2-29. Thermodynamic Vent Device

intercepted by the heat exchanger coils. A schematic of the thermal conditioning system is shown in Figure 2-30. Heat exchanger coils will be wrapped around the outside of the start basket to assure that no vapor is formed within it. Mixer flow will heat the vent fluid from the outside of the start basket, while conduction on the inside of the basket will tend to heat the vent fluid and subcool the start basket fluid. The engine feed line is then coiled with tubing to keep vapor from forming there. Tubing is then wrapped around the tank to provide maximum cooling efficiency of the vented hydrogen. The LOX tank is then coiled with the GH_2 heat exchanger tubing around the start basket and feed line area to eliminate formation of oxygen vapor. Local overcooling of the tank wall is a possibility however. Thoroughly mixing S-IVC LOX tank contents should prevent solid oxygen from forming inside the tank.

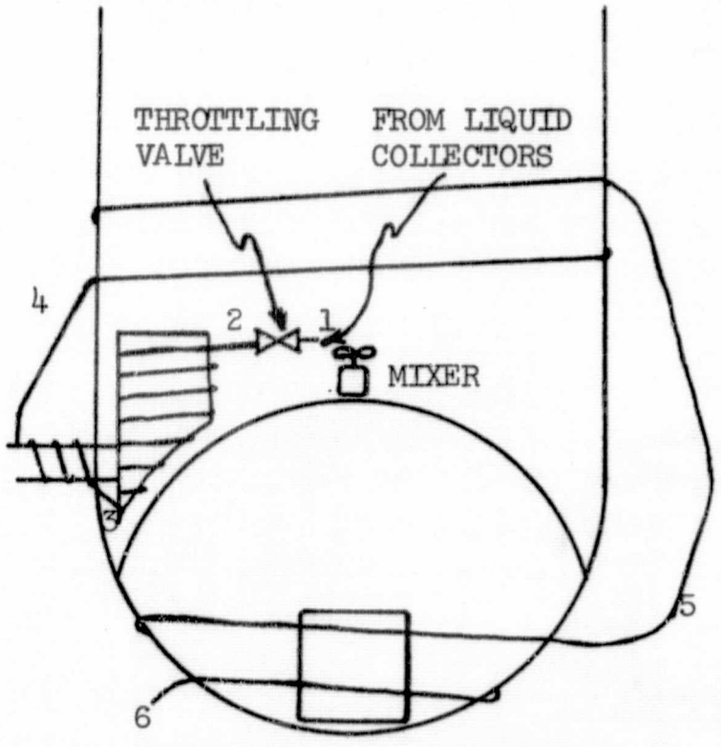


Figure 2-30. Schematic of S-IVC Heat Exchanger Vent System

Heat exchanger sizing for start basket cooling and tank pressure venting is based on the basic first law relationship of Reference 4.

$$\dot{m}_v = \left[\frac{q + P}{h_2 + e\lambda/(1 - e) - h_L} \right]_{P_T = C} \tag{10}$$

where:

$\dot{m}_v$ is the vent flow rate

h_2 is the exit enthalpy

h_L is the liquid enthalpy

e is the vapor density/liquid density

λ is the heat of vaporization

q is the heat input

P is any power input

The basic sizing problem is to assure that for a given flow rate, the desired exit enthalpy of equation 1 is attained. This equation must be satisfied in addition to $\dot{m}_V = q_e/(h_o - h_2)$ where q_e is the engine feed line heating and h_o is the exit enthalpy of the vent fluid after cooling the feed line. This creates a possible sensitive matching of heat transfer coefficients unless some valving and bypass heat exchanger tubing is added to the system.

For the cold side of the tube, heat transfer in a vaporizing two-phase fluid flowing in a tube is computed by considering the process to consist of three phases (x indicates quality - % vapor):

1. nucleate boiling, $0 \leq x \leq 0.90$
2. fully developed turbulent flow at constant temperature (saturation) $0.90 < x \leq 1.0$.
3. fully developed turbulent gas flow with increasing temperature $T > T_{SAT}$.

A computer program has been written to facilitate calculation of heat exchanger design parameters. Input data are: fluid properties, exterior heat transfer coefficients, tube geometry, and inlet conditions. The program yields the following information: tube length for each heat transfer region, pressure drop, and temperatures. If desired, a tube length can be input and the program will compute fluid properties at the end of the tube.

Heat transfer coefficients on the outside of the tube can take on a wide range of values depending on the external fluid conditions. Because the inside coefficients are so high the tube design is controlled by the exterior coefficients. Some of the possible fluid conditions and resulting external heat transfer coefficient ranges are:

1. liquid free convection, $0.1 < h < 1.0$ Btu/hr-ft^2-°F
2. liquid forced convection, $1.0 < h < 100$ Btu/hr-ft^2-°F
3. film condensation with free vapor convection, $0.1 < h < 1.0$ Btu/hr-ft^2-°F
4. film condensation with forced vapor convection, $1.0 < h < 100$ Btu/hr-ft^2-°F

Tube lengths required to provide the desired exit enthalpy have been computed for the low range of exterior heat transfer coefficient and are excessively long. In order to provide forced convection heat transfer coefficients, rather than free convection at low-g, mixing can be utilized. Small flow velocities will produce considerable increase in external heat transfer coefficients.

In a complicated tank configuration the strength and direction of circulation currents are very difficult to predict.

The main objective which must be met by a circulation system is to minimize temperature stratification. Location, quality and size of fans or pumps to accomplish this objective will be determined in Phase II.

A major source for heat input to the S-IVC LH_2 tank is the engine feed line and elbow. This line, whether liquid filled or dry, is connected to a heat source from which it cannot be effectively insulated. The central problems are how to best remove the heat introduced into the tank from the feed line and how to ensure that the propellant feed system will function properly when called upon.

Initially, the feed line will be wet, and any subsequent evaporation of the contained liquid may cause expulsion of a volume of liquid approximately 240 times the volume of liquid evaporated. It is thus essential to either eliminate evaporation completely or to provide a vent for the evaporated fluid. Elimination of vaporization entirely requires removal of all incident heat, part of which is radiation from the warm end of the tube. Radiation, unlike convection and conduction cannot be taken out at the warm end because it can penetrate the liquid. A cooled optical baffle could be used at the warm end of the pipe, but since heat is continuously entering the liquid through the insulation on the pipe, some cooling over the entire surface will be necessary.

Heat to be removed from the propellant feed line is tabulated below, assuming that a four-inch gap exists between the heat source and the liquid/vapor interface.

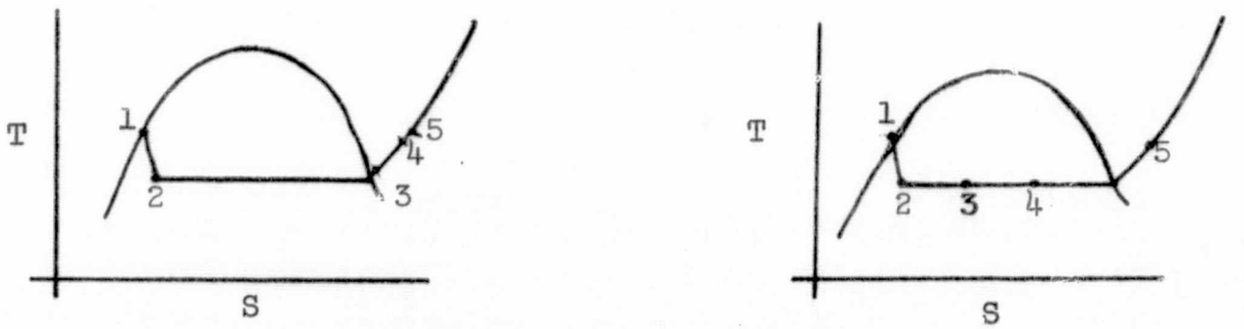
Radiation	24.5 Btu/hr
Gas Conduction	25.7 Btu/hr
Metal Conduction	45.2 Btu/hr
Insulation Heat Leak	5.3 Btu/hr

Heat from gas conduction and metal conduction can be removed at the warm end of the pipe by heat exchanger coils wrapped on the outside of the pipe under the insulation. The remaining 30 Btu/hr can be removed over the entire pipe surface by heat exchanger tubes, coiled on the outside surface of the pipe, under the insulation.

For the S-IVC LO_2 tank the heat transfer coefficient in the vent tube will be in the fully developed turbulent flow regime. Tubes are wrapped around the tank near the start basket area. Heat transfer coefficients inside the tank must be determined from mixing correlations and test data.

In order to assure effective operation of the S-IVC thermodynamic vent device cooling system, it is necessary to provide safeguards for system operation. For example, heat transfer coefficients on the hot side of the start basket cooling system will differ depending upon whether gas or liquid surrounds the start basket. If the system is sized for condensing gas surrounding the start basket, steady state heat transfer rates will be low compared to forced convection within the liquid. Thus, a relatively long heat exchanger will be required to control tank pressure. If, by chance, liquid is present outside the start basket, greater heat transfer rates will be present and the cooling capacity of the fluid inside the cooling coils will be used up without cooling the engine feed line.

Designing the system for liquid around the start basket allows a shorter heat exchanger length to be used. If gas is present, less heat will be removed around the start basket and additional cooling coils must be provided for the fluid coming out of the engine feed line area. The feed line tubing must be sized for the liquid inlet case since cooling fluid will then be at a higher inlet enthalpy. The possible state conditions present are illustrated in the T-s diagram shown below in Figure 2-31. State numbers correspond to locations shown in Figure 2-30.



A) LIQUID SURROUNDING THE START BASKET

B) VAPOR SURROUNDING THE START BASKET

Figure 2-31. Thermodynamic Performance of Figure 2-30 Configuration

Another configuration which may have some advantages is shown in Figure 2-32. In this case the vent fluid removes only enough heat from the start basket region so that no vapor is formed within it. The vent fluid then cools the feed line and is brought back to the tank to a thermodynamic vent system complete with mixer, which is sized to control tank pressure. Start basket coils would be sized for all gas

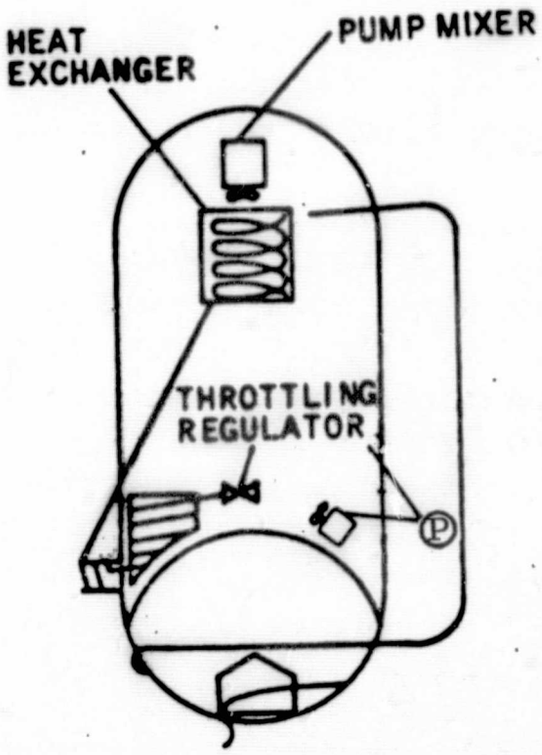


Figure 2-32. Schematic of Alternate S-IVC Heat Exchanger Vent System

surrounding the start basket. Engine feed line coils would be sized for all liquid surrounding the start basket. This system is very similar to the one proposed in Figure 2-30, however, it will be easier to fabricate the start basket with less cooling coils. This system is also less sensitive to start basket heat transfer coefficients in cooling the engine feed line.

One drawback may occur due to the sensitivity of external heat transfer coefficients to small flow velocities. In order to keep the tank fully mixed with the mixer of Figure 2-32, it is possible that high heat transfer coefficients resulting at the start basket will cause all the heat into the tank to be removed for the heat exchanger length required to produce a given degree of subcooling. Several possibilities exist to obviate this condition. A lower degree of subcooling may be one solution. Another is to size one mixer for providing high heat transfer coefficients to the thermodynamic separator and another mixer to operate intermittently and destratify the tank. During the stratification and destratification period, high heating rates may develop on the start basket causing vapor to form within it.

Both systems appear feasible and will be examined in more detail during Phase II of the program.

2.2.2 LOX TANKER THERMAL ANALYSIS. To prevent vapor formation in the liquid oxygen collection channels a heat exchange system was designed to intercept

incident heating. Oxygen vented from the tanker is the heat exchanger medium and can be ducted through the collector channels as shown in Figure 2-32 or as in Figure 2-33.

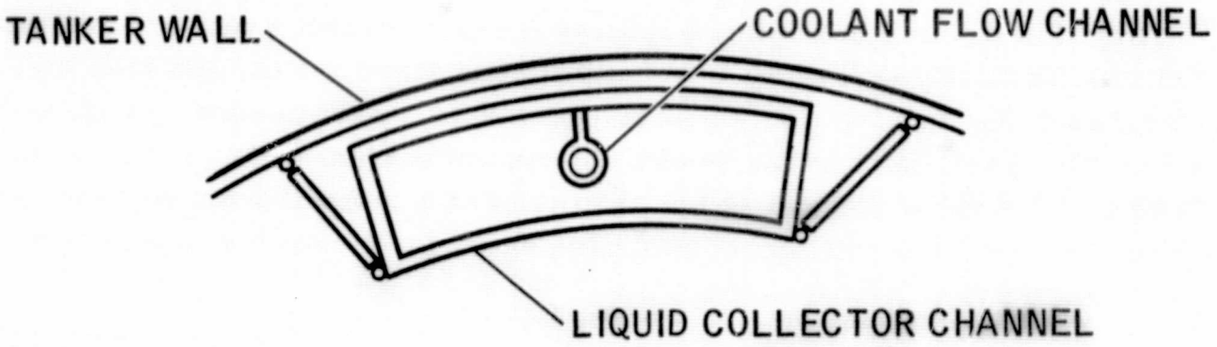


Figure 2-33. LOX Tanker Cooling With Cooling Channels Inside the Collector Channels

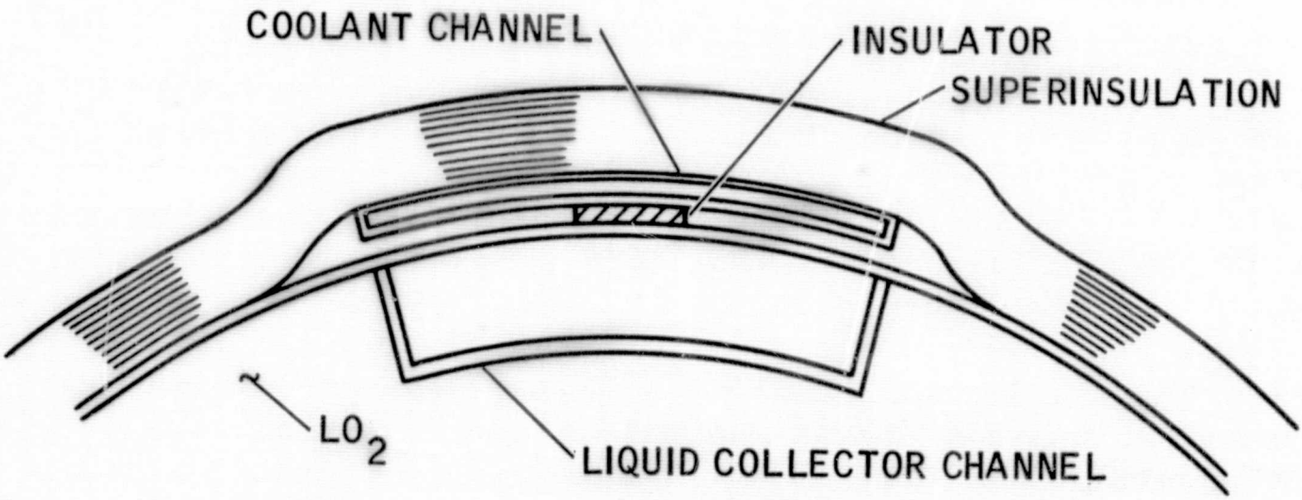


Figure 2-34. LOX Tanker Cooling With Coolant Channels Outside the Tank Wall

Venting oxygen is bled from the tanker through an expansion valve where it is lowered in temperature; the resulting temperature loss is the ΔT available for heat transfer. The available flow rate is determined by requiring that the tank pressure remain constant. If all of the heat added to the venting fluid comes either directly or indirectly from the tank liquid, then equation 10 can be used to relate the flow rate to the exit enthalpy for constant pressure venting.

Either liquid or vapor can be introduced into the vent system, but after consulting a T-S diagram for oxygen one sees that the heat capacity of vented vapor is insufficient to remove a significant fraction of the incident heat rate. Liquid, therefore, is

drawn from the tank and circulated through the heat exchanger tubing where it rises in enthalpy to h_{exit}. Values of $\dot{m}_v$ computed from (10) are shown in Figure 2-35.

Expanding the vent liquid to low pressures provides a small ΔP for flow through the tubes, and results in a large ΔT (in the boiling region) for heat transfer from the saturated tank fluid. By expanding to pressures only slightly less than tank pressure, the ΔP for flow in the tubes is increased and the ΔT for heat transfer is reduced. The Δh available for energy absorption is only slightly decreased, however, because the sensible heat of the vapor at these temperatures is only a small fraction of the heat of vaporization. Also the enthalpy of saturated vapor is insensitive to pressure in the range considered.

A balance in energy exchange rates is sought whereby the expanded vent fluid absorbs enough energy to prevent vaporization in the collector channels and can be exhausted from the O_2 tanker at the flow rate and exit enthalpy which results in constant tank pressure.

A mixer is required within the tank to assure a homogeneous thermodynamic condition within the tank.

Any heat incident on the tank skin must be removed if a possibility exists that it will enter the collector channel. After the initial chilldown period all of the collected liquid will have reached steady state at temperatures at or below saturation. The The channel thus becomes a heat sink and the heat exchanger must remove (a) heat incident on the tank skin, and (b) heat convected to the collector channel by the liquid propellant.

During the 690 hour coast period at least seven of the eight channels will be wetted. For this reason and because liquid oxygen has less heat transfer resistance than vapor, the heat exchanger load is computed for wetted conditions.

Each liquid collection channel occupies 14 inches of tank circumference and is 1.4 inches deep. The heat exchanger duct length in which boiling heat transfer occurs is determined by

$$L = \frac{\dot{\omega}\,\lambda}{(8)\,Q/L}$$

where

$\dot{\omega}$ = total vent rate

λ = Δh between the expanded quality and 0.9

Q/L = heat input to heat exchanger duct per unit length

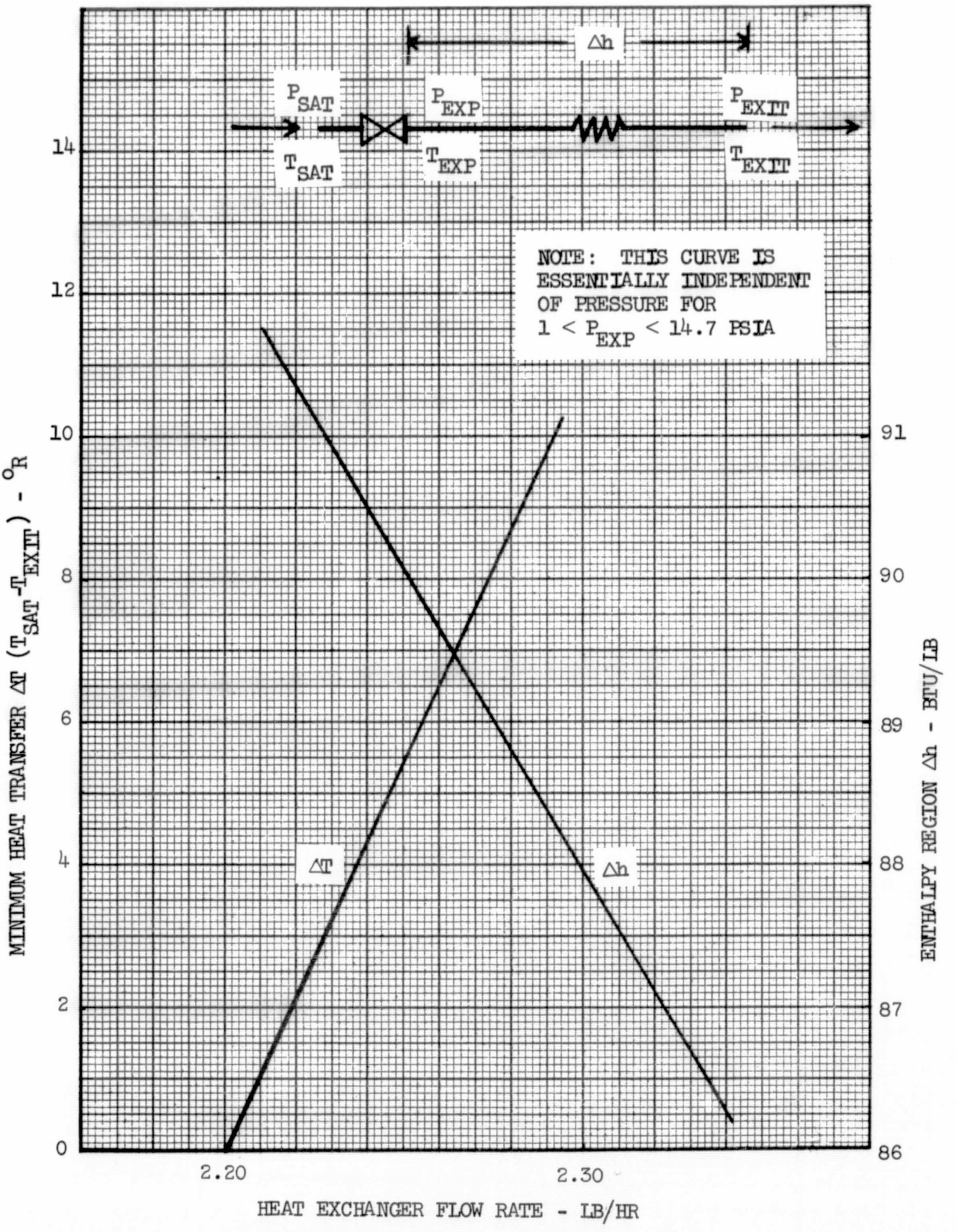


Figure 2-35. O_2 Tanker Vent Flow Rate Required for Constant Tank Pressure

The flow rate is divided by eight because one eighth of the vented propellant is used to cool each channel.

Two thermal models of collector channels (Figures 2-33 and 2-34) were set up and conditions were varied so that the heat exchange fluid would remain a two-phase mixture over most of the tube length. Since only a small fraction of the total h available is derived from sensible heat changes, the portion of heat exchanger length where the quality is greater than 0.9 should also be small.

Heat exchanger duct locations, shapes and surface areas were adjusted and the two phase fluid temperature was altered by the expansion pressure until heat transfer into the tube was approximately correct.

To meet these conditions the liquid should be expanded to a temperature of 158-162°R and the heat exchanger tube should be located either in the center of the collector duct with minimum surface area or on the outside of the tank. Lower fluid temperatures or higher surface areas result in excessively rapid vaporization of the heat exchanger fluid.

In addition to the tubing used to cool the channels some additional tubing may be placed either around the tank wall or within the tank near the reservoir depending upon the design utilized. This assures that the maximum use is being made of vented oxygen. The cooling flow is split into eight parts.

The model of Figure 2-33 requires some subcooling of the collected liquid in order to remove all the heat entering the collector channel from the outside. To avoid extracting an excessive amount of heat from the tank liquid, however, the collected liquid must remain quite close to the saturation temperature.

Figure 2-34 shows another design approach where the cooling channel is installed on the outside of the tank under the insulation and with a conduction resistance between the heat exchanger duct and the tank wall. By establishing the thickness and material of the spacer, heat from the tank into the duct can be regulated.

Several points worth considering are: The outside heat exchanger permits the liquid collection channel to be fastened to the tank wall with no supports using the tank wall as the fourth side of the channel. This method would minimize liquid transfer residuals. The 1.4" × 14" channels must then be increased in size corresponding to the flow area removed by using the tank wall as a collector wall. With the exterior heat exchanger insulator pads are required and the envelope of the tank is increased.

Cooling the LO_2 tanker, although considerably more difficult than the S-IVC LO_2 and LH_2 tanks because of the larger capillary device area, appears to be possible for the mission conditions under consideration. More detailed calculations in Phase II will verify these conclusions.

Evaporative Effects on Screen Liquid Retention

Tests were conducted using pentane with square weave and dutch twill screens to examine the influence of vaporization on the stability of the liquid vapor interface at a capillary barrier. Tests indicated that evaporation of liquid from the surface of a screen did not cause immediate drying out and retentive failure, but was accompanied by a wetting film closing about the ejected vapor. Dutch twill screens, due to their wicking properties, exhibited greater resistance to drying out than non-wicking square weave screens and are thus recommended for cryogenic capillary devices.

Bench tests with room temperature fluids were designed to evaluate the effect of evaporation on the liquid retention capability of screens. The flight condition of interest is that which occurs when liquid contained within a screened device is heated during constant tank pressure venting. The sketches below indicate a potentially

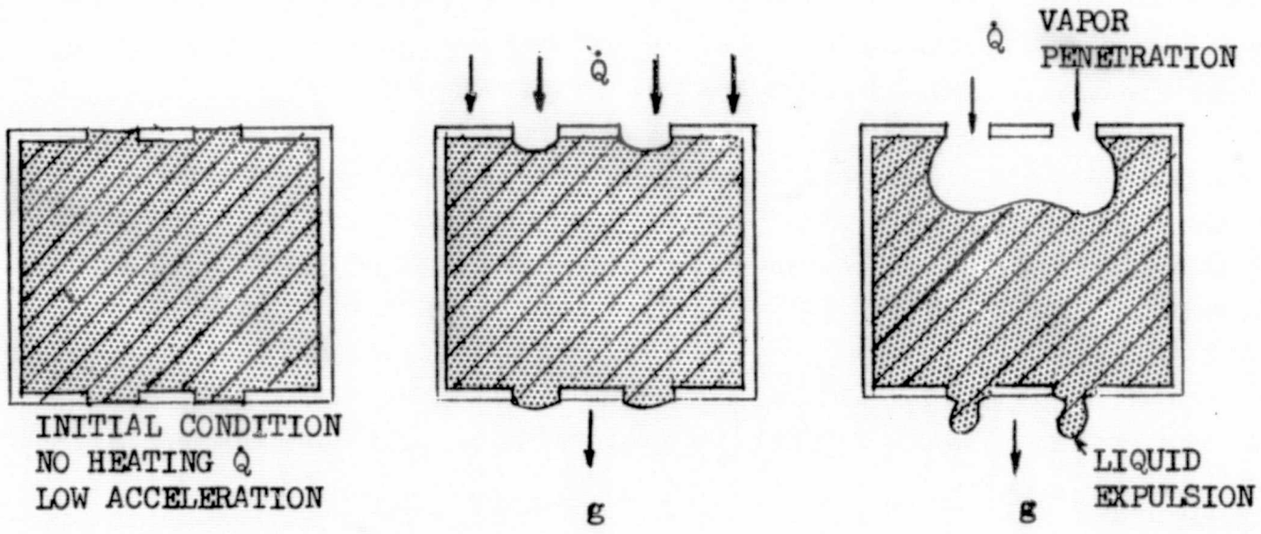


Figure 2-36. Vapor Formation in Bench Test Specimen

adverse condition that may arise during venting. The first sketch shows a filled container prior to the introduction of heat. The next two sketches show how evaporation at the screen will enable vapor to penetrate the screen. The question that arises is whether the generated vapor will dry the screen or leave a liquid film. The outcome is important because a wetted screen will retain its liquid holding capability, whereas a dry screen would permit the penetration of vapor, and therefore, the expulsion of liquid in a gravity environment.

It was decided to approximate inflight evaporation by evacuating the vapor space surrounding screened contained with liquid. Figure 2-37 shows the test configuration and the method selected for evaporating liquid at the screen surface. The test configuration was constructed of plexiglas and consisted of three adjacent chambers. The central chamber was separated from the other two by fine mesh screens. Each

chamber had a fill and drain line and shut-off valve at the bottom. The chambers were plumbed to a vacuum pump for individual or collective pressure reduction, as shown in Figure 2-37.

A typical test was conducted in the following manner:

1. Fill all chambers with pentane at 73°F (8.5 psia vapor pressure).
2. Drain most of liquid from outer chambers.
3. Pump down outer chambers at low rate (liquid will begin to evaporate when pressure drops to 8.5 psia). Freon was initially used as the test fluid, however, it was found necessary to use a fluid with a higher σ/ρ since slight disturbances of the test article tended to perturb the liquid vapor interface at the screen. Pentane was chosen as the test fluid because it has a relatively high vapor pressure at room temperature and a high σ/ρ, approximately 2/3rds higher than Freon TF.

   Tests run with pentane indicated that bubbles forming at the screen interface do not cause breakdown of the liquid vapor interface if liquid is present at one side of the screen. For example, if liquid fills the center compartment and vapor fills the two outer compartments, bubbles forming at the screen will detach from the screen and the screen will be rewetted without total collapse of the liquid vapor interface across the screen. As vapor forms in the center compartment, eventually both sides of the screen are exposed to vapor and, since the square mesh 150 × 150 screen does not wick, the liquid wetting the screen evaporates and is not replaced. This causes breakdown of the liquid vapor interface across the screen. This condition could possibly occur in a typical mission if screens are not wicking.

The absolute micron rating of the 150 square mesh screen used is approximately 100 microns. Equating surface forces to gravity forces indicates that a 350 micron diameter bubble can be supported at the top screen without liquid running out the bottom screen. Observations indicated that the bubbles grew well beyond this critical diameter without breaking off.

With the central compartment full of liquid and the two outer compartments containing only vapor, small bubbles tend to form at the underside of the screen and grow slowly. As the bubble exceeds a size of approximately 350 microns, the bubble growth accelerates rapidly. This is due to liquid spilling through the bottom screen at this critical diameter. Liquid spillage causes a corresponding volume of gas to enter the central compartment from the top. The inertia of the gas entering the screen causes the bubbles to grow rapidly to about 1200μ before breaking off because of dynamic instability. Liquid outflow then ceases and a new bubble begins to grow. The inertia of the bubble has allowed the screen to reseal itself in spite of its non-wicking properties. This process continued until insufficient liquid remained near the screen to

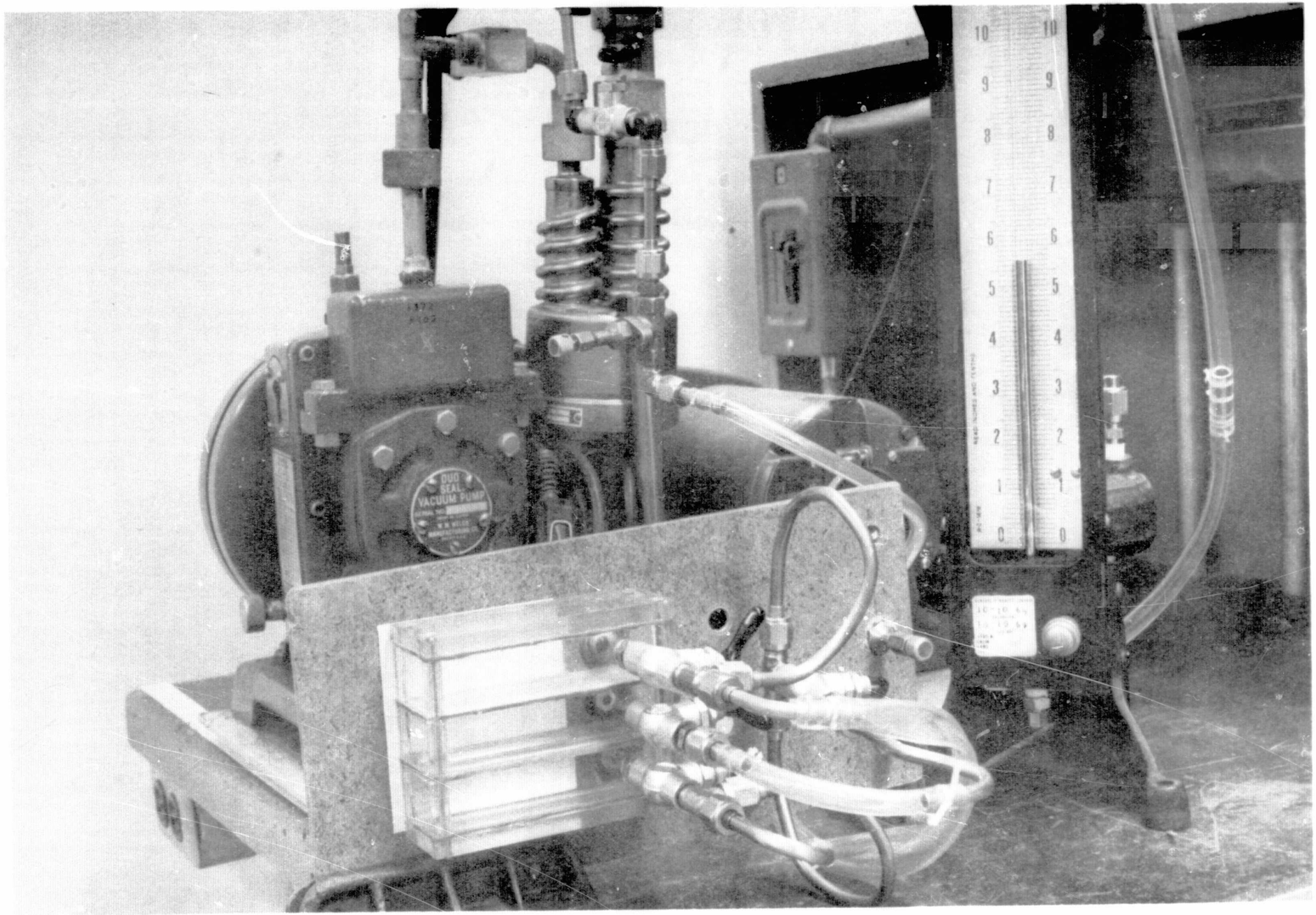


Figure 2-37. Screen Retention-Evaporation Test Apparatus

rewet the screen behind the bubbles. All liquid is then lost through the bottom screen.

Dutch twill screens have wicking properties which prolong the liquid-holding capacity of the test article. In order to evaluate the effect of wicking on drying out of the screen, a piece of dutch twill, 80 × 700 screen with a 30μ bubble point was put into the test article as a replacement for one of the 150 square mesh screens. Repeating the tests illustrated that the dutch twill screen will remain wetted for a considerably longer period of time due to the wicking action of the screen.

2.3 PHASE I DESIGN

2.3.1 PRELIMINARY DESIGN CONCEPTS. The objective of the preliminary design effort was to establish configurations for both the S-IVC restart and LOX tanker missions. Feasibility of these configurations has been examined in other sections of this report. Included in determining the feasibility of particular designs are the factors of system performance (which can be expressed as weight) manufacturing feasibility, cost and reliability.

Additional preliminary information relating to the capillary device designs considered is presented in Reference 5. This information has been summarized in the following paragraphs. For the latest design examples and philosophy see the design handbook, Reference 6 and Phase II final designs, Reference 7.

For the missions considered several design approaches were examined for each tank which required a surface tension device. These preliminary designs are presented with weight estimates for each design considered in detail. Detailed structural analysis concerning liquid impingement forces, vibration effects, temperature gradients, etc., was beyond the intent of this initial effort, thus conservative nodes were selected and the basic structural integrity of the designs were checked. The calculations enclosed were used as aides in determining or adjusting the magnitude of weight allowances. For example, if an area appeared marginal,conservative weight values were assigned to compensate for items that may appear in a detailed design.

2.3.1.1 S-IVC LH_2 and LO_2 Restart Reservoir Concepts. Designs were developed based on considerations of minimum weight, no vapor formation in the start basket and minimum spillage during restart. Six configurations were examined for volumes ranging from 60 ft^3 to approximately 2000 ft^3 for the fuel tank. This wide range of volumes was considered because of difficulty in predicting the settling time of the uncontained propellants. Curves were developed showing surface tension system volume vs. weight for both cylindrical and annular shaped start baskets.

Initially cylindrical baskets were designed for the low volume range since they appeared to be the lowest weight configuration. Fluid analysis of the cylinders indicated that, due to their greater height, they would have greater percentages of unuseful volume due to spillage than an annulus shape. Thus, from a useful volume standpoint annulus shapes presented the lowest weight configurations. Data for both the cylindrical and annular configurations considered is presented in the following paragraphs.

A LOX tank surface tension system design is presented for a 100 ft^3 capacity. This volume will be sufficient to assure liquid flow to the engine until the bulk of the LOX is settled. This design represents a conservative approach to the LOX surface tension restart basket. Weights derived from this design are combined with the LH_2 system weights for comparison purposes.

S-IVC Fuel Reservoir

The fuel reservoir structure is subject to numerous load combinations from vibrations, accelerations, and fluid impingements. The capillary screen should be supported in such a manner that the micron rating will not be altered during manufacturing or operating conditions. It, therefore, appears reasonable to base the weight estimate upon a perforated skin (ring stiffened) structure with the capillary screen applied over the skin areas. This should also yield values representative of an open frame work structure. Weight calculations were made on the basis of steel and aluminum using minimum gages of .020 and .032 respectively. The perforated skins were assumed at minimum gages and the stiffener rings estimated for external loading per Appendix A. A summary of the components and related weights are given for a 60 ft^3 unit in Figure 2-38.

The forward bulkhead primary loading mode is assumed to be tension with the possibility of a small reversed loading during tanking. No material is removed due to the perforations since stiffeners or gage adjustments may be required due to vibration and reversed loading conditions. Loading conditions are discussed in Figures A-1, A-2 and A-3. The ring at the base of the bulkhead was checked per Figures A-1 and A-2 and a conservative cross section used to compensate for unknown factors. 40% of the material for the cylindrical shell sections was assumed removed due to the perforations and the stiffener rings sized per Figure A-1. For simplicity, the stiffener ring cross sections were assumed angular with the attachment leg fixed at 3/4-inch length and the adjacent or radial leg varied per the amount of inertia requirements. The three stiffener rings and two flange rings used in the 48-inch diameter section of the shell are assumed equal in cross section. Discussions for the cylindrical shell sections are given in Figure A-4.

The stiffener rings for the aft transition section are non-circular, therefore, an equivalent diameter (based upon estimates from a lay-out) was assigned to these rings and the cross sections estimated per Figure A-1 procedures. For the 11-inch diameter outlet, two channel shaped members were used as the equivalent structure.

For steel applications, the capillary screen is attached by welding or brazing. For aluminum, the screen is attached by mechanical, soldering or seam welding methods. The latter process is preferred.

For weight calculations, two heat exchanger coils between each stiffener ring on the forward cylindrical section was assumed (1210 inches). For the aft section 50% of this value was used giving a total coil length of 1815 inches. For steel applications, the coils are brazed or welded to the shell. For aluminum, the tubes and the local attachment areas on the shell may be gold plated and soldered with a 50% lead/50% indium alloy or seam welded. See Section 2.3.3 for discussion of heat exchanger attachment methods.

The forward support struts are tubular fiberglass units with titanium inserts equipped with spherical ball end fittings. This type of strut has been developed by Convair under a program aimed at developing low conductive attachments. The weights assigned therefore are based on the Convair designs with additional allowances made for tank wall and reservoir ring fittings.

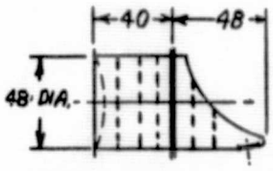
The forward section, aft section and the 11-inch outlet required mechanical attachments at the interfaces using a system of bolts, nut plates and gaskets. Fittings for the coil terminals will also be required to permit assembly. Weight allowances for such items are included in the contingency column of Figure 2-38. Additional weight estimates were made for the following cases using aluminum alloy:

1. A 60 ft^3 cylindrical unit sized to fit through a 40-inch access opening (Figures 2-39 and 2-40).
2. A 1970 ft^3 (approx.) unit which follows the tank wall profile per Figure 2-41.
3. A 1015 ft^3 annulus type unit per Figure 2-42.
4. 500 ft^3 cylindrical unit per Figure 2-43.
5. 180 ft^3 annulus type unit per Figures 2-44 and 2-45.

A summary of these weights are shown on Figure 2-46. Percentages of material removed due to shell perforations; contingency allowances; and basic loads were varied slightly between cases depending upon the type of configuration, and expected degree of design complexities. Each unit is equipped with capillary screens and heat exchanger coils.

Case 1: (Figures 2-39 and 2-40)

The basic diameter was reduced 11.0 inches which increased the shell length, decreased the moment of inertia of the rings, and increased the quantity of rings. A 6.3 lb weight increase was experienced over that shown for the 48.0 diameter unit, per Figure 2-39. The support system is essentially common to both configurations.



C= Steel
A= Al. Aly

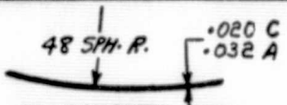
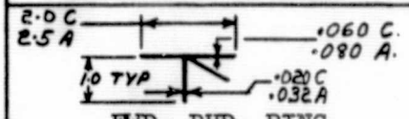
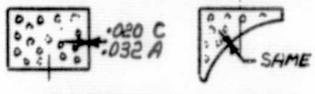
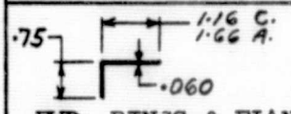
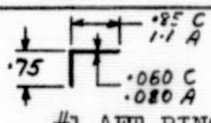
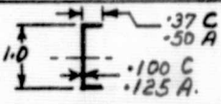
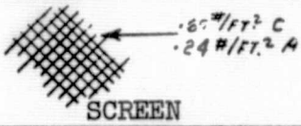
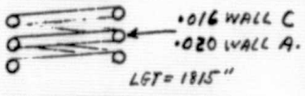
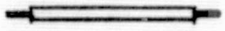
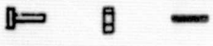
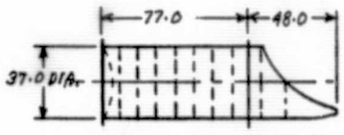
OVERALL CONFIGURATION	WEIGHTS LBS. STEEL	WEIGHTS LBS. AL. ALY.	REMARKS
 PERFORATED BHD.	11.75	6.26	1960 IN^2 SURFACE AREA.
 FWD. BHD. RING	8.15	4.00	RING DIA= 48.0
 PERFORATED SHELLS	41.8	22.2	9995 IN^2 SURFACE AREA
 FWD. RINGS & FLANGES (5)	26.00	10.90	RING DIA.=48.0
 #1 AFT RING	3.16	1.63	EQUIVALENT RING DIA.=35.0
 #2 AFT RING	2.26	1.16	SAME AS FOR #1 AFT RING EXCEPT EQUIV. DIA. 25.0
 EQUIV. REINF. RING/OUTLET	3.96	2.00	RING DIA. =12.0
 SCREEN	49.80	19.60	
 HEAT EXCHANGER COILS	6.96	2.90	1/4" O.D. TUBING
 SUPPORT STRUTS	2.00	2.00	INCLUDES TANK WALL FITTINGS.
 MISC. BOLTS, NUTS & GASKETS	2.00	3.00	
TOTAL WT.	157.84	75.65	
10% CONTINGENCIES	15.78	7.56	
GRAND TOTAL	173.62	83.21	

Figure 2-38. Weight Estimates/Fuel Reservoir, 60 Ft^3



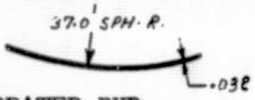
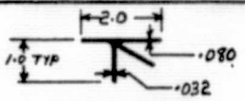
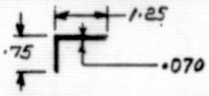
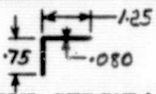
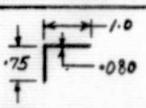
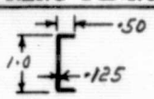
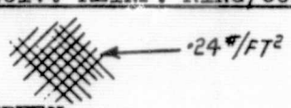
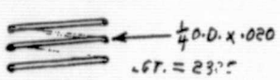
OVERALL CONFIGURATION	WT. LBS AL. ALY	REMARKS
 PERFORATED BHD.	3.86	
 BHD. RING	2.70	DIA. = 37.0
 PERFORATED SHELLS	26.3	SURFACE AREA = 11,740 IN^2
 CIRCULAR RINGS (8)	13.0	DIA. = 37.0
 NON CIRCULAR RING (1)	1.2	23.0 EQUIV. DIA.
 RING FLANGES (2)	3.25	DIA. - 37.0
 EQUIV. REINF. RING/OUTLET (2)	2.00	DIA. = 12.0
 SCREEN	21.40	
 HEAT EXCHANGER COILS	3.64	
 SUPPORT STRUTS	2.00	INCLUDES TANK WALL FITTINGS
 MSC. BOLTS, NUTS, GASKETS, ETC.	2.00	
TOTAL WT.	81.35	
10% CONTINGENCIES	8.13	
GRAND TOTAL	89.48	

Figure 2-39. Weight Estimate/Fuel Reservoir, 60 Ft^3

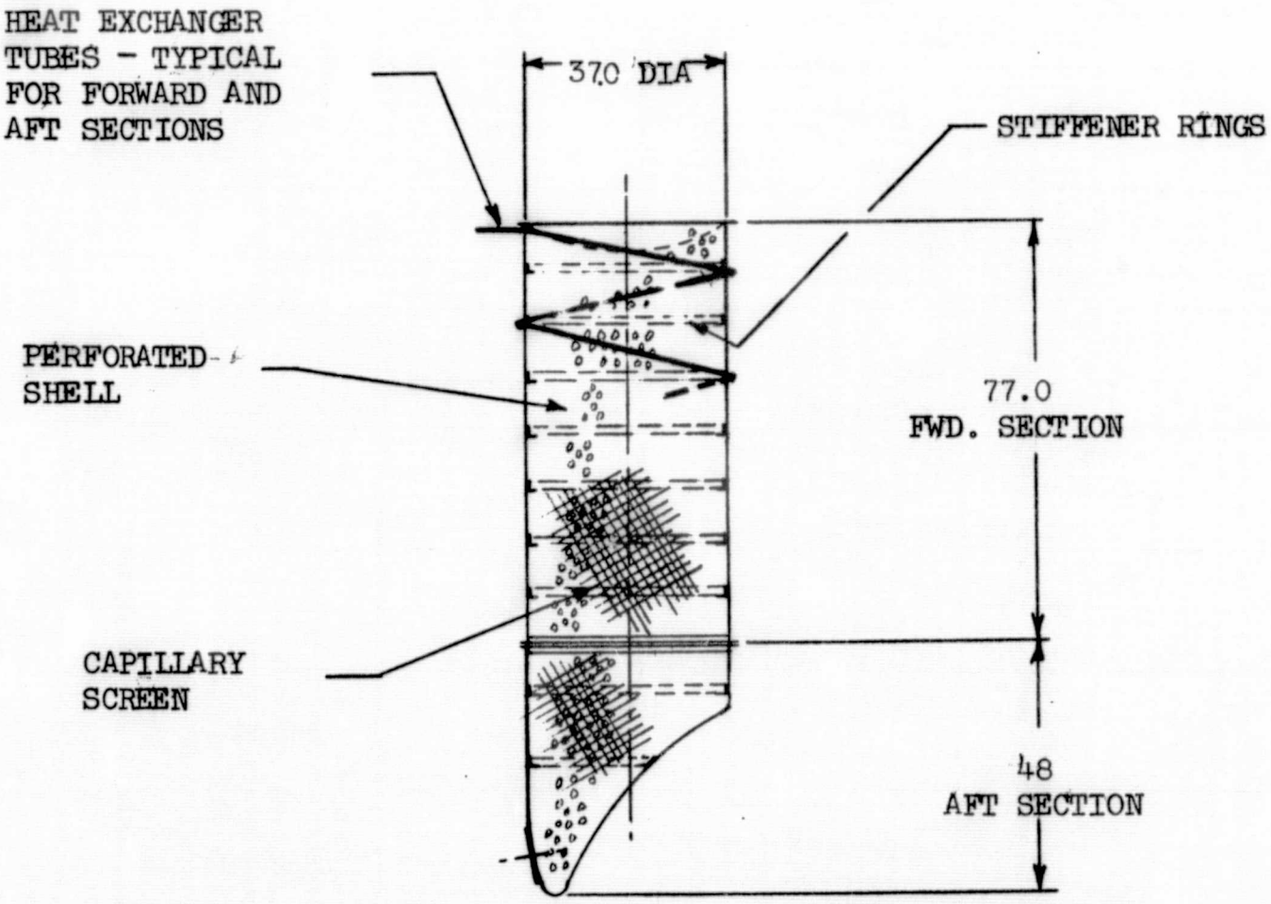
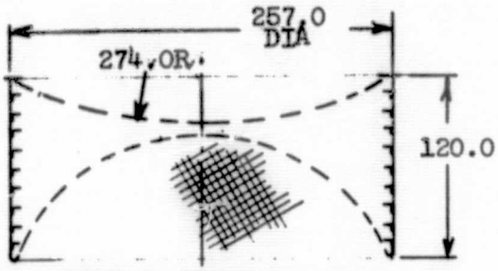


Figure 2-40. Fuel Reservoir Sized for 40.0 Inch Dia Tank Access Opening (Approx. 60 Ft^3 Vol)

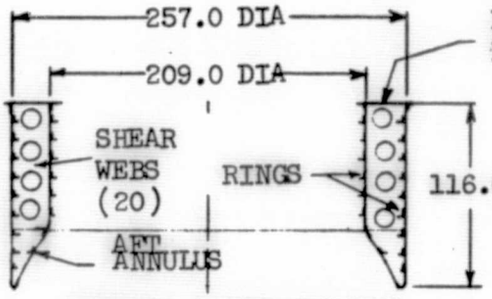


OVERALL CONFIGURATION

LOADS: 3 PSI ON FWD BHD
1 PSI ON CYL. SHELL

	WT. LBS. AL. ALY.	REMARKS
.032 FORWARD BULKHEAD	165.0	
.032 AFT BULKHEAD	216.0	
.032 CYLINDRICAL SECTION	248.0	
11.0, 1.0 TYP., .060, .125 FWD. BHD. RING (1)	148.0	
.75, 4.0, .060, .50 STIFFENER RINGS (9)	180.0	
.080, .75 TYP FWD. FIANGE (1)	10.0	
.080, .75 TYP AFT END RING (1)	20.0	
24#/FT² SCREEN	359.0	1495 FT²
¼ O.D. x .020 HEAT EXCHANGER COILS	40.0	25,200 INCHES
SUPPORT STRUTS AND END FITTINGS	30.0	40 STRUTS & 80 FITTINGS
MSC. BOLTS, NUTS, RIVETS, GASKETS, ETC.	20.0	
TOTAL WT.	1436.0	
5% CONTINGENCIES	72.0	
GRAND TOTAL	1505.0	

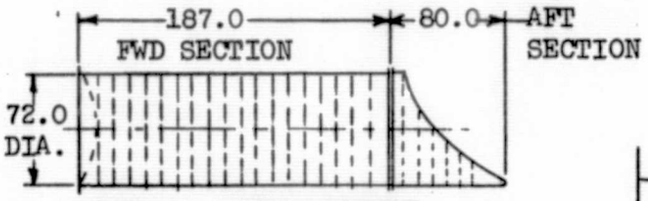
Figure 2-41. Weight Estimate/Fuel Reservoir, 1970 Ft³



LOADS: 3 PSI ON FWD ANNULUS
1 PSI ON CYLINDERS

GENERAL CONFIGURATION	WT. LBS AL. ALY.	REMARKS
FWD. ANNULUS SECTION (1)	71.0	
FWD ANNULUS STIFFENERS (135)	55.0	EACH STIFF. 26.0" LG'T.
FWD ANNULUS RINGS - INNER & OUTER	26.0	
AFT ANNULUS (1)	72.0	
AFT ANNULUS RING (1)	20.0	
SHEAR WEBS (20)	74.0	
INNER CYLINDER (1)	134.0	20% OF THE MATERIAL REMOVED DUE TO PERFORATIONS.
OUTER CYLINDER	240.0	
OUTER CYL. STIFF. RINGS(9)	180.0	
INNER SHELL STIFF. RINGS (8)	71.0	TWO RINGS ADDED FOR AFT ANNULUS
SCREENS	320.0	1330 FT^2
HEAT EXCHANGER COILS	47.0	30,000 INCH LG'T.
SUPPORTS	30.0	
MSC. BOLTS, NUTS, RIVETS, ETC.	20.0	
TOTAL WT.	1360.0	
5% CONTINGENCIES	68.0	
GRAND TOTAL	1428.0	

Figure 2-42. Weight Estimate/Fuel Reservoir 1015 ft^3



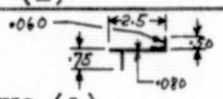
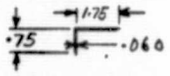
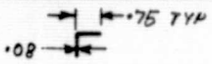
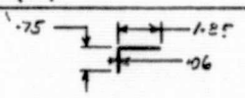
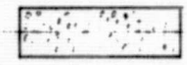
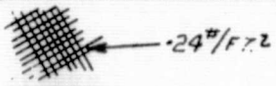
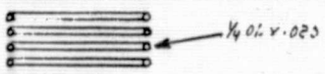
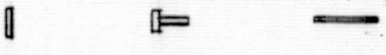
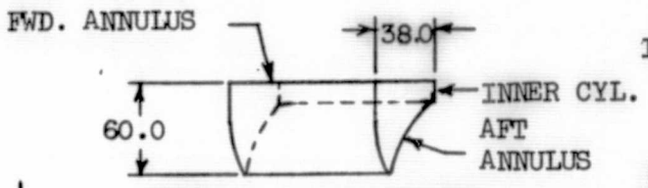
GENERAL CONFIGURATION	WT. LBS. AL. ALY.	REMARKS
 FORWARD BH'D. (1)	15.0	
 FORWARD BH'D. RING (1)	7.0	
 FWD SECTION STIFF. RINGS (18)	61.2	
 INTERFACE RINGS (2)	5.4	
 AFT SECTION STIFF RINGS (6)	7.0	30.0 EQUIV. DIA.USED
 FWD. CYL. SECTION	108.0	
 AFT SECTION SHELL	25.0	
 SCREEN	91.0	
 HEAT EXCHANGER COILS	17.0	10,750 INCHES
 SUPPORTS	20.0	
 MSC. BOLTS, NUTS, GASKETS, ETC.	6.0	
TOTAL WEIGHT	362.6	
5% CONTINGENCIES	18.1	
GRAND TOTAL	380.7	

Figure 2-43. Weight Estimate/Fuel Reservoir, 500 Ft^3



GENERAL CONFIGURATION	WT. LBS. AL. ALY.	REMARKS
180 I.D. 38.0 .050 FWD. ANNULUS SECTION (1)	43.3	ACCESS DOOR INCLUDED
.060 1.75 1.0 FWD. ANNULUS STIFFENERS	11.27	18 REQ'D. 38" LGT EA.
.060 1.0 2.0 FWD. ANNULUS RINGS - INNER AND OUTER	8.20	457" LGT. TOTAL
.032 AFT ANNULUS	42.50	
.080 .75 TYP. AFT ANNULUS RING	3.40	189" LG'T
.032 SHEAR WEBS	46.18	10# INCL. FOR STIFFENING TWO END WEBS
.032 OUTER CYL. PERFORATED INNER CYL. NOT PERFORATED (.036) INNER AND OUTER CYL. SHELLS	57.52	
4.0 .75 .060 .50	25.40	3 REQUIRED 805" LGT TOTAL
1.50 .060 .75 INNER CYL. SHELL STIFFENERS	11.88	4 REQ'D 879" LG'T TOTAL
.24#/FT^2 SCREENS	14.40	60 FT^2
1/4 O.L. x .020 HEAT EXCHANGER COILS	12.50	8,000 INCHES
SUPPORTS	12.0	
MSC. BOLTS, NUTS, RIVETS, ETC.	8.0	
TOTAL WT.	296.5	
10% CONTINGENCIES	29.6	
GRAND TOTAL	326.1	

Figure 2-44. Weight Estimate/Fuel Reservoir, 180 Ft^3

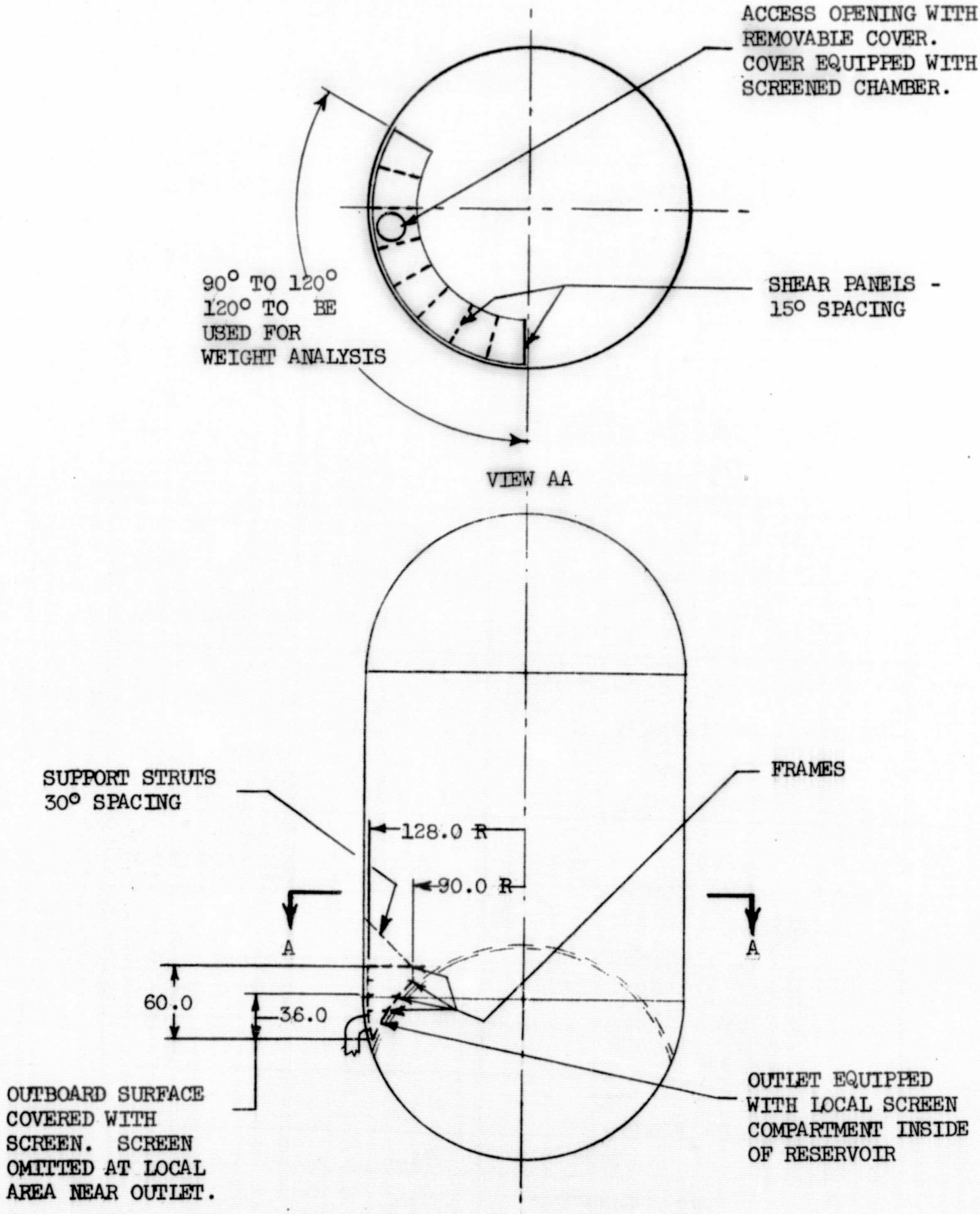


Figure 2-45. Fuel Reservoir Annular Reservoir

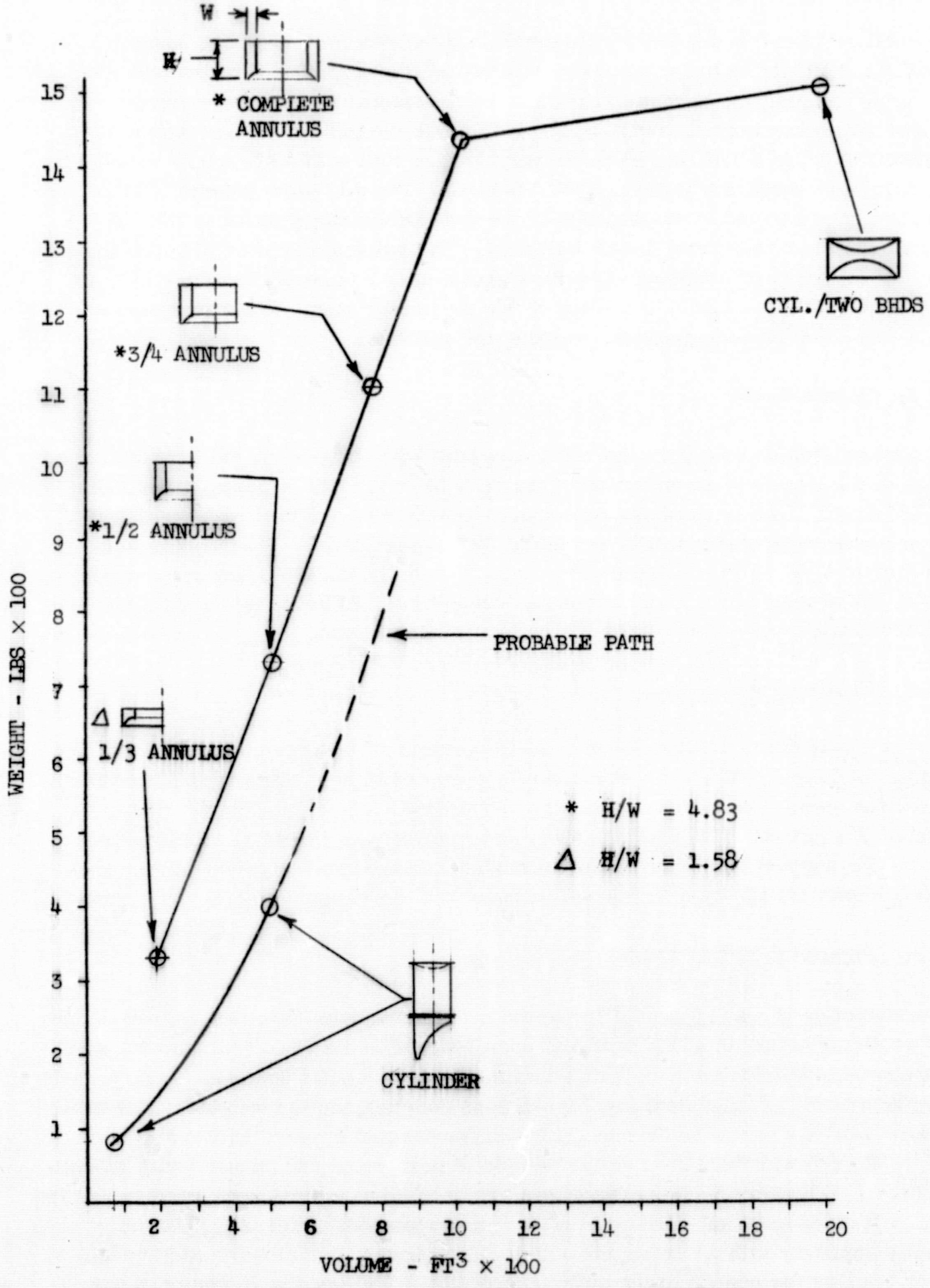


Figure 2-46. Fuel Reservoir Weights Versus Volume

Case 2: (Figure 2-41)

This configuration follows the profile formed by the vehicle tank. The assembly is basically a stiffened cylinder equipped with two bulkheads. The forward bulkhead can be a removable unit for access to the 11.0-inch diameter outlet connection or a fixed unit with an access opening and closure provided in the bulkhead. The assembly is supported at the forward ring from the vehicle tank wall with a system of adjustable low conduction struts arranged in a "V" pattern. The minimum volume for this configuration is controlled by the location of the forward bulkhead which in turn is influenced by clearances from the aft bulkhead. The volume also depends upon the profile of the forward member. The case shown uses a spherical surface with a radius selected for reasonable loading on the perimeter ring. Final analysis would reflect tradeoffs between profiles, weights and volumes.

Case 3: (Figure 2-42)

Case 3 is an annulus configuration which contours with the cylindrical section and a portion of the intermediate bulkhead of the vehicle tank. The forward end is a flat stiffened panel. The inboard and outboard cylinders are stiffened with rings and interconnected with shear panels located at the support points. The support system is similar to that used for Case 2. An opening would be required through the inboard cylinder for access to the 11.0-inch outlet connection. An increase of weight penalty per unit volume is experienced due to the large surface area.

Case 4: (Figure 2-43)

Case 4 is a cylindrical design using a 500 ft^3 volume. The construction is basically the same as Case 1. The support system is expected to be more complex than that used for the smaller units due to the size and weight. The 11.0-inch outlet may be incapable of supporting major loads, therefore, additional weight allowances are given for the support system. The shell stiffener rings have larger cross sections than that shown for the 60 ft^3 reservoirs due to the increased diameter.

Case 5: (Figures 2-44 and 2-45)

The construction of Case 5 is similar to the previous annulus type design except the cross sectional height to width ratio has been reduced and a 90 to 120° annulus section assumed. Weights were calculated on the basis of a 120° annulus. Figure 2-44 shows the overall arrangement and Figure 2-45 summarized the weights. The basic structure is shear panels interconnected with frames and covered with a stiffened skin. A 36-inch wide belt area on the outside is perforated and covered with a capillary screen. The screen and perforations are omitted at a local area surrounding the outlet. All other external surface areas are unperforated. Internally, the outlet area is locally boxed-in with a screen assembly. The forward end closure section contains an opening for access to the outlet connection. The opening is equipped with a

removable cover which incorporates a cylindrical screened riser chamber. The support system consists of tubular struts and fittings attached between the tank wall and the shear panels.

The curve of Figure 2-46 summarizes the weights for the above configurations. It is evident that the weight is affected by the type of design. Cylinders may become impracticable at high volume levels. The cross over point between the cylinder and the annulus is not known, therefore a probable projection for the cylinder is shown. As mentioned previously, the annulus shapes provide a greater percent useful volume than the taller cylindrical shaped configurations. This factor makes the annular devices lower weight systems than the cylindrical devices when compared on a weight versus useful volume basis.

Oxidizer Reservoir/S-IVC (Figures 2-47, 2-48 ,2-49)

The reservoir is basically an open frame type structure consisting of aluminum alloy angles, channels and tee-shaped members interconnected by welding. A 96-inch diameter cylindrical section capped off at the forward end by a conical section forms the total assembly. The entire surface area is covered with a capillary screen assembly equipped with a back-up support screen. The assembly is attached directly to the tank shell. Two heat exchanger coils are provided at the attachment zone. Figure 2-47 summarizes the weight estimate and Figures 2-48 and 2-49 show the design details.

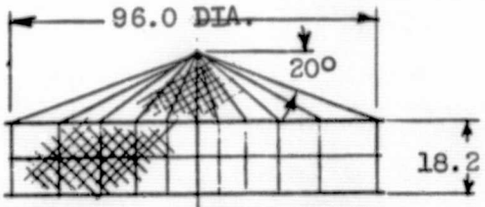
Cylindrical Section

The cylindrical portion consists of a forward ring, an intermediate ring and an aft ring interconnected by ribs. The forward ring is a channel shaped member which resists the kick loads from the forward conical section and provides a corner attachment between the cylinder and the cone (see Figure 2-48). The depth of the ring is controlled by the 3 psi loading assumed for the forward conical section.

The intermediate ring is a tee section equipped with a lip section at the inboard edge of the radial leg. The ring was sized for external loading equal to 13.5#/in. using the procedures of Figure A-1. The base of the tee cross section is attached to the ribs by welding.

The aft ring has an angle type cross section with one leg interfacing with a land area which is integral with the tank wall. Since the ring is supported from the tank wall, the size of the legs are controlled primarily by the attachments to the tank and to the adjacent support ribs.

The vertical ribs are tee shaped members which interconnect the rings. These ribs are subjected to the simultaneous actions of column loading from the forward conical section and a bending type load from the pressure acting on the screen surfaces. The



100 FT^3 VOLUME

OVERALL CONFIGURATION	WT. LBS. AL. ALY.	REMARKS
HEAT EXCHANGER EXTRUSION	4.0	600 INCH LGT.
TANK WALL ATTACHMENT ZONE	4.0	LOCAL BOSSES FOR BOLTS + LAND FOR SEAL
AFT RING	3.4	
INTM. RING	5.6	
FWD. RING	10.0	
RIBS	4.6	24 REQD.
CONE RINGS	8.1	4 REQD.
APEX FITTING	2.0	MONOCOQUE SHELL TYPE
CONE STRINGERS	14.6	24 REQD @ 45 INCH LGT.
CAPILLARY SCREEN	27.5 14.0 ←	BACK-UP SUPPORT SCREEN
OUTLET FITTING	2.0	
MSC. BOLTS, GASKETS, ETC.	2.5	
TOTAL WT.	102.30	
10% CONTINGENCIES	10.20	
GRAND TOTAL	112.50	

Figure 2-47. Weight Estimate/Oxidizer Reservoir/S-IVC Tank

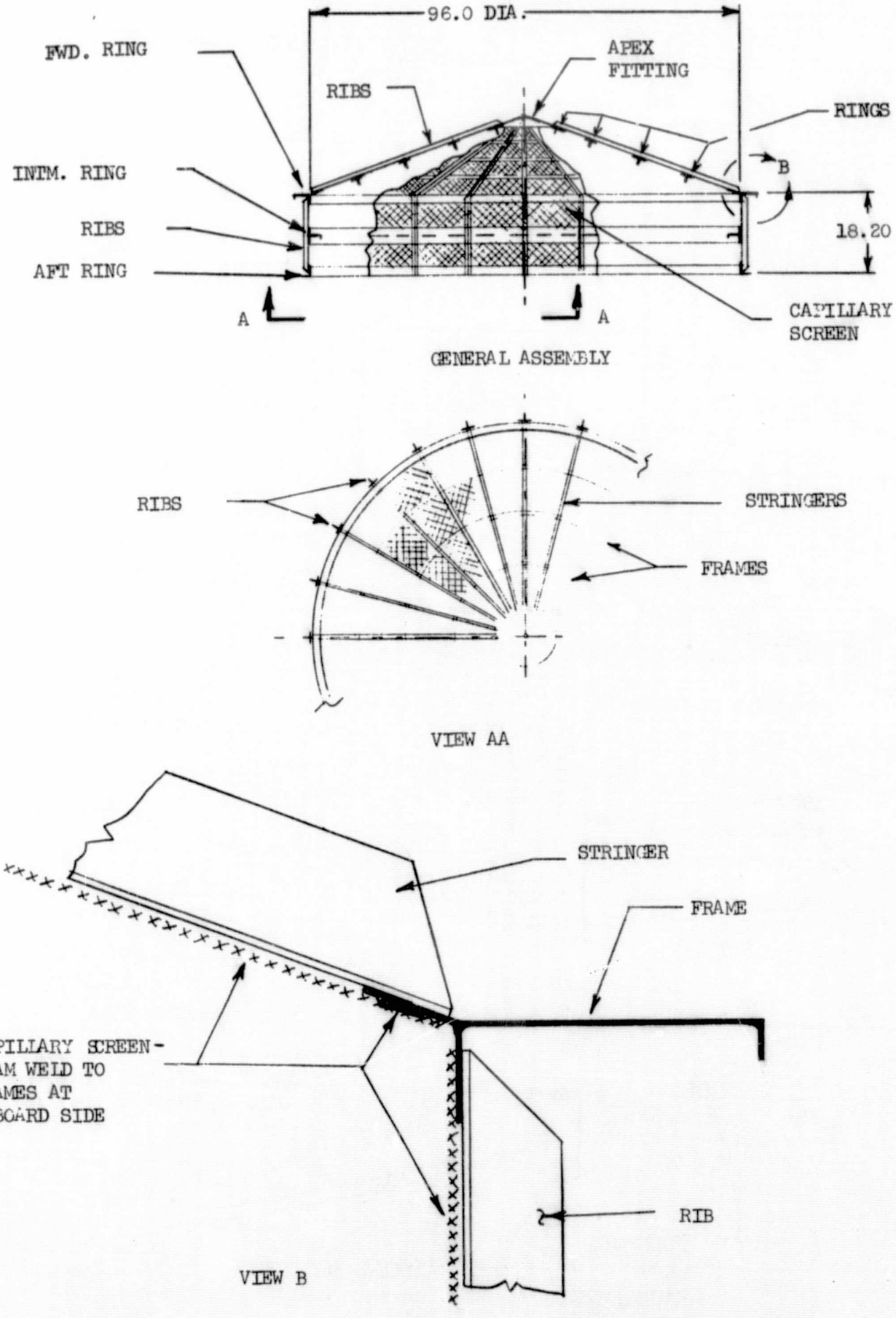


Figure 2-48. S-IVC Oxidizer Assembly

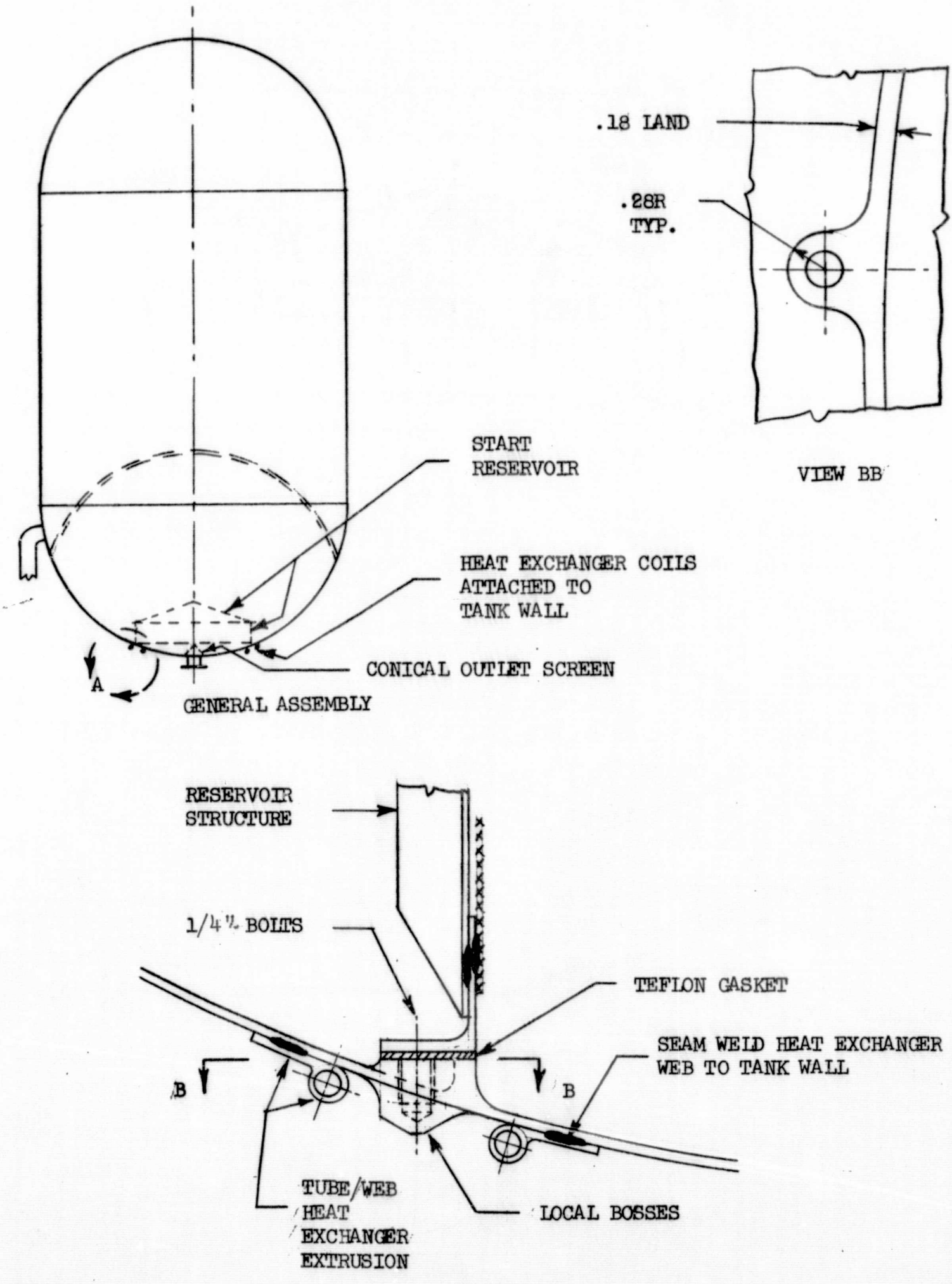


Figure 2-49. Oxidizer Start Reservoir Concept/S-IVC Tank

member was checked for column instability and conservative values used for the cross section due to the beam column type loading.

The open areas of the cylindrical structure are covered with a capillary screen attached to the through rings at the inboard side. The micron rating of the capillary screen can be altered if the stresses become excessive, therefore, a back-up support screen is assumed in the weight estimate. Both screens are seam welded to the legs of the frames. Intermediate attachments can be made to the ribs providing spacer strips placed between the screen and the ribs or the use of offset bends at the ends of the ribs. Tradeoffs exist between the quantity of ribs, number of rings, and type of back-up screens. Alternate designs are also available which would replace the support screen with a perforated sheet metal skin. The weight assignments of Figure 2-47 are representative of the range of values that can be encountered with a representative series of designs.

Forward Section

A 140° (included angle) conical structure was chosen for the forward closure. The open frame structure consists of four tee shaped rings, 24 stringers spaced at 15° intervals, and an apex fitting. The rings and stringers were estimated for external loading and beam column actions respectively. The rings are welded to the stringers and the ends of the stringers in turn are attached to the forward ring of the cylindrical section and to the apex fitting. The apex fitting is a stiffened sheet metal conical member with a 14-inch diameter base. The base diameter is controlled by the quantity of stringers and the attachment methods. A capillary screen and a back-up support screen is attached to the inboard faces of the cone structure using the methods described for the cylindrical section.

Tank Wall Attachment

The reservoir assembly is attached to the tank by bolting the aft flange of the cylindrical section to a ring boss which is integral with the tank shell (see Figure 2-49). A teflon gasket is used between the two mating surfaces. The ring boss is a local 3/16 wide × 96 inch I. D. land section equipped with local bosses containing 1/4-inch tapped holes for receiving the attachment bolts (see View BB of Figure 2-49). The outboard faces of the bosses are flanked by two heat exchanger coils. The coils are tubular web type construction and are attached by seam welding the web section to the tank wall.

2. 3. 2 LOX TANKER PROPELLANT TRANSFER DESIGNS. Several designs were considered for this surface tension device. Two capillary systems using a central cylindrical reservoir connected to eight retrieving channels were considered (see Figure 2-50). The reservoir design and weight estimate shown per Figure 2-51 is common to both systems. The retrieving channels, however, differ for the two arrangements. The estimate shown per Figure 2-52 uses gore type channels having

variable depth and a 16.0 inch width. An average channel depth of three inches was used for the Figure 2-52 weight estimate. The design per Figures 2-50 and 2-53 is basically the same as that shown in Figure 2-52 except the gore channels are interconnected at the equator by channel sections; the cross section is reduced to a 1.4 inch depth × 14.0 inch width (no taper); the micron rating and density of the screen reduced; and the number of supports are increased. The change in designs was based on pressure drop information given in Reference 8 and the possibility of high residuals without the interconnecting channel across the equator as indicated in Section 2.1.

A third oxidizer system using a screen liner mounted inside the tank was evaluated per Figures 2-54, 2-55, and 2-56. The design is basically a frame work suspended from the tank wall and covered with a capillary screen. Steel frames and screen are used. This design is more difficult to fabricate and thermally isolate.

Stress calculations for the LOX tanker designs are given in Appendix B.

Oxidizer Reservoir (Figure 2-51)

Similar to the fuel system, the oxidizer reservoir structure (Figure 2-51) must support load combinations due to vibrations, and accelerations. The capillary screen must be supported to prevent alterations to the micron ratings during manufacturing, checkout, and mission operations. Loads due to fluid impingements are expected to be small. The primary loading would be that due to boost phase accelerations and vibration. It is, therefore, assumed that a minimum gage type structure is adequate with conservative allowances for interface and stiffener areas. This should also yield values representative for an open framework structure. Weight calculations were made on the basis of steel and aluminum gages of .020 and .032 respectively. The perforated skins were assumed at minimum gages using the stiffener ring cross sections calculated for the fuel reservoir. A low conductive type support system is used. A summary of the components and related weights are given in Figure 2-51.

The perforated forward bulkhead and ring combination examined for the S-IVC LH_2 system was used. The purpose of the spherical shaped member is reduce the ring cross sectional area that is required when using a flat diaphragm and to provide a stable surface under vibrational modes. The five stiffener rings used in the cylindrical shell have cross sections equal to the 48.0 inch diameter units selected for the fuel system.

The aft end of the reservoir is equipped with eight rectangular shaped openings equipped with flanges for attachment to the retrieving channels. A detail design would position these openings between two stiffener rings, equipped with intercostals and local skin reinforcements. The flange section shown in Figure 2-51, is structurally conservative to compensate for these details. A .25 inch lip was used on the outboard edges of the flange for distributing the bolt loads.

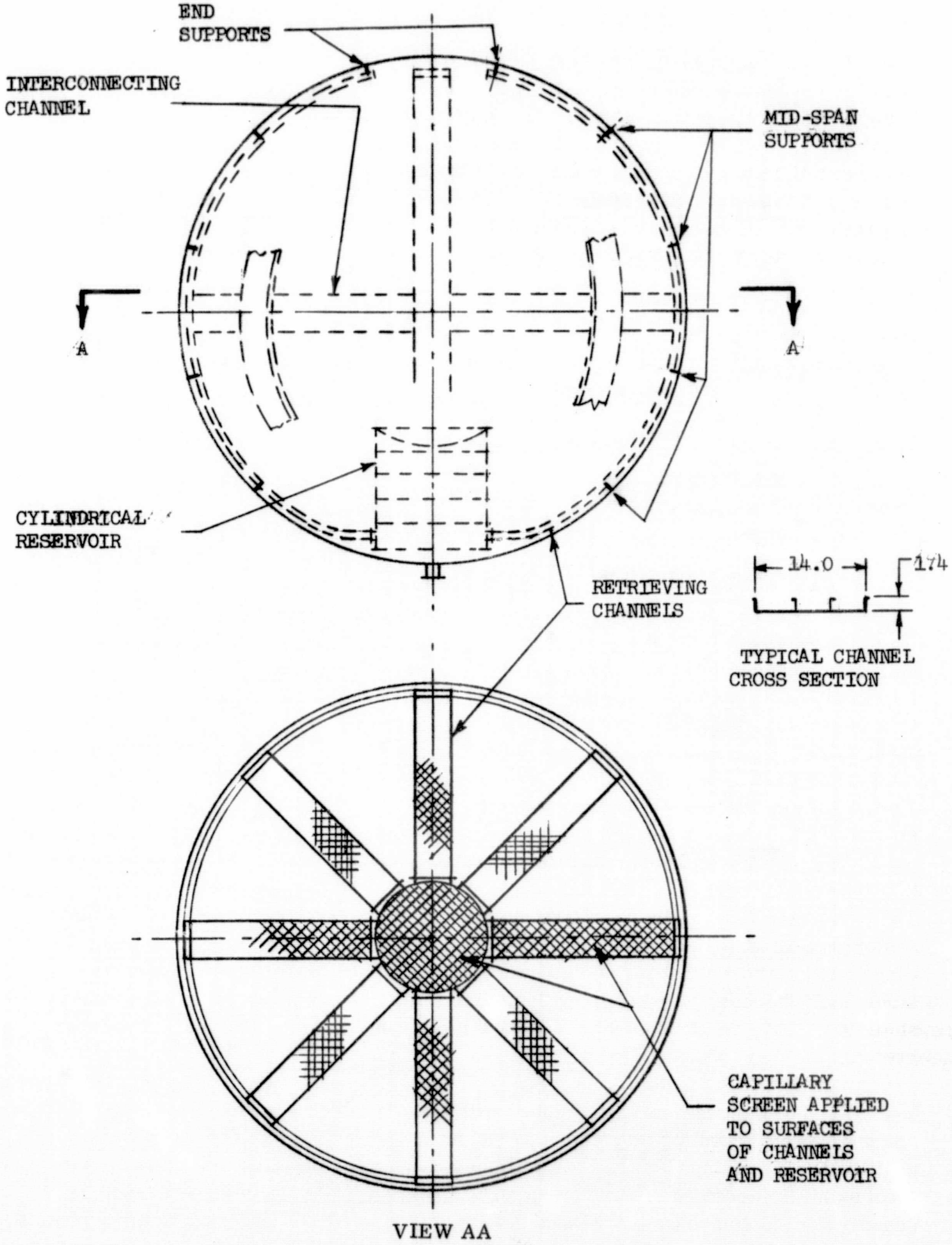
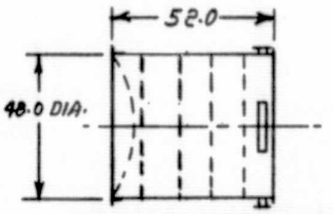


Figure 2-50. Oxidizer Collector System



C = STEEL
A = AL. ALY.

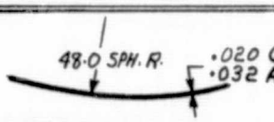
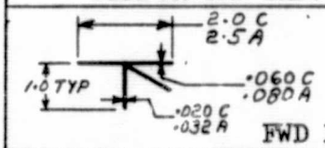
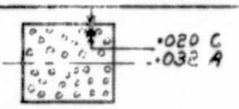
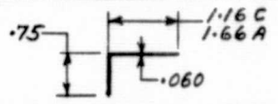
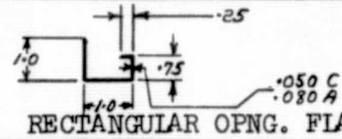
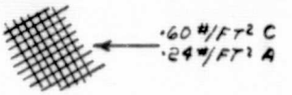
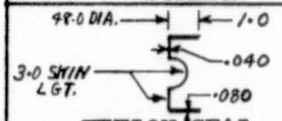
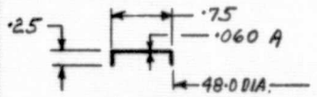
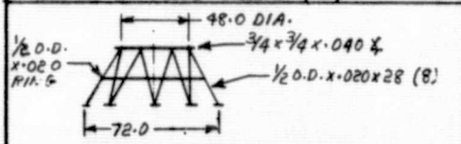
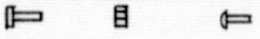
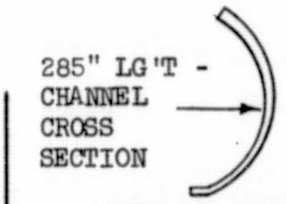
OVERALL CONFIGURATION	WEIGHT LBS. STEEL	WEIGHT LBS. AL. ALY.	REMARKS
 PERFORATED BHD.	7.05	3.76	1960 IN^2 SURFACE AREA. 40% OF MATL REMOVED
 FWD BHD RING	8.15	4.00	RING DIA = 48.0
 PERFORATED CYL. SHELL	47.00	25.00	7830 IN^2 SURFACE AREA. 40% OF MATL REMOVED
 STIFFENER RINGS (5)	26.00	10.90	RING DIAS = 48.0
 RECTANGULAR OPNG. FLANGE	13.00	6.06	RECTANGULAR 2×16 OPNG. 8 REQUIRED
 SCREEN	40.70	16.30	68 FT^2 REQUIRED
 TEFLON SEAL	3.00	3.00	
 SEAL BACKUP RING (2)	2.30	2.30	
 STEEL SUPPORT CAGE	10.65	10.65	
 MSC. BOLTS, NUTS, RIVETS, ETC	1.50	2.00	
TOTAL WEIGHT	154.38	79.00	
10% CONTINGENCIES	15.40	7.90	
TOTAL	169.78	86.90	

Figure 2-51. Weight Estimate/Oxidizer Reservoir

285" LG'T - CHANNEL CROSS SECTION



C = STEEL
A = AL. ALY.

"h" is based on 3.0 inches for weights shown. Will probably be reduced to 2.0 @ next design cut.

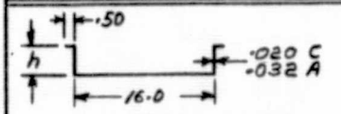
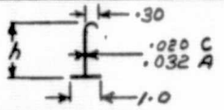
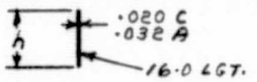
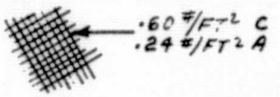
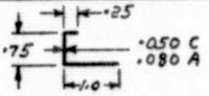
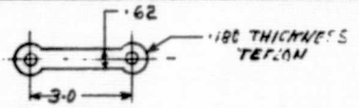
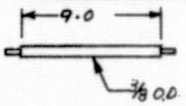
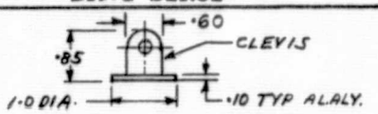
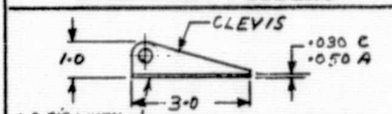
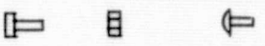
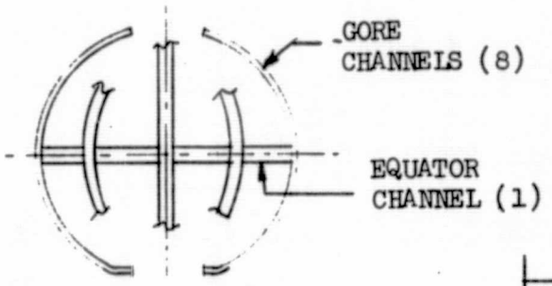
OVERALL CONFIGURATION	WEIGHT LBS STEEL	WEIGHT LBS AL. ALY.	REMARKS
 BASIC SHELL	314.00	168.00	285 INCH LGT. - 8 REQUIRED
 SUPPORT WEBS	176.00	94.00	285 INCH LGT. - 24 REQUIRED
 SUPPORT WEB	23.30	12.30	WT. BASED ON 80 @ h = 3.0 MAY INCREASE TO 144 @ h = 2.0.
 SCREEN	161.50	64.50	269 FT^2 REQUIRED
 RESERVOIR INTERFACE FLANGE	12.98	6.05	2x16 OPNG. 8 REQUIRED
 SUPPORT LINK	2.30	2.30	64 REQUIRED
 DRAG STRUT	6.75	6.75	24 REQUIRED
 TANK WALL FITTING	1.60	1.80	72 REQUIRED
 SUPPORT FITTING	4.80	2.40	48 REQUIRED
 MSC. BOLTS, NUTS, RIVETS, ETC.	2.00	2.00	
TOTAL WEIGHT	705.43	338.80	
10% CONTINGENCIES	70.50	33.80	
TOTAL	775.93	372.60	

Figure 2-52. Weight Estimate/Oxidizer Retrieving Channels

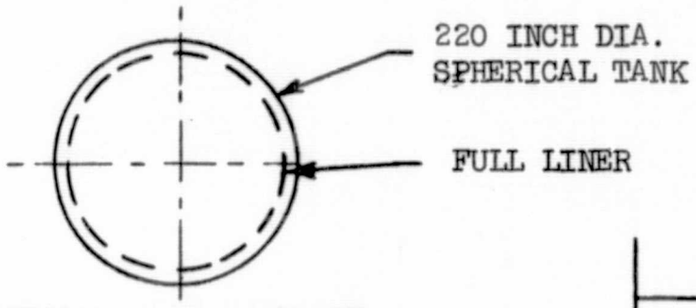


C = STEEL
A = AL ALY.

OVERALL CONFIGURATION	WT. LBS. STEEL	WT. LBS. AL ALY.	REMARKS
.50 → 14.0 → .020 C .032 A, 1.4 — BASIC SHELL	305.0	162.5	2858 IN LG'T TOTAL
1.4, .30, .080 C .032 A, 1.0 — SUPPORT WEBS	92.2	49.2	2 PER CHANNEL
1.4, .020 C .032 A — SUPPORT WEBS	21.2	11.30	180 REQ'D.
200x1400 MESH .16 #/FT² C .0544 #/FT² A. — SCREEN	143.0*	49.1*	ALL SIDES OF CHANNEL COVERED
.75, .25, .050 C .080 A, 1.0 — INTERFACE FLANGES	38.9	18.2	FOR RESERVOIR AND EQUATOR CONNECTIONS 24 REQ'D.
.62, .180 TEFLON, 3.0 — SUPPORT LINK	3.78	3.78	80 REQ'D.
C. 3/8 D.C. x .020 — DRAG STRUT	6.75	6.75	24 REQ'D.
.85, .60, CLEVIS, .8 TYP, 1.0 DIA. — TANK WALL FITTING	2.60	2.60	104 REQ'D.
CLEVIS, 1.0, .030 C .050 A, 3.0, 1.3 F.C. WITH — SUPPORT FITTING	8.0	4.0	80 REQ'D.
MSC. BOLTS, NUTS, RIVETS, ETC.	2.50	2.50	
TOTAL WT.	623.93	309.93	
10% CONTINGENCIES	62.39	30.99	
TOTAL	686.32	340.92	

* Includes back-up screen at 14.0 inch open face area.
44.0# for steel and 15.4# for al aly.
4 × 4 mesh × .025 Wire Dia.

Figure 2-53. Weight Estimate/Oxidizer Retrieving Channels



OVERALL CONFIGURATION

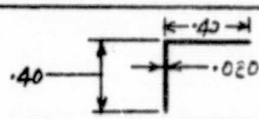
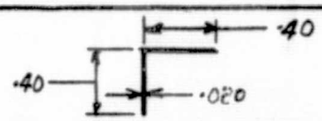
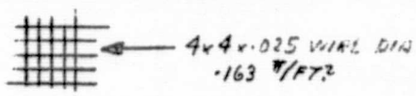
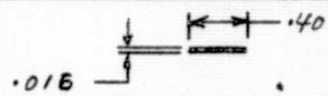
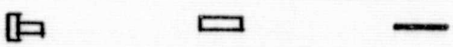
	WT. LBS. STEEL	REMARKS
 GORE PERIMETER FRAMES	86.7	18,100 INCH LGT. TOTAL
 GORE REINFORCEMENTS	61.8	12,880 INCH LGT. TOTAL 13 PER GORE
 CAPILLARY SCREEN	158.0	1052 FT^2 REQD.
	172.0	
 ACCESS OPN'G TRANSITION SECTION	15.0	
 OUTLET TRANSITION SECTION	12.0	
 BACK-UP STRIPS @ SCREEN ATTACHMENTS	59.5	SAME IF BRAZE IS USED DUE TO BRAZE MATL.
 SUPPORT FITTINGS	37.4	9 SUPPORTS PER GORE LINE 216 TOTAL
 MSC. RIVETS, SPACERS, GASKETS, BOLTS, ETC.	20.0	
TOTAL WT.	622.4	
10% CONTINGENCIES	62.2	
TOTAL	684.6	

Figure 2-54. Weight Estimate/Oxidizer Collector System

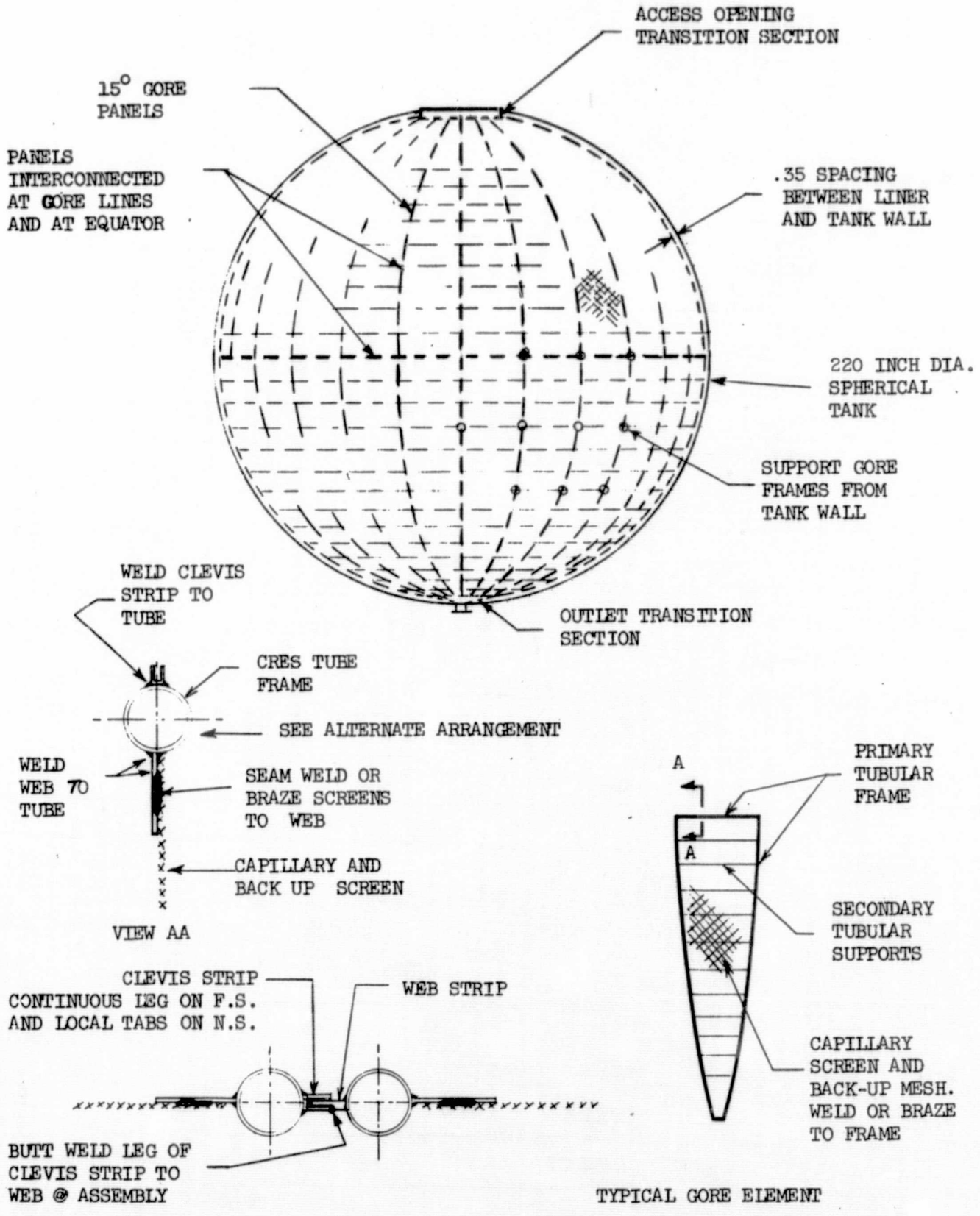
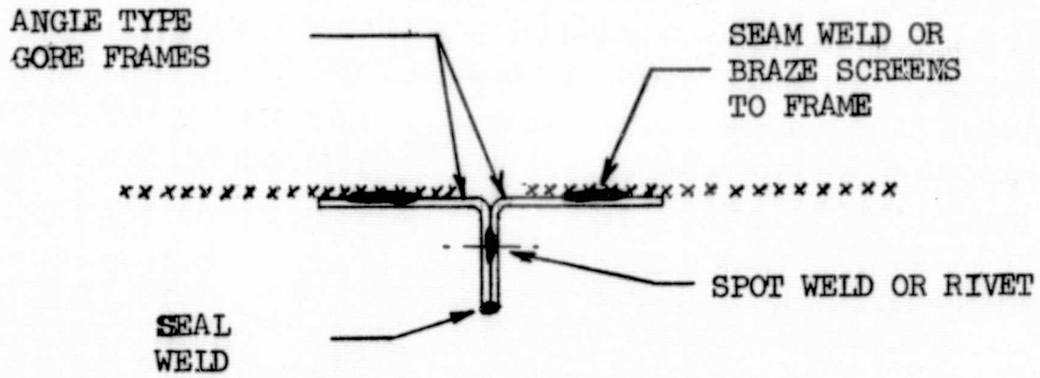


Figure 2-55. Oxidizer Collector System/Full Liner Concept



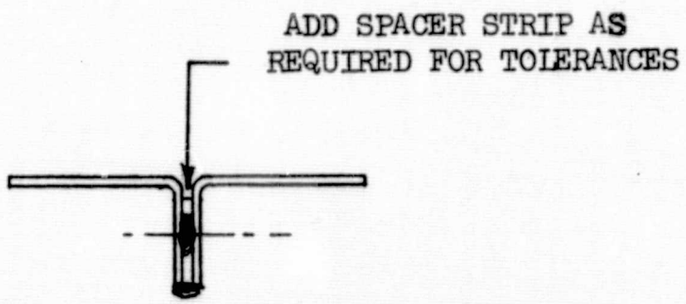


Figure 2-56. Alternate Gore Panel Construction and Interconnecting Arrangements

The screen weights are for the screen meshes initially used for the fuel system. These meshes values were changed to account for spillage and adjustments made to screen weight in Section 2.4. The screen attachment methods assume welding or brazing for the cases using steel and soldering or mechanical fastening for the arrangements using aluminum alloys. Weight variations between methods are small and are absorbed in the conservative areas of the estimate.

Since a low conductive type support arrangement is assumed, the aft end of the reservoir is connected to the tank wall using an omega shaped teflon, KEL F, or Mylar ring equipped with interface flanges and back-up rings. Detail designs may show that one flange can be removed by riveting the forward end of the plastic ring to the reservoir structure. For weight purposes, however, two flanges are assumed since the riveting method may require local stiffening provisions to assure a reasonable seal. Aluminum back-up rings with channel shaped cross sections are used for distributing the fastener loads. These rings are the split type to permit assembly.

A tubular type structural cage is used to support the reservoir assembly from the tank wall. Steel is used for this assembly and the lengths of the tubular members assumed at 28 inches (see Figure 2-51). These tube lengths are influenced by the slope of the cage; the cross sectional dimensions of the retrieving channels, clearances between the tubes and the channels, and the heat path length. The legs of the structure are attached to the tank wall at eight local points.

Bolts, rivets and pins are used to connect the retrieving channels and reservoir to the tank wall and for the interfaces between reservoir and channels. Therefore, an allowance in the miscellaneous column of Figure 2-51 is included. The allowance for the case using aluminum exceeds that shown for steel due to the anticipated increased complexity of attaching aluminum screen.

Oxidizer Retrieving Channels (Figure 2-52)

The retrieving channels, Figure 2-52, are basically curved beams with a channel cross section formed from flat panels. The span between support points is approximately 72 inches, therefore, the flat panel sections must resist local buckling and crippling actions from loads due to accelerations, vibrations and fluid impingements. This is accomplished by using a system of stiffeners which are attached to the panels, integrally formed with the panels or a combination of these methods. General instability of the beam is not considered a problem since large moment of inertia values are obtainable from the channel shaped cross section. The external loads are believed to be small, therefore, minimum gage materials (.020 for steel and .032 for aluminum) are used for the flat panel areas. A low conductive support system is assumed. The component breakdown and weight estimates are summarized in Figure 2-52.

The channel section shown in Figure 2-52 has flanged edges on the side panels to act as stiffeners for the free edge condition and to serve as stiffeners for the 16.0 inch wide panel and act as aides for vapor migration. The webs are tee or "Z" sections with a flange on one leg to stabilize the free edge and to prevent screen damage. The base of the webs are spot or seam welded to the channel wall. Figure B-6 , Appendix B, shows a structural check for the webs.

Support members oriented 90° to the above webs are required to give the beam a load carrying capability along the width direction and to act as a shear panel under side load conditions. The width of the web is assumed equal to the channel depth. Final designs will likely reflect large rectangular cutouts in the webs to permit liquid and gas flow. These cutouts are disregarded for this estimate since attachments will be required at the intersections between the webs and the stiffeners. Final designs will also reflect flanges at the edges of these members for attachment to the channel walls by spot or seam welding. The weight for these flanges are offset by neglecting the material removed from the cutouts.

The screen is not a structural member and is attached to the flanged sections of the channel by mechanical, braze or soldering methods. The assembly is non-removable and does not include a separate perimeter frame. Intermediate attachments can be made to the channel webs for stabilizing any diagram actions.

The aft ends of the channels terminate with a rectangular shaped flange for connecting to the reservoir. The flange section used contains a one-inch neck section for riveting or welding to the channel walls. Additional reinforcements and minor transitions parts may be required in the final design but are neglected at this time since the flange configuration is conservative.

A low conductive support system is used employing short links for the radial restraint attachments and tubular drag struts for lateral loads. The supports can be designed using teflon or steel. The weight summary of Figure 2-52 also includes allowances for the clevis type support fittings used on the channels and tank walls. Structural analysis and designs for the supports are shown in Figures B-1 , B-2 , B-3 , B-4 , B-5 , B-6 , B-7 , B-8 , B-10, B-11, B-12, and B-13. Earlier estimates indicated that channel depths ranging from the tapered configuration shown in Figure 2-52 to a fixed depth of 2.0 inches were to be included in the study, therefore, the 2.0 inch value was used in the structural analysis.

An allowance is included in the contingency column for fasteners such as bolts, nuts, rivets, gaskets, solder, etc.

Oxidizer Retrieving Channels (Figures 2-50 and 2-53)

The channels shown per Figures 2-50 and 2-53 are basically the same as that shown in Figure 2-52 except for reductions in the cross section and the addition of channel

units at the equator. The number of supports have been increased to compensate for the decrease in the channel depth and the added loads from the equator equal to that used at the ends which interface with the reservoir. The quantity of flanges was, therefore, increased from eight shown in Figure 2-51 to 24. The capillary screen micron rating and density were revised, and weight allowances added for a back-up support screen required at the open side of the channel. The capillary screen is applied to the four faces of the channel. The three sheet metal sides are perforated such that approximately 30 to 40% of the material is removed. The minimum gages previously established are assumed adequate for the Figure 2-53 design. The previous structural analysis was used as a guide for the weight assignments.

Oxidizer Collector System/Full Liner Concept

Figure 2-55 shows a 220-inch diameter tank fully lined with a steel capillary screen. The liner is basically a system of 15° gore elements which are interconnected at the meridians, the equator and supported from the tank shell. Transition collars are included at the access opening and outlet areas. These collars support the ends of the gore elements and serve as adapters between the profile of liner and the tank openings. A weight estimate is shown in Figure 2-54.

Gore Element Construction

The liner is subject to acceleration and vibration loads during the boost phase and minor pressure differentials during coast and unloading periods. The assembly, therefore, must include a structure which will resist these loads and provide sufficient stiffness such that the parts can be handled and assembled without altering the capillary screen properties. A typical gore element is shown in Figure 2-55. The unit consists of a primary tubular perimeter frame equipped with secondary cross members. Web sections welded to the tubes provide a land area for attaching the screens (see Figure 2-55, View AA). Clevis and web-type strips attached to the outboard edges of the perimeter frame provide the interconnections between gore elements. The transition collars are designed to interface with the tongue and groove edges of the tubes. The capillary screen is equipped with a back-up mesh. Both screens are seam-welded to the web sections.

General assembly consists of positioning the gore elements onto the transition collars while engaging the tongue and groove surfaces. The mating edges are held together with tools, while a permanent connection is made by butt welding the web sections to the clevis strips (see Figure 2-55). Accumulative tolerances are accommodated by full or partial engagement of the tongue and grooves.

The tubular framework shown in Figure 2-55 requires the attachment of strips to tubes or the procurement of extrusions having similar cross sections. The tubes create channels which are inaccessible for cleaning. The framework also protrudes into

the .35 inch spacing required between the tank wall and the screen surface. When considering tolerances the tubes may touch the tank wall at some areas. Figure 2-56 shows an alternate design which simplifies the framework and eliminates extensions beyond the outboard surface of the screen. The alternate method uses angle type frames and stiffeners with the screens seam welded to one leg of the angles. Structural connections at the gore and equator lines are made by spot welding or riveting the legs of the angles. A seal is formed by welding the inboard edges of the angle legs. Spacers may be added between the angles for absorbing tolerances.

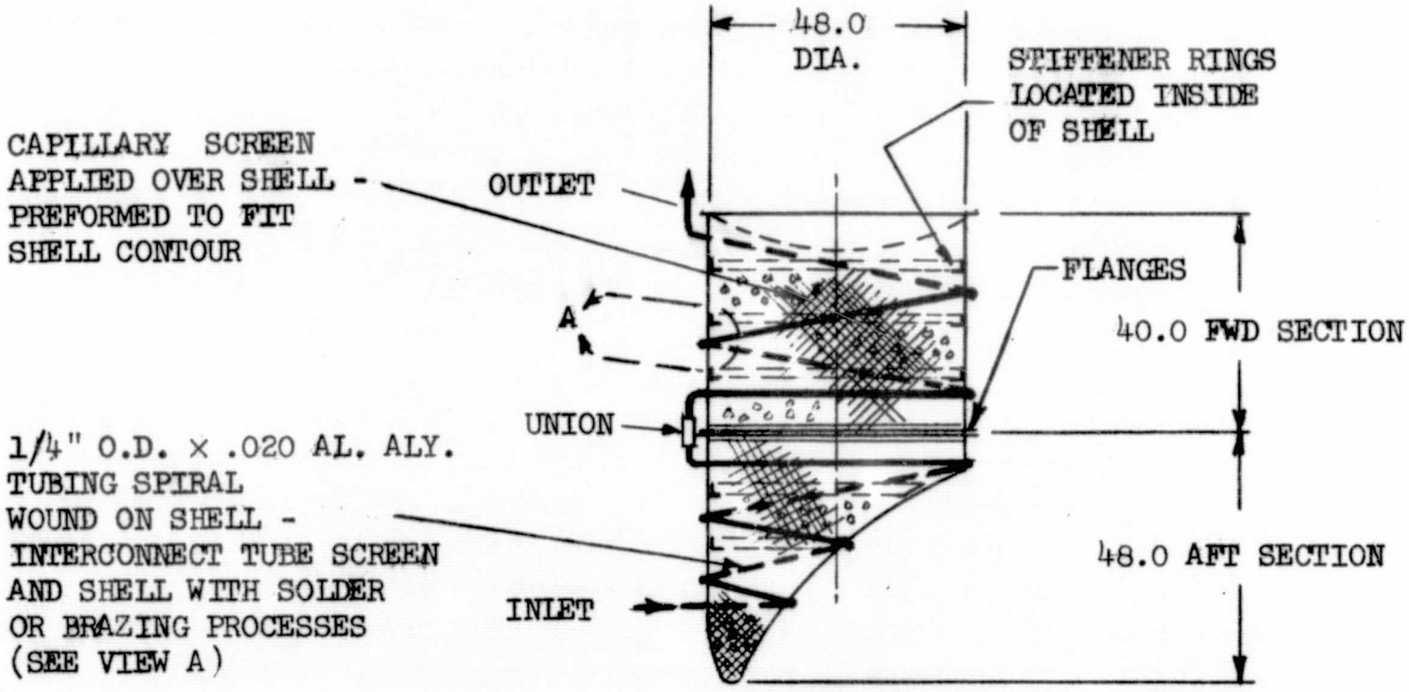
Supports

The liner is supported from the tank wall along the meridian and equator lines as shown in Figure 2-55. Since the spacing between the screen and the tank wall is .35 inches, the gore frames must include local structural fittings with attachment points located inboard approximately two inches from the screen surface. Fittings welded to the tank wall provide the mating attachment points. The supports are required to resist the external loads imposed on the liner while compensating for relative movements between tank and screen. The attachments must also be capable of absorbing tolerances at assembly. Support fitting details were not defined, however, a weight estimate was made per the general profile shown in Figure 2-54. The configuration employs a sheet metal can-type fitting equipped with a rod and spring device. The can and rod are attached to the liner frame and the tank wall respectively.

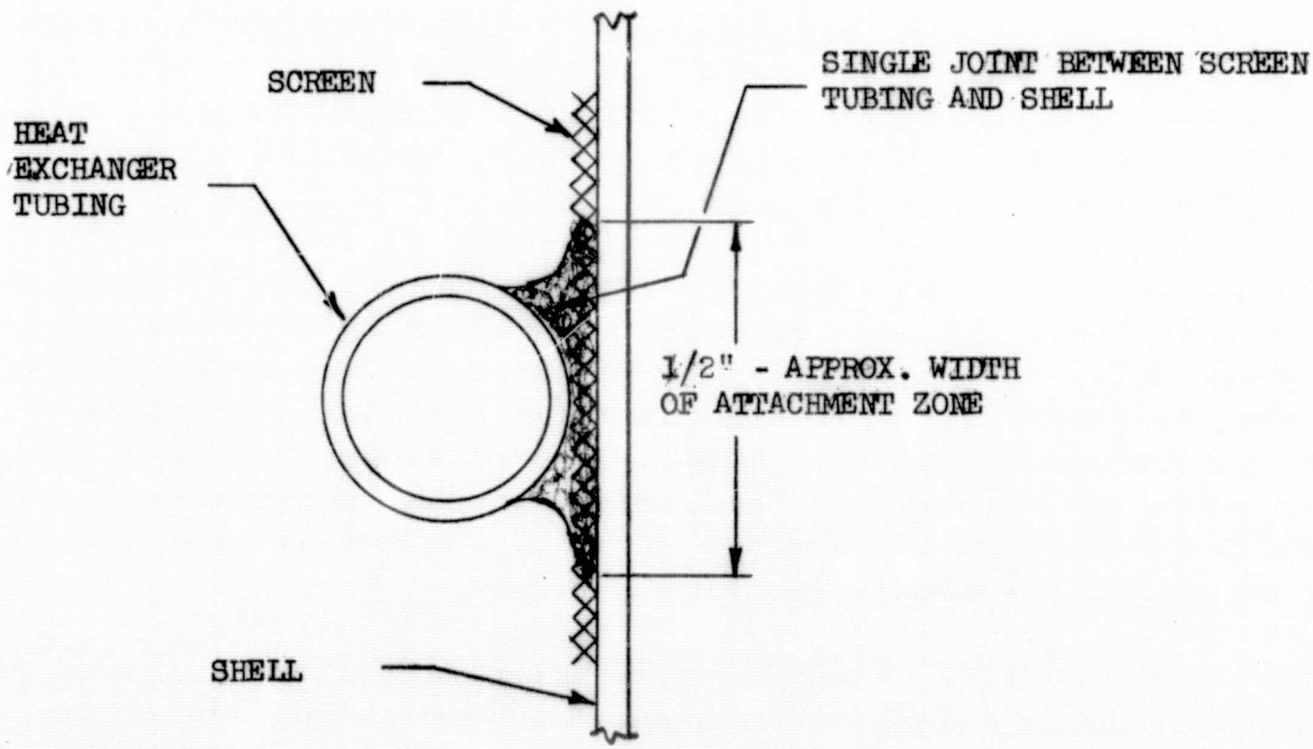
2.3.3 HEAT EXCHANGER ATTACHMENTS. Several heat exchanger attachment methods were considered including locating heat exchanger coils outside the stiffening rings, using hat shaped rings, positioning the coil on the stiffener ring and the recommended method; using a webbed tube for the heat exchanger coil and seam welding the tubes in as part of the structure.

The basic reservoir structure is a stiffened sheet metal shell covered with a capillary screen. It is required to cool the outboard face of this shell with a system of heat exchanger coils. A continuous conductive path between the coils and the reservoir surface is essential. From a manufacturing and structural basis, the location of the coils may become important. Tubes which are soldered or brazed to the skin surfaces between stiffeners may present warpage and material metallurgical problems which in turn may cause structural degrading. Cases 1, 2, 3 and 4 were generated for evaluting tube locations and methods of attachment.

Case 1 uses a spiral type coil for the forward and aft sections of the reservoir. At installation, the two coil sections are connected with a single union fitting. The capillary screen is preformed, placed over the shell and attached (using a seam connection) at the interface flanges and the forward ring. The coil is placed over the screen and continuously attached along the spiral path such that a common bond between shell, screen and tube is formed. This system is thermally advantageous, but may present warpage problems since the major portion of the coils are located



GENERAL ASSEMBLY



VIEW A
TYPICAL TUBE/SCREEN SHELL ATTACHMENT

Figure 2-57. Fuel Reservoir Heat Exchanger Installation, Case 1

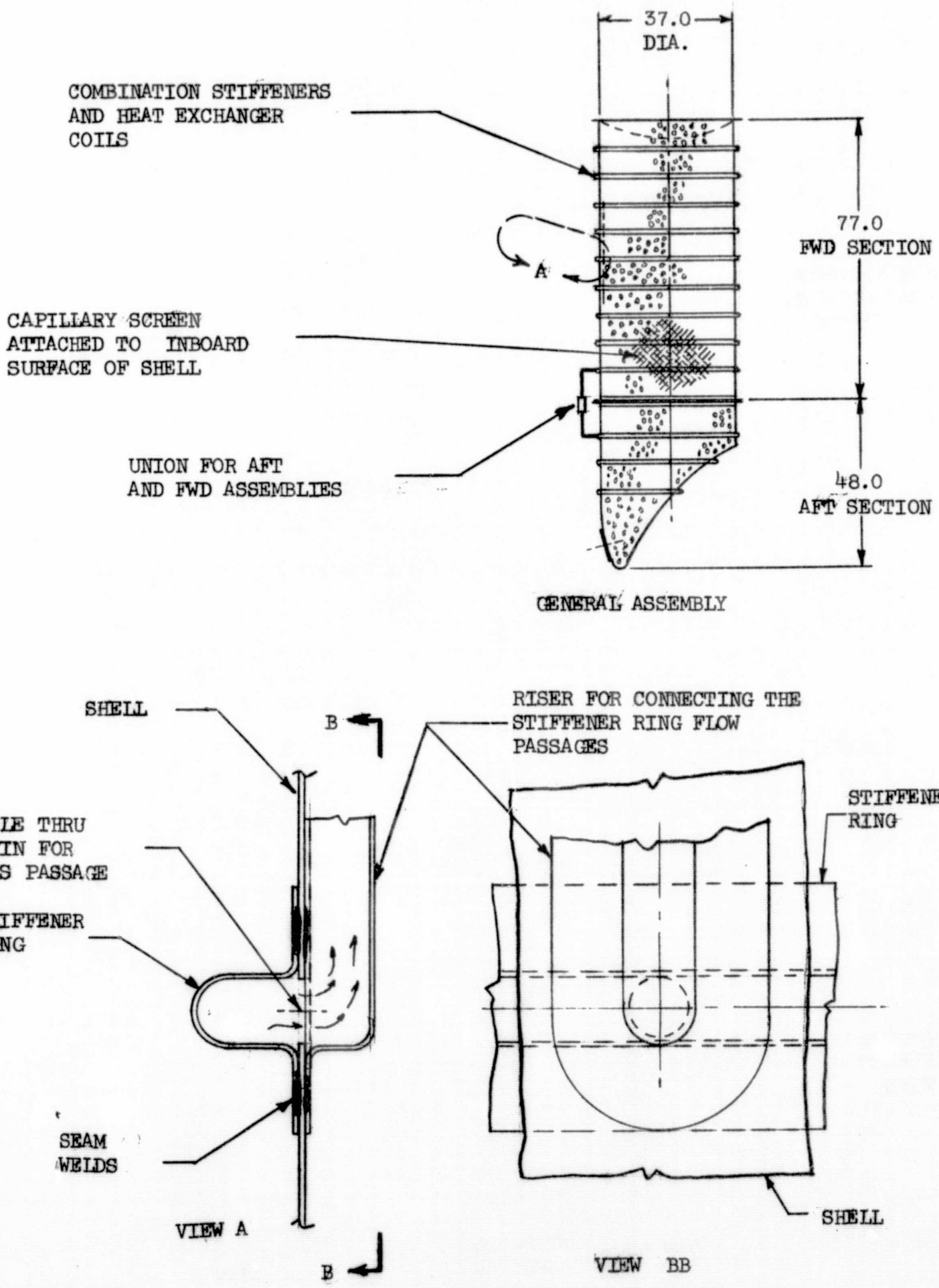


Figure 2-58. Fuel Reservoir HeatExchanger Installation, Case 2

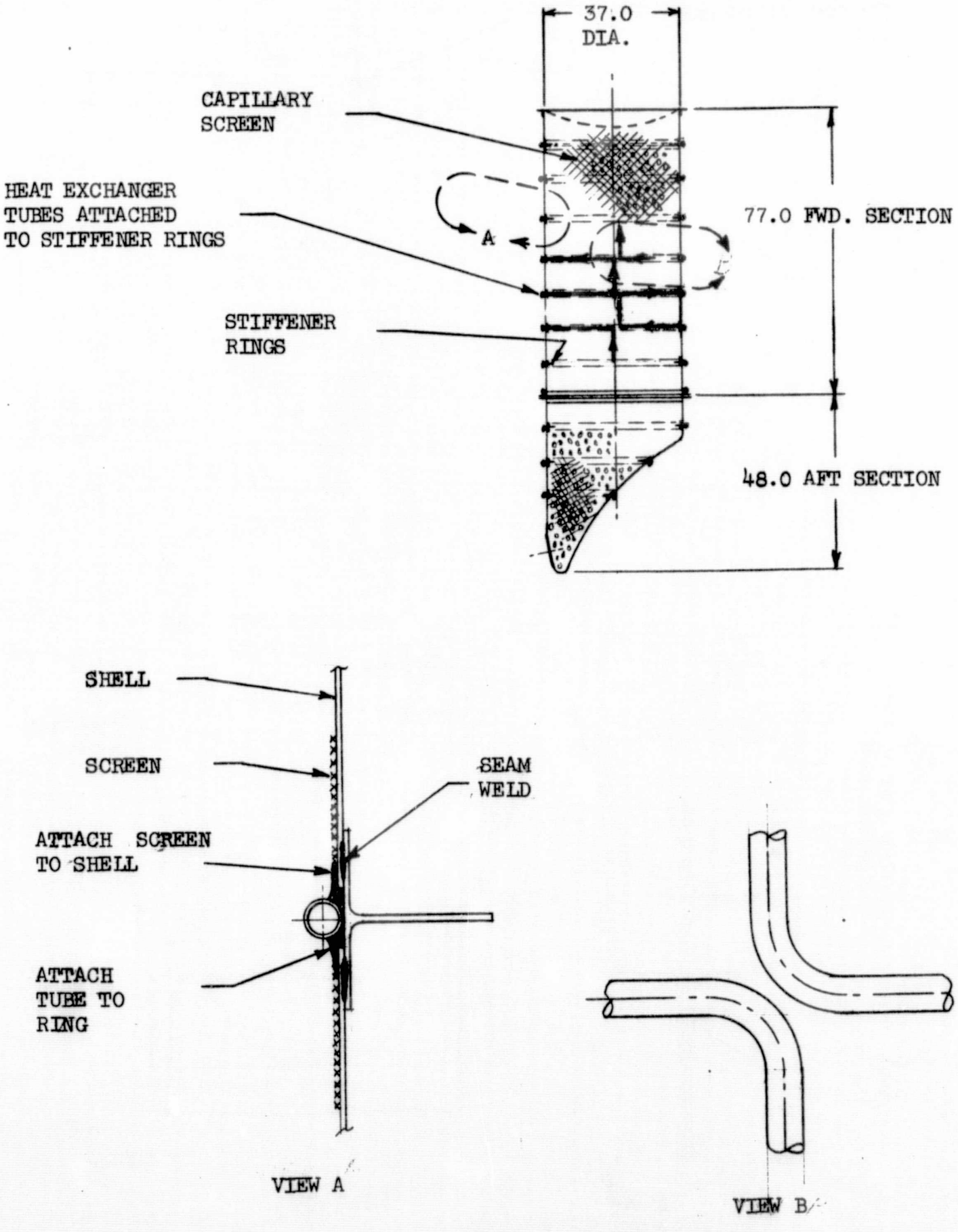


Figure 2-59. Fuel Reservoir Heat Exchanger Installation, Case 3

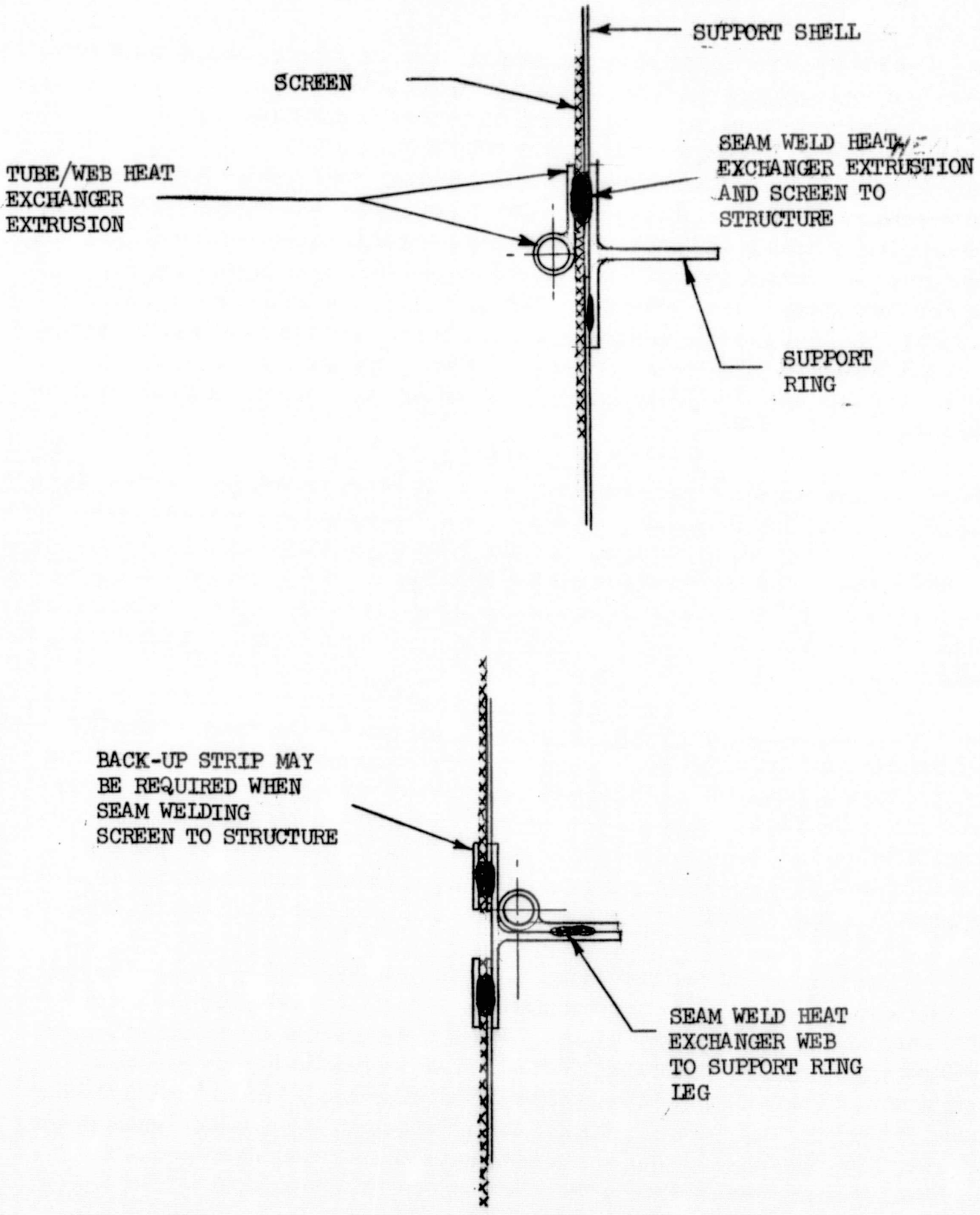


Figure 2-60. Heat Exchanger Installation, Case 4

outside the stiffener rings. With respect to manufacturing, Case 1 is not recommended.

Case 2 eliminates the coils by using hat shaped rings which serve as structural stiffeners and heat exchangers. The rings are interconnected using stringer type riser sections, with one end of each ring blanked off to provide a continuous flow path. The flow is, therefore, circumferential at each ring; through a hole in the structural skin; and through the riser section to the next adjacent ring. This type of construction reduces warpage problems since the rings and risers can be seam-welded to the shell. The capillary screen is applied separately with seam type attachments near each ring. The ring cross sections are non-circular and depend upon the structural loads. This requirement promotes non-uniform flow paths which may be a disadvantage for heat exchange. The flat sections of the flow path walls are sensitive to pressure, therefore, leak checks at pressures above operating would require close monitoring. Cleaning procedures are also complicated due to the numerous faying surfaces in the flow path.

Case 3 positions a coil on each stiffener ring which reduces warpage since the ring is a rigid member. The coils may be attached as a separate assembly to the rings or installed as a one piece circuit after the completion of the structural shell. The former method would use brazed or welded connections at the terminals (depending upon material) with the fittings and the tube ends spaced from the shell for tool clearances. The screen is applied in belt sections between the coils and attached near the stiffener rings.

The prime requirement for heat exchanger attachments is a continuous conductive path between tube and tank wall surfaces. Brazing provides a good conductive path and structural support, but promotes metallurgical changes to the mating material due to the brazing temperatures. Locally brazing by using a torch is considered impractical since the base material temperature is difficult to monitor and general structural warpage may result. If a dip brazing process is used, the complete assembly would require handling with special procedures protecting the screen openings.

A second approach is the use of solder. An area of the structure and a portion of the tube are gold plated. The attachment is made using a solder alloy (50% lead + 50% indium) which melts at approximately 450°F and is ductile at low temperatures. Although a good conductive path and adequate structural capability are attained, the method is not readily adaptable to positive temperature control of the base materials during soldering. For example, if a gun or torch is used, the operator (unknowingly) may over heat some areas. Uniform temperature control using an oven would be required. It is also questionable what effects the 450°F temperature will have upon the base material. The process is also complex and costly due to the local gold plating on the joining surfaces.

A third method mechanically attaches the tubes using a series of studs welded to the structure and equipped with tube clips. A continuous conductive path is provided

by filling the cavity between the tank wall and the tube with a conductive bonding mix which adheres to the tube and mating surfaces. This approach relieves the temperature problems, but presents new difficulties. Thermal gradients cause dimensional variations which may not correspond with the bonding alloy changes due to differences in thermal and elastic properties. Stresses are, therefore, developed at the bonding planes are through the conductive path. When these conditions are combined with vibrational modes, it becomes questionable if an effective conductive path is maintained. Inspection is also difficult since the arrangement is not readily adaptable to positive acceptance or rejection.

A recommended design (case 4) uses a soft aluminum (1100) extrusion consisting of a tube attached to a web. The web is seam-welded to a structure. An alternate construction is available which replaces the special extrusion with an assembly consisting of a web brazed to a tube. The design per Case 4 provides a positive conductive path, adequate support, adaptability to standard inspection procedures, and can be applied without metallurgical changes to the base material beyond the weld zones. Stresses from the thermal gradients are not considered a problem due to the small temperature differences between the fluid in the tubes and the support structure. Contributions to discontinuity stresses are considered negligible due to the small cross sectional area of the web tube combination and the low yield point of the material. To simplify the seam welding procedures it is recommended that the tubes be installed in a series of circles using jumper tubes to interconnect each circular element (similar to that shown for Case 3). The seam welding is discontinued near the ends of each circle, a section of web removed, and the tube bent away from the tank surface to permit a butt welding attachment to a jumper tube. The space between the end of the tube and the tank wall will vary depending upon the welding technique employed. The location of the weld is optional along the span of the jumper. An orbit arc type system is recommended.

The seam welding of aluminum screen to a support structure is sensitive to the mechanical actions of the welding roller and the current. In some cases, the process is improved by using a back-up strip which sandwiches the screen between two metal layers. For cases requiring attachment of the heat exchanger coils to the screen surfaces, the web section of the coil replaces the back-up strip.

2.4 SYSTEMS COMPARISONS

Based on the analysis and design of Phase I, promising capillary control system designs were chosen for comparison with other means of propellant transfer. From the designs considered, recommendations are made for the S-IVC restart mission and LOX tanker mission. Comparisons were made based on system weight, reliability, and cost. A summary of the comparison is given in Figure 2-62 and Tables 2-3 through 2-8.

2.4.1 S-IVC SYSTEM COMPARISONS. Promising capillary control systems were compared with linear acceleration, bladder and dielectrophoretic systems for accomplishing the S-IVC mission restart requirements.

Weights

System weights were assessed based on differences in component weights needed for accomplishing the required mission. However, no other pressurization system weights were determined since it was felt that pressurization systems would be similar for the other transfer systems being compared. The incremental increase in pressurant system weight required by the bladder system compared to the other systems is included in the comparison. On the other hand, since vent systems would be slightly different for the various restart systems, vent system weight and reliability must be included in the comparison. Because of the uncertainty in settling time, a range of restart system volumes was considered.

Capillary Devices

For means of comparison the surface tension weight penalty consists of the restart systems and the collector for the vented liquid. Residuals for a high g level outflow are assumed to be similar for the settling, surface tension and dielectrophoretic system comparisons.

The range of start basket volumes considered initially are shown in Figure 2-46. The annular shapes proved to be more efficient that the cylindrical shapes due to the increased vapor ingestion and liquid spillage problems with the cylindrical shape. Based on the usable volume (total-residuals-spillage) available with the annular shapes, a curve of weight vs. usable volume was generated.

Screen weights generated had been for higher screen microrating than eventually dictated by fluid analysis. Thus, for comparison purposes, screen weight estimates of .60 lb/ft^2 used in the weight breakdowns for stainless steel screen were reduced to .16 lb/ft^2. Corresponding adjustments were made for aluminum screen. These changes represent approximately a 15% decrease in system weight. For the engine flow rate of 17.3 cps the usable volume was converted to engine firing time. Within the volume required for the S-IVC mission the start basket weight is given by the curve of Figure 2-61. The weight of the oxidizer start basket was conservatively calculated to be 97.1 lbs (see Figure 2-47). In order to properly cool the start baskets it is necessary to use the cooling capacity of a thermodynamic vent system. A liquid inlet to this system is required for sufficient cooling capacity. The collector system for a thermodynamic separator system which is constructed of tubular screens will be 19.3 lbs. Thus, the total system weight penalty using aluminum components is given by the curve of Figure 2-61.

For the fine mesh screen required for efficient system operation some manufacturing

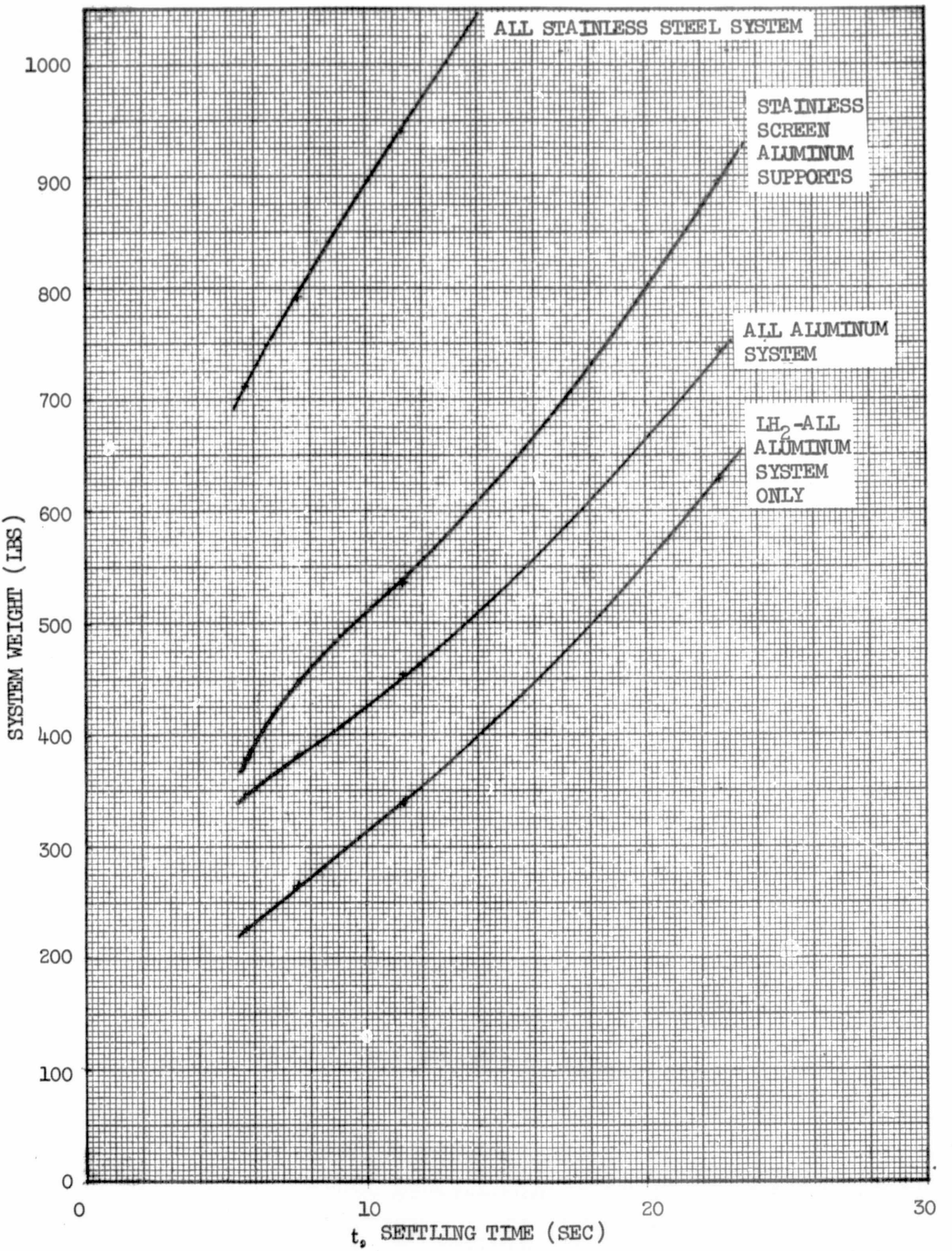


Figure 2-61. S-IVC Screen System Weights

development was required to draw fine aluminum wires. There is considerable weight savings using aluminum screens compared to using stainless steel. A comparable system in stainless steel according to Section 2.3 weight estimates will be as shown in Figure 2-61. Since aluminum screens were not available at this time an aluminum structure with stainless screens was considered. This system would weigh approximately as shown in Figure 2-61.

Dielectrophoresis

Weights for dielectrophoretic systems were determined based on a configuration employing conical electrodes near the tank outlet and ribbon electrodes to collect propellant. Rather than keep the system continuously on during orbit, several hours before restart the system is turned on and the cryogenic is collected by the ribbons and stored in the closely spaced conical electrode system. The ribbon electrodes were sized and spaced based on information in Reference 4. Conical electrode spacing was determined using the equation

$$S = \sqrt{\frac{V^2 (K - 1) \epsilon_o}{\rho g h}}$$

where S is the plate spacing, V is the voltage, K is the dielectric constant, ϵ_o is the permeability of free space, ρ is the density of the fluid, g is the acceleration level, and h is the head to be contained. Spacing was limited by the electrical breakdown in gaseous hydrogen that may occur with high voltages. The influence of helium on spacing limits was not included.

System weight was based on using a 10 KV power source and 10^{-6} g's ambient gravity level. This system will allow liquid to spill out at a fairly rapid rate at .337 g's. It was found, however, that a system to retain liquid at .337 g's, even with a 100 KV power source, would require plate spacing which would allow electric breakdown. Thus, some spillage must be accepted. By fashioning the outer screen of the cone of similar mesh and design as the surface tension start basket, the usable volume within the DEP system should be proportional to the usable volumes in the surface tension device. Support weights were found based on the average ratio of support weight to surface area for the surface tension device. Electrical system weights include the power supply including transformer and rectifier, the high voltage cables, wiring, feed throughs, transistors, diodes, resistors and capacitors. The energy source for the electrical power supply is a fuel cell consisting of reactants and tankage. No liquid collectors are required for the thermodynamic vent system since propellants will be collected just before restart minimizing required restart system cooling. The following table gives a system weight breakdown for the S-IVC DEP system.

Table 2-3. S-IVC Mission, DEP Weights

Engine Firing Time, t (Sec)	LH_2-Cone Electrode + Supports	LO_2-Cone Electrodes + Supports	Ribbon Electrodes	Power Supply	Electrical System	Total Weight
2.5	174	32	38	30	30	304
3.6	222	32	43	30	30	357
7.3	535	32	63	30	30	690
9.4	719	32	71	30	30	882

Linear Acceleration

The maximum weight penalty for settling the propellants using the main engine flow is W= 483.5 t. This is based on all liquid flow to the engine, where t is the engine firing time (sec).

For the S-IVC mission considered 1.33 lbs of stage weight = 1 lb propellant. Thus, putting the settling weight penalty in terms of hardware weight yields W = 642 t.

For all gas settling in the idle mode, the fluid will impinge the aft bulkhead after 8.1 seconds. The idle mode flow rate is 18 lb/sec, with the exchange ratio of 1.33. This represents the minimum hardware weight penalty for settling of 24 t. In order to cover the feedline an engine firing time of well in excess of 8.1 seconds will be required. It was felt that this time would exceed 24.3 seconds which will make the weight penalty greater than the surface tension system. This assumption is based on the empirically derived practice of using three times the initial impingement time for the collection time in relatively low Weber number cases (Reference 14).

The main problem with the linear acceleration method of providing settled propellant is the uncertainty in the liquid or vapor proportions which might exist in the feedline. Thus, in order to assure that settled propellant exists over the outlet, the settling time must approach 25 seconds even though some liquid may be flowing in the feedline prior to this time.

Another assumption is that fluid used to settle the propellants is actually wasted propellant and not available for useful propulsion.

Positive Expulsion

A review of current technology in cryogenic positive expulsion devices included consideration of diaphragms, bellows, metal and polymeric bladders. Current technology assessments indicated that polymeric bladders were most applicable for the S-IVC mission.

Several bladder designs were considered for the S-IVC mission. For large tanks bladders are difficult to deploy due to general lack of "clean" tank walls. However, weight estimates were made based on References 10 and 12. The transfer systems would consist of a perforated standpipe along the vertical axis of the tanks with the bladder tight against the standpipe. Pressurant gas flowing through the standpipe would inflate the bladder forcing liquid out the engine feed line. For the LH_2 tank, .25 mil Mylar was used, while for the LOX tank, .5 mil Kapton was the bladder material.

System weight consists of standpipe weight, bladder weight and vent system weight. At the start of the thirty day coast period the bladder is expanded from the initial run of the S-IVC_2. As the tank is heated in orbit the bladder can be vented until it corresponds to its minimum volume configuration. After this, a thermodynamic separator must be used to vent the tank. Vapor formed in the main bulk of propellants can be condensed before restart by pressurizing the bladders, assuring pure liquid flow to the engine. However, since helium, the pressurant, weighs more than the boiled off hydrogen gas, it is more efficient to maintain the bladder in its expanded state and vent solely through the thermodynamic separator. Before restart the bladder is expanded to compress the vapor formed. Additional pressurant gas is required for this mode of transfer. For the 2140 Btu/hr heat flux to the LH_2 tank, 509 lbs of helium will be required to condense the vapor formed. Using the 1.33 exchange ratio which is optimistic for pressurant penalty gives 676 lbs of equivalent hardware weight.

Total system weight includes: LH_2 tank, bladder weight = 41 lbs, hardware weight = 290 lbs. Thus, total LH_2 system = 331 lbs. For the LOX tank: bladder weight = 33 lbs, hardware weight = 92 lbs. Thus, total LOX system weight = 125 lbs. Total S-IVC bladder system hardware weight is 456 lbs. Residuals in the bladder case could be much less than other systems if "clean" tanks are used. The presence of the vent system and support structure of the standpipe will probably increase residuals to approximately the level of the other systems. System hardware weight penalty will thus be equal to 1132 lbs.

Weight comparisons for S-IVC propellant transfer systems are shown in Figure 2-62. The curves show that aluminum screen system is the lowest weight system for the range of reorientation times considered realistic. Ten seconds is the best estimate for full flow settling, while 24 seconds is estimated for idle mode method settling. Subsequent to this comparison, aluminum screens were fabricated in the mesh sizes required for the S-IVC start baskets. This gives the capillary devices a marked weight advantage over the other methods considered.

Reliability

Relative reliability for 30 days was determined for the candidate systems based on the settling system having a reliability of 1.0. Adding a thermodynamic vent system

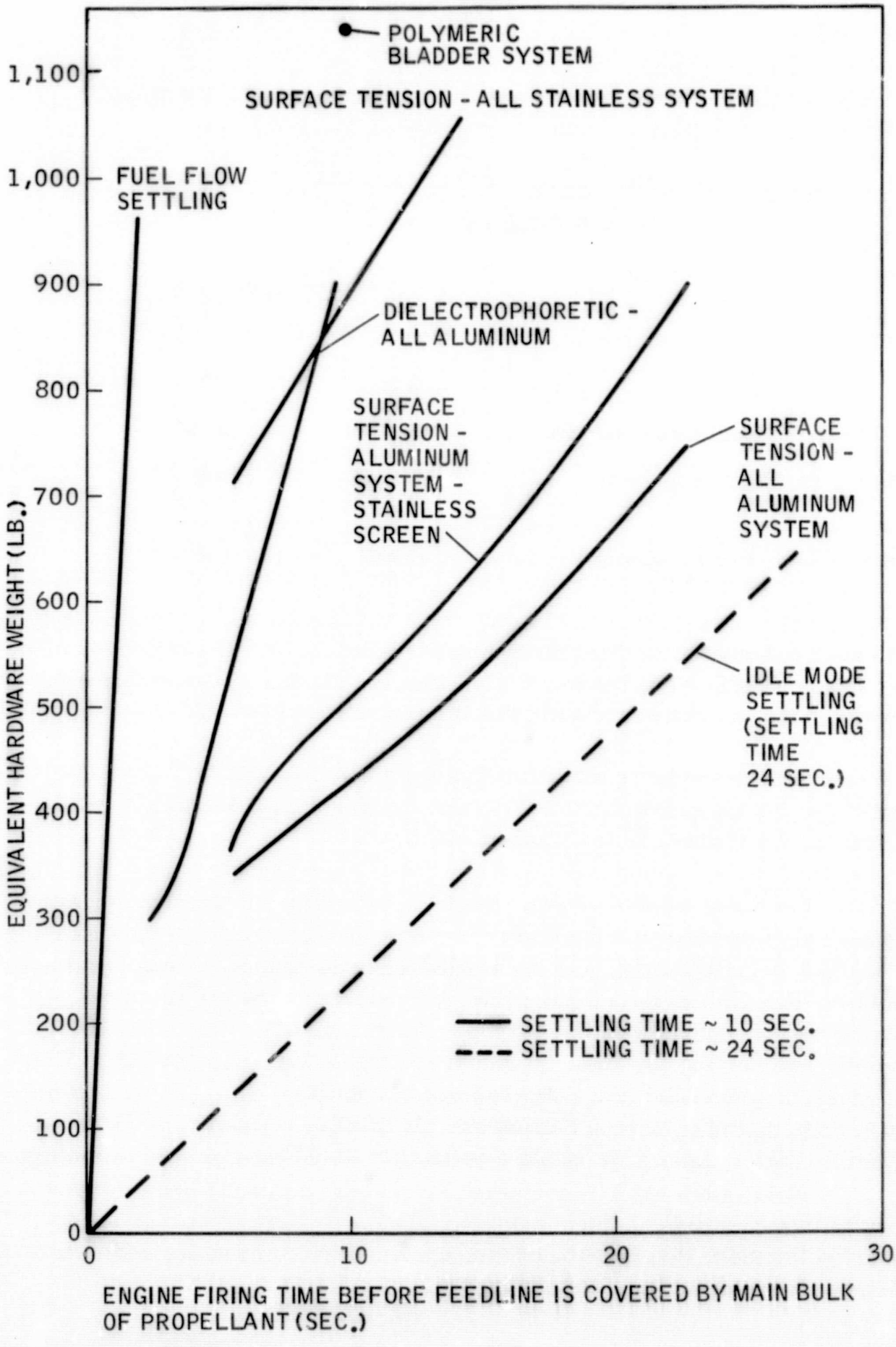


Figure 2-62. Equivalent Hardware Weight Comparison for S-IVC Mission Restart

to the settling system reduces its reliability to .9505. Adding surface tension components with a comparatively high structural reliability decreases the LH_2 system reliability to .9495. The dielectrophoretic system has the reduced reliability of electrical components. Reliability numbers are given below in Table 2-4 .

Table 2-4. S-IVC Restart Systems LH_2 Tank — Relative Reliability

System	Relative Reliability	
	LH_2 Tank	$LH_2 + LO_2$ Tank
Settling	1.00	1.00
Settling With Thermodynamic Vent System	.9505	.9505
Surface Tension With Thermodynamic Vent System	.9495	.9484
Dielectrophoresis With Thermodynamic Vent System	.9431	.9400

Relative Reliability was not determined for the bladder system due to a lack of available data for cryogenic operation, however, a bladder system with a thermodynamic vent system would have the lowest reliability of the systems considered.

The data used to determine these relative reliabilities were obtained from FARADA using a factor of one for the coast phase and the recommended missile factor for the boost phase, i.e. 10 for diodes, 25 for transistors, etc.

For the LOX tank, there are possible safety problems with the dielectrophoretic and bladder systems. Dielectrophoretic system arcing in a LOX environment was considered in Reference 9 . Similarly, polymeric bladder materials have been found to be impact sensitive in a LOX environment. Boeing is currently testing Mylar and Kapton film in order to dispense with this problem (Reference 10). Assuming these potential problems are solved, the rankings would still remain as given in Table 2-4. with bladders at the bottom of the list. The relative reliability of the settling system would remain the same, while surface tension overall relative reliability would decrease to .9484 and dielectrophoretic relative reliability would become approximately .940.

The data presented indicates that surface tension systems are competitive with other types of restart systems when compared on the basis of relative reliability.

Costs

Relative costs were determined for the S-IVC restart systems based on vendor contacts in-house estimates and information obtained from References 4 and 11. System cost

is based on restart systems for both tanks including baffling and installation of these systems in the S-IVC tankage.

Table 2-5. S-IVC Restart Systems — Relative Cost

System	Relative Cost
Linear Acceleration	1.0
Surface Tension	2.1
Dielectrophoresis	2.5
Bladder System	3.1

Relative costs indicate that surface tension systems compare favorably with systems other than linear acceleration. The significant weight reduction which is possible using a surface tension system may justify this increased cost.

Manufacturing Feasibility

Fabrication of fine mesh aluminum screen capillary devices may require some additional manufacturing development. Fabricating a dielectrophoretic device to work safely in a LOX environment is likely to be more difficult than the screen development required. Bladder system reliability and impact resistance in LOX must also be proven.

Conclusions

Surface tension systems appears to have substantial weight advantages over other types of systems. The linear acceleration system has a lower cost and a higher reliability. The surface tension system weight advantage should offset the cost of the system considering the high cost of putting the additional weight in orbit. Also, if more than one restart is anticipated, the fixed weight of the surface tension system would become less of a relative weight penalty, increasing the weight advantage of this system.

2.4.2 LOX TANKER SYSTEM COMPARISONS. For the LOX tanker weight comparison, pressurization, secondary propulsion and transfer system weights were considered. (For the mission ground rules used see Table 2-2.) The transfer systems considered were linear acceleration (settling), surface tension dielectrophoresis and bladder. Comparisons are made for the third tanker of the mission.

Weight

Pressurization system weights were assumed equal for all the systems except for the bladder system. Vent system weights are included for all systems, as are

differences in propellant transfer hardware. Secondary propulsion system weight penalties are included for all the systems with the exception of the bladder system.

Surface tension system weight is as described in Figures 2-50 and 2-53. The vent system is a thermodynamic separator with cooling channels inside the retriever channels of Figure 2-33. This approach is a modification to the design indicated necessary by the thermal analysis. In order to reduce system weight penalties due to excess residuals, the secondary propulsion system is utilized for scavenging the tanker during the final portion of transfer. The full liner system of Figure 2-55 was also weighed out and is presented in Figure 2-54.

Two settling systems were considered for purposes of comparison. One system utilized a low g settling acceleration (3×10^{-5}) throughout the transfer. The other method used an increased acceleration of 6.5×10^{-4} g's at the end of the transfer (200 seconds) to reduce residuals. A thermodynamic vent system was used to control tank pressure. A more compact vent system than used with the surface tension device is possible because cooling of the tank walls is not required. System weight penalty is shown in Table 2-6.

For the dielectrophoretic system, the system design is similar to the S-IVC case with a central reservoir of concentric cones and a set of ribbon electrodes to collect the propellant before transfer. In sizing this system to resist the 10^{-3} g disturbing acceleration it was necessary to go to excessively high voltage requirements (500 KV) to obtain a plate spacing which would not cause excessive weight penalty. In spite of this, the system chosen will still have an electrode spacing less than the breakdown spacing. Thus, successful operation of this system without serious safety hazards is doubtful. The vent system used for weight comparison is similar to the one used for the settling system. Secondary propulsion requirements are similar to those of the surface tension system. A weight breakdown is given in Table 2-6.

Bladder system weight was determined based on using a bladder of 10 layers of .5 mil Kapton and an aluminum standpipe in a configuration similar to the one suggested for the S-IVC LOX tank. As in the S-IVC case, excess pressurant must be used to collapse ullage formed from venting. Also, residuals will exceed those estimated for other methods unless the SPS is used to reduce residuals. If this is the case, SPS + residuals will be 777 + 33 lbs = 810 lbs as compared to 925 lbs for draining without using thrusting. The presence of standpipe supports and the thermodynamic vent system indicate that a relatively high amount of residuals will occur.

Table 2-6 shows that the all aluminum channel surface tension system weight penalty is less than all systems considered with the exception of the bladder system. For the bladder to operate properly the tank must be free of baffles, PU probes and other obstructions which would interfere with proper bladder expansion.

Table 2-6. LO_2 Tanker Weight Comparisons

TYPE OF PENALTY	SETTLING	SETTLING WITH SCAVENGING	ALUMINUM SURFACE TENSION (CHANNELS)	ALUMINUM SURFACE TENSION CHANNELS (STAINLESS SCREENS)	STAINLESS SURFACE TENSION (FULL LINER)	DIELECTRO-PHORESIS	BLADDER	ALL STAINLESS (SURFACE TENSION CHANNELS)
VENT SYSTEM	10	10	25	25	50	10	10	2
TRANSFER SYSTEM	100	100	417	522	685	488	163	828
RESIDUALS	1,883	33	33	33	33	33	925	33
SECONDARY PROPULSION	700	1,467	777	777	777	777	-	777
ADDED PRESSURANT	-	-	-	-	-	-	30	-
	2,693	1,610	1,252	1,357	1,512	1,308	1,128	1,663

Looking at the surface tension systems, the weight penalty for the full liner concept is slightly less than the weight penalty for the channel and reservoir system. This does not take into account increased boiloff which would be required to prevent vapor from forming inside the liner. The magnitude of this boiloff may be more than sufficient to compensate for the reduced hardware weight. From a feasibility standpoint, however, it was felt that a channel design could be shown to be practical using cooling means which are normally available without increasing boiloff losses. The cryogenic full liner system is not desirable from a thermal design standpoint because all the heat incident on the tank surface must be removed by the thermodynamic vent system to prevent vapor formation within the screen liner. This requires that portions of the tank be overcooled (this overcooling can be reduced if the tank can be effectively mixed) causing the vent flow rate to exceed the normal boiloff rate, allowing the tank pressure to decay. This is unlikely to be a satisfactory requirement for the LO_2 tanker mission where a 30 day orbital stay time is needed. In either case, however, weights are competitive with other systems. Considering potential safety hazards with other low weight systems, the surface tension propellant transfer system certainly warrants additional study.

Reliability

For the 163-day mission relative reliability was determined for the systems considered in a manner similar to that in the S-IVC case.

Linear acceleration was assumed to have a reliability of 1.0.

Reliabilities of the candidate systems are given below in Table 2-7 in order of relative reliability.

Table 2-7. Relative Reliability of LOX Tanker Transfer Systems

Transfer Systems	Relative Reliability
Linear Acceleration (Settling With Thermodynamic Separator)	.7689
Surface Tension With Thermodynamic Separator	.7581
Dielectrophoresis	.7240

Bladder reliabilities were not determined due to lack of available information, however, reliability should be lower than the other systems considered. Failure rates were determined as described for the S-IVC mission.

As mentioned previously, serious potential safety problems exist with the dielectrophoretic and bladder systems which may seriously impair their usefulness in a LOX environment. Manufacturing feasibility problems are similar to those discussed for the S-IVC system comparison.

Costs

Relative costs were determined from vendor contacts, in-house estimates and information from previous studies (References 4 , 11 and 12).

Table 2-8. Relative Cost of LOX Tanker Transfer System

Settling System	1.0
Surface Tension System	2.5
Bladder System	2.5
Delectrophoretic System	2.7

This includes the cost of the actual transfer system including baffles, vortex suppressors and transfer devices plus assembly of the system into the tanker.

Conclusions

The surface tension system appears to be competitive with other transfer systems. Bladder compatibility in a LOX environment does present an additional drawback of this system. Surface tension systems, since they are relatively low in weight and do not present the safety problems of the dielectrophoretic or bladder systems, appear to warrant further study.

3

REFERENCES

1. Masica, W. J. and Petrash, D. A., "Motion of the Liquid-Vapor Interface in Response to Imposed Acceleration," NASA TND-3005, September 1965.

2. J. A. Salzman and W. J. Masica, "Experimental Investigation of Liquid Propellant Reorientation," NASA TN D-3789, January 1967.

3. Tucker, R. H., "The Development and Verification of Theoretical Models of Performance of Wire Cloth Filter Media," PhD Thesis, Oklahoma State University, 1966.

4. Mitchell, R. C., Hudson, V., Stark, J. A., and White, R. C., "Study of Zero Gravity, Vapor/Liquid Separators," GDC-DDB65-009, Contract NAS8-20146, January 1966.

5. Blatt, M. H., Burton, K. R., Evans, E. A., Merino, F., and Siden, L. E., "Low Gravity Propellant Control Using Capillary Devices in Large Scale Cryogenic Vehicles," First Quarterly Progress Report, 584-4-208, Contract NAS8-21465, October 1968.

6. Blatt, M. H., Stark, J. A., and Siden, L. E., "Low Gravity Propellant Control Using Capillary Devices in Large Scale Cryogenic Vehicles," Design Handbook GDC-DDB70-006, Contract NAS8-21465, August, 1970.

7. Blatt, M. H., Betts, W. S., Burton, K. R., Merino, F., Perkins, C. K., Siden, L. E., and Stark, J. A., "Low Gravity Control Using Capillary Devices in Large Scale Cryogenic Vehicles," Phase II Final Report, GDC-DDB70-008, Contract NAS8-21465, August 1970.

8. Blatt, M. H., Burton, K. R., and Evans, E. A., "Low Gravity Propellant Control Using Capillary Devcies in Large Scale Cryogenic Vehicles," Related IRAD Studies GDC-DDB70-00 , Contract NAS8-21465, August, 1970.

9. Blutt, J. R., "Operating Safety of Dielectrophoretic Propellant Management Systems," Dynatech Report No. 768, NAS8-20553, March 31, 1968.

10. Hoggatt, J. T., "Polymeric Positive Expulsion Bladders for Liquid Oxygen Systems," NASA-CR-72418, Contract NAS3-7952, June 1968.

11. Stark, J. A., and Blatt, M. H., "Study of Zero-Gravity Vapor-Liquid Separators," Fifth Monthly Report," 584-4-128, NAS8-20146, Dec. 1967.

12. Morgan, L., "Orbital Refueling and Checkout Study," T1-51-67-21, NAS10-4606, Feb. 1968.

13. Reynolds, W. C., Saad, M. A., and Satterlee, H. M., "Capillary Hydrostatics and Hydrodynamics at Low g," LG-3, NSF-G-20090, September 1, 1964.

14. Hollister, M. P., Satterlee, H. M., and Cohan, H., "Liquid Propellant Behavior During Periods of Varying Acceleration," LMSL A874728 Code Y-87-67-1, NAS9-5174, June 30, 1967.

APPENDIX A

S-IVC STRESS CALCULATIONS

FUEL RESERVOIR BULKHEAD RING ESTIMATE

The bulkhead ring is subjected to the external load condition shown in Figure

$$F_K = F_T \text{ (cos } 26.5^\circ)$$

$$= (120)(.894)$$

$$= 107.2 \text{ \#/in}$$

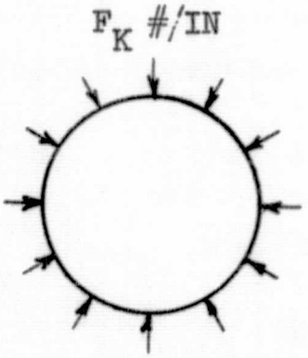


Figure A-1. Ring Load Condition

The critical unit load p' is expressed by

$$p' = \frac{3EI}{R^3}$$

where

E = modulus of elasticity = 10×10^6

I = cross section moment of inertia

Replacing p' with 107.2

$$I = \frac{107.2\ (24)^3}{3(10)(10)^6} = .0494 \text{ in}^4 \text{ for aluminum and } .0170 \text{ for steel.}$$

No design factor is used since F_K is conservative. Due to torsional modes from F_T and point loads from the support, the ring configurations chosen for the weight estimate exceeds the above I values.

The stiffener rings for the forward and aft sections of the reservoir were determined per the above procedures using $F_K = 50$ #/in.

FUEL RESERVOIR BHD. TENSION LOADING

The flat diagram and spherical dished type bulkheads were considered for the reservoir end closure. When a uniform pressure "p" is applied, a circumferential load

develops which must be reacted by r ring. For the case using a flat diaphragm, the expression for the stress at the edge is

$$S = 0.328\left[\frac{E\,p^2\,R^2}{t^2}\right]^{1/3}$$

per formulas for stress and strain by Roark, 3rd adition, 1964, page 223.

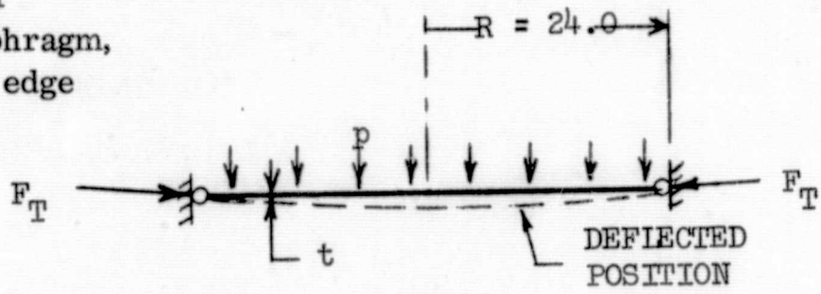


Figure A-2. Flat Diaphragm

Using aluminum alloy:

E = modulus of elasticity = 10×10^6, t = .024 (due to perforations), p = 5.0 psi.

This arbitrary value for "p" is considered sufficient coverage for unknown load combinations resulting from supports, vibrations, fluid impingements, temperature gradients, etc.

$$S = 0.328\left[\frac{10\times10^6\,(5)^2\,(24)^2}{(.032)^2}\right]^{1/3}$$

$$= 0.328\ (63,000)$$

$$= 20,700 \text{ psi}$$

F_T then becomes

$$20,700 \times .024 = 497.0 \text{ \#/in}$$

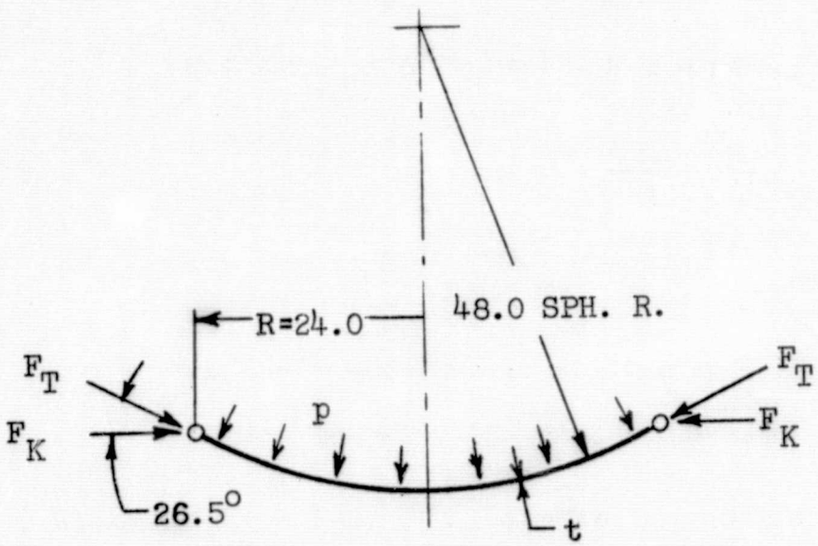


Figure A-3. Spherical Diaphragm

For the case using a spherical dished bulkhead, the stress

$$S = \frac{pR}{2t} = \frac{5 \times 48}{2 \times .024} = 5,000 \text{ psi}$$

$$F_T = 5000 \times .024 = 120 \text{ \#/in}$$

$$F_K = 120 \times \cos 26.5 = 107.2 \text{ \#/in}$$

Due to the lower F_T and less sensitivity to vibrational modes, the spherical type bulkhead was used for the weight estimate.

FUEL RESERVOIR BHD. REVERSE LOADING

For cases where propellant loading will be through the reservoir, the forward bulkhead would be exposed to the reversed loading condition shown. The magnitude of

of this load depends upon the tanking rate, screen surface area and the screen micron rating. This condition may be augmented by perculating effects at start of tanking due to large temperature gradients and gas formations. The buckling pressure is determined for a minimum gage type bulkhead.

The critical value is controlled by the stability of the shell, therefore, from "Theory of Elastic Stability" by S. P. Timoshenko and J. M. Gere, 2nd Edition, 1961, page 519:

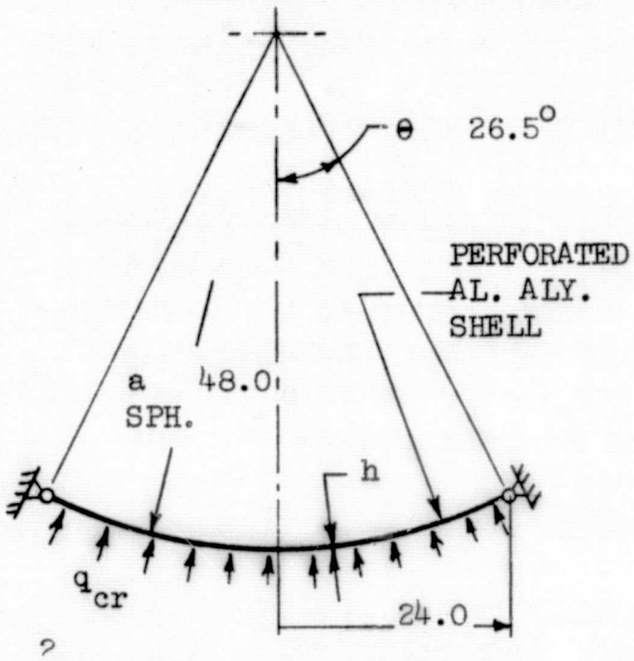


Figure A-4. Load Condition

$$q_{cr} = \left[1 - 0.175\ \frac{\theta^\circ - 20^\circ}{20^\circ}\right] \left[1 - \frac{(0.07)(a/h)}{400}\right] (0.3E) \left(\frac{h}{a}\right)^2$$

where E = Modulus of elasticity = 10×10^6

h = Effective material thickness (use 75% of basic gage)

= (.75) (.032) = .024

Using the parameters of Figure ,

$$q_{cr} = \left[1 - 0.175\ \frac{26.5 - 20}{20}\right]\left[1 - \frac{(0.07)(48)/.024}{400}\right] (0.3)(10)(10)^6 \left[\frac{.024}{48}\right]^2$$

= (.9432)(.65)(.75)

= .460 psi

If h is fixed at .024 and "a" and "θ" adjusted to the allowable limits for the above equation,

θ = 60°

and a = 27.5 inches

q_{cr} = (.65)(.8)(2.29)

= 1.19 psi

Final designs should reflect stiffeners or a gage increase to reduce the sensitivity. The weight estimate for Figure includes allowances for these deviations.

FUEL RESERVOIR CYLINDRICAL SECTION

The forward section of the reservoir is a cylindrical skin stiffened by a system of end and intermediate rings. Heat exchanger coils are attached to the skin between the stiffeners which contributes to the reinforcement system. If it is assumed that the effects of these coils permits using the full skin gage, then:

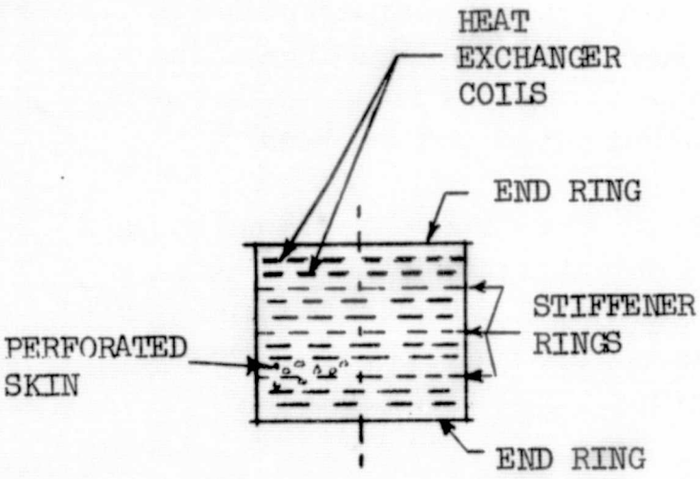


Figure A-5. Forward Cyl. Assembly

$$p' = 0.807 \frac{Et^2}{\ell R} \left[\left(\frac{1}{(1-\gamma^2)} \right)^3 \frac{t^2}{R^2} \right]^{1/4} \quad *$$

where

E = modulus of elasticity

29×10^6 for steel and 10×10^6 for aluminum

t = skin gage = .032 for aluminum and .020 for steel

R = shell radius = 24.0 inches

ℓ = distance between stiffeners = 10.0 inches

γ = Poisson's ratio .30

p' = external radial pressure at which elastic buckling occurs

From which

p' = 1.35 psi for aluminum and 1.20 psi for steel

For a compression loading in the axial direction, the critical stress at which elastic buckling occurs

$$S' = \left(\frac{1}{\sqrt{3}} \right) \left(\frac{E}{\sqrt{1-r^2}} \right) \left(\frac{t}{R} \right) \quad *$$

S' = 8070 psi for aluminum and 15,100 psi for steel

* Formulas for stress and strain by R. Roark, 3rd ed. 1954, p. 316 and 318

The imposed stress due to a 5 psi acting on the forward bulkhead is 1,875 for aluminum and 3000 psi for steel.

For axial loading, the minimum gage shell appears adequate, however, for radial and combination loading, additional stiffening may be required. These possible additions are accounted for in the weight estimate by using conservative values for the ring stiffener cross sections and the amount of material removed for the skin perforations.

APPENDIX B

LOX TANKER STRESS CALCULATIONS

OXIDIZER RETRIEVING CHANNEL SUPPORT LINKS

The retrieving channels are supported in the radial direction from the tank wall using eight links as shown and a reservoir attachment. With respect to heat transfer, it is desirable to use teflon or Kel-F materials for these components. The members are checked for tension and compression loading per the following.

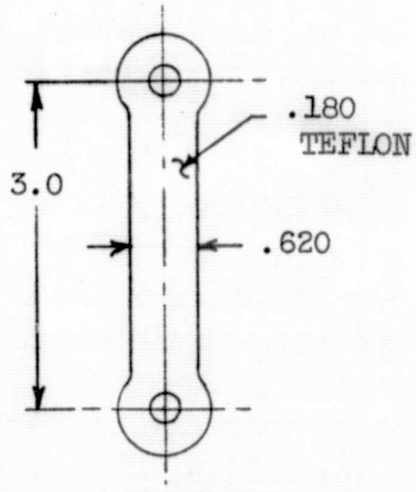


Figure B-1. Typical Radial Support Link

A typical aluminum channel weighs approximately 46.5 pounds. The force per link is related to the direction of loading, the radial components from the drag struts, and the distribution of loads to the support points. The latter is influenced by manufacturing tolerances and the curvature of the channel. To compensate for unknowns, a 10-g field is assumed, two links considered inactive, and the support at the reservoir neglected. The load per support

$$P = \pm\frac{46.5 \times 10}{6} = 77.5\,\#$$

The tension or compressive stress

$$S = \frac{77.5}{.62 \times .180} = 695 \text{ psi}$$

The member may be critical for column type loading, therefore assuming a hinged end condition, the critical buckling load

$$P_{CR} = \frac{\pi^2 E I}{L^2}$$

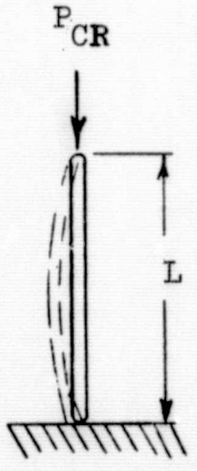


Figure B-2. Column Load Condition

where

E = modulus of elasticity = 600,000

I = least moment of inertia

$$I = \frac{.62 \times (.180)^3}{12} = .000301 \text{ in}^4$$

$$P_{CR} = \frac{(\pi)^2 (600,000) (.000300)}{(3)^2} = 197\#$$

The links appear satisfactory for the assumed conditions. For the case of steel retrieving channels, an increase in the cross sections or quantity of supports; the use of reinforcements, or a combination of these methods may be required. Loads due to pressure gradients across the screen areas are not expected to exceed two pounds per square foot. Loads due to liquid impingement are considered negligible.

OXIDIZER RETRIEVING CHANNEL BASIC STRUCTURE

The retrieving channels are "U" shaped sections with stiffening ribs as shown. The moment of inertia "I" for the section shown is approximately .417 in^4. A typical channel is divided into four sections and treated as a uniformly loaded beam as shown.

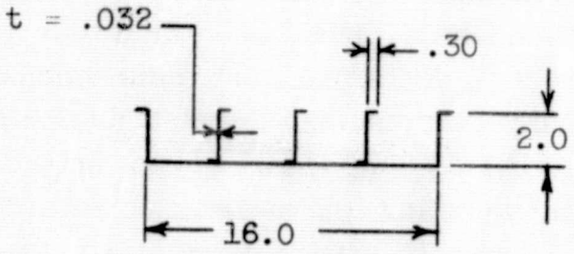


Figure B-3. Channel Cross Section

$$W = \frac{(\text{WEIGHT PER CHANNEL}) (10 \text{ gs})}{4}$$

$$= \frac{46.5 \times 10}{4} = 116.2 \text{ lb}$$

The maximum bending moment

$$M = \frac{W\ell}{8} = \frac{116.2 \times 72}{8} = 1048 \text{ in-lb}$$

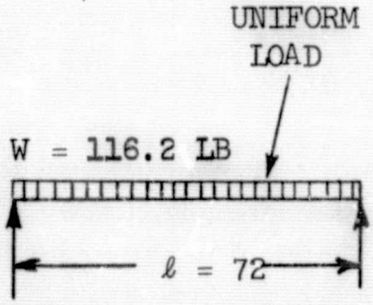


Figure B-4. Beam Load Condition

The deflection at mid-span

$$\Delta Y = \frac{5 W \ell^3}{384 EI}$$

where

E = modulus of elasticity = 10^7

Therefore

$$\Delta Y = \frac{(5)(116.2)(72)^3}{384 \times 10^7 \times .417} = .135 \text{ inches}$$

The deflection shown will permit locating the channel near the tank wall.

The bending moment subjects the 16.0 inch wide flat skin section to a compressive stress

$$S_C = \frac{MC}{I}$$

where

C = distance from the skin to the centroid of the section = .471

$$S_C = \frac{1048 \times .471}{.417} = 1185 \text{ psi}$$

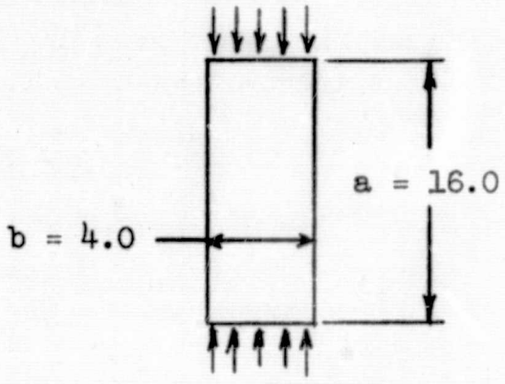


Figure B-5. Panel Load Condition (simply Supported Edges

The wide skin section is divided into 16.0 × 4.0 inch panels by a system of stiffener ribs. The boundary edge conditions of these panels are assumed to be simply supported. The critical buckling stress under the load conditions shown is:

$$S_{C_{CR}} = \frac{\pi^2 K_C E}{12(1-\gamma^2)} \left(\frac{t}{b}\right)^2 *$$

where

K_C = the buckling coefficient

= 4.0

γ = Poisson's ratio = .30

$$S_{C_{CR}} = \frac{(\pi^2)(4)(10)^7}{12(1-.09)} \left(\frac{.032}{4.0}\right)^2 = 2300 \text{ psi}$$

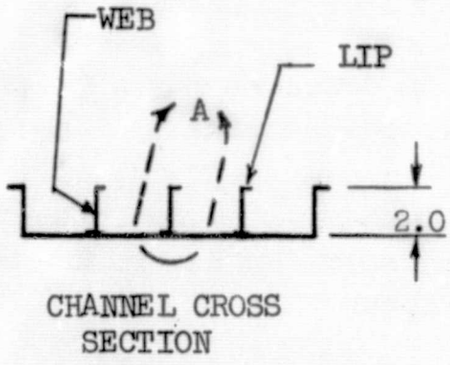
Since the buckling stress exceeds the stress due to bending, the panels will not buckle.

The bending stresses imposed on the beam channels may cause buckling of the stiffener web sections. The free edge of the webs are flanged or are equipped with

* Analysis and Design of Flight Vehicle Structures," by E. F. Bruhn, 1965, page C5.11, or "Theory of Elastic Stability," by S. P. Timoshenko, 2nd edition, 1961, pages 351, 352 and 353.

a lip angle. For this analysis, the angle is used. From Figure B-3, the bending moment M = 1048 in #. The stress near the lip angle due to the bending moment

$$S = \frac{MY}{I} = \frac{1048 \times 1.50}{.417} = 3770 \text{ psi}$$



CHANNEL CROSS SECTION

Figure B-6. Channel Cross Section

The critical bending buckling stress

$$F_{b_{CR}} = \frac{\pi^2 K E}{12(1-\gamma^2)} \left(\frac{t}{Y}\right)^2 *$$

where

Y = distance from base of web to lip angle = 1.50

γ = Poisson's ratio = .30

E = modulus of elasticity = $(10)(10)^6$

*K = buckling coefficient

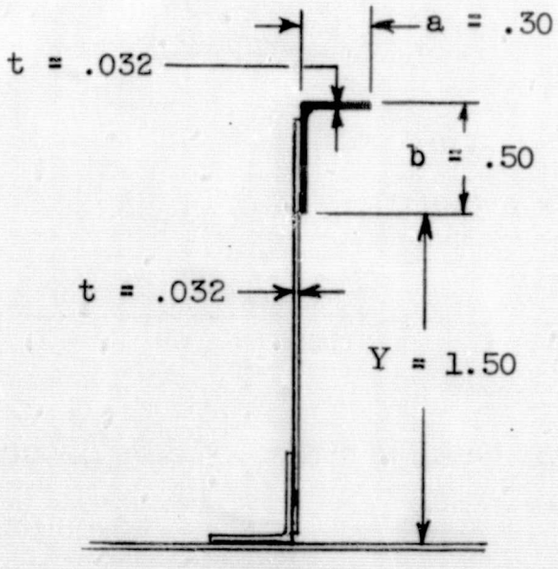
= 24.5

This assumes simple supported edges with an a/b ratio of 16/1.5 = 10.67

Therefore

$$F_{b_{CR}} = \frac{(\pi^2)(24.5)(10)(10)^6}{12\left[1-(.3)^2\right]} \left(\frac{.032}{1.5}\right)^2$$

= 100,000 psi



View A

The cutoff stress for $F_{b_{CR}}$ would be near the yield stress. The web is adequate for the bending mode.

The lip section of the web may fail by crippling or column buckling. For the crippling condition

*Analysis and Design of Flight Vehicle Structures," by E. F. Bruhn, 1965.

$$\frac{F_{CS}}{\sqrt{F_{CY}E}} = .0475$$

where the .0475 value is taken from page C7.3 of Bruhn*

$$\frac{a+b}{2t} = \frac{.3+.5}{(2)(.032)} = 12.50$$

F_{CS} = crippling stress

F_{CY} = material yield stress = 40,000

From the above

$$F_{CS} = .0475\ \sqrt{(40,000)(10)^7} = 30,000 \text{ psi}$$

The webs are adequate for crippling.

For column buckling, the Johnson-Euler expression is

$$F_C = F_{CS} - \frac{(F_{CS})^2}{4\pi^2 E}\ (\frac{L'}{\sigma})^2 *$$

where

F_C = column failing stress

F_{CS} = crippling stress

L' = $L/\sqrt{C}$ where L = column length = 16.0 inches and C is the end fixity coefficient taken as 1.50.

σ = radius of gyration of the lip angle = .176

Using the above,

$$F_C = 30,000 - \frac{(30,000)^2}{4\pi^2\ 10^7}\ \left[\frac{16/\sqrt{1.5}}{.176}\right]^2 = 17,450 \text{ psi}$$

The lip region therefore is satisfactory for column buckling.

---

* Analysis and Design of Flight Vehicle Structures," by E. F. Bruhn, 1965.

OXIDIZER RETRIEVING CHANNEL SUPPORT STRUTS

Each channel is supported in the lateral direction by four drag struts and a connection at the reservoir. Due to heat transfer requirements, it is desirable to compare teflon with steel per the designs shown in Figures B-12 and B-13. The components are checked for tension and compression loading to determine the feasibility for this application. For the case using teflon, the tubing is attached to aluminum end fittings with one of these fittings incorporating designs for adjusting the length of the strut at assembly. With this length adjustment capability, it is assumed that each strut will carry 1/4 of the total load. The attachment at the reservoir is neglected. Using the load conditions from the radial restraint links (Figure B-1), the force

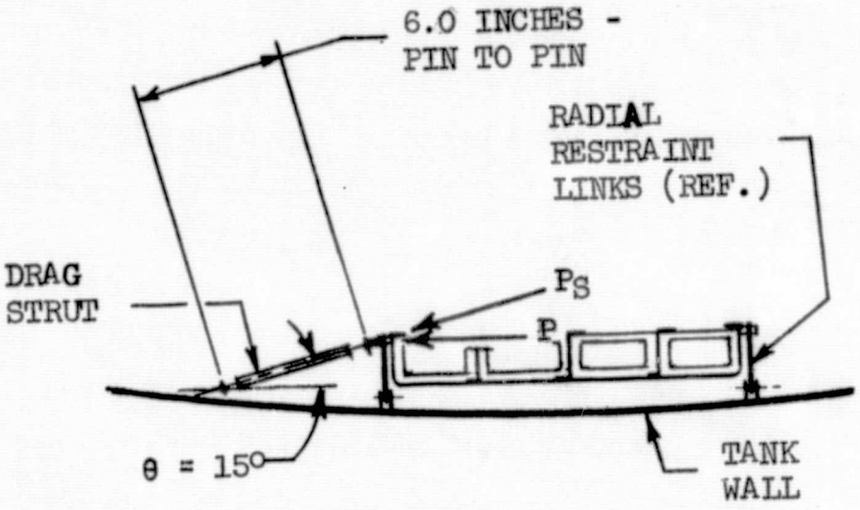


Figure B-7. Typical Drag Strut Arrangement

$$P = \pm\frac{46.5 \times 10}{4} \quad \pm 116.2\#$$

The load directed to the strut axis =

$$P_S = \pm \frac{P}{\cos\theta}$$

$$= \pm\frac{116.2}{.965} = 120.5\#$$

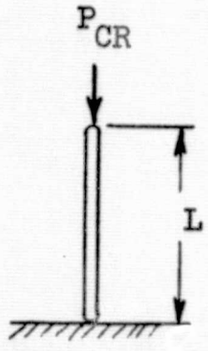


Figure B-8. Column Loading Condition

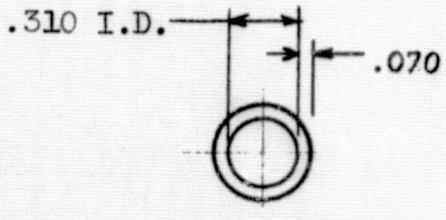


Figure B-9. Teflon Tube Cross Section

The strut may be critical for column type loading, therefore assuming a pinned end condition and using teflon, the critical buckling load

$$P_{CR} = \frac{\pi^2 EI}{L^2}$$

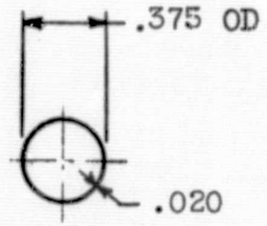


Figure B-10. Steel Tube Cross Section

where

E = modulus of elasticity

= 600,000

I = moment of inertia for the tube cross section shown for teflon

= .001438 in^4

L = 6.00 inches from center to center of pin connections. This is conservative and should compensate for manufacturing and material tolerances.

Using the above:

$$P_{CR} = \frac{\pi^2 (600,000)(.001438)}{(6)^2}$$

$$= 236\ \#$$

If the teflon tubing is replaced by steel tubing with the cross section shown:

I = .000414

P_{CR} = 3290 #

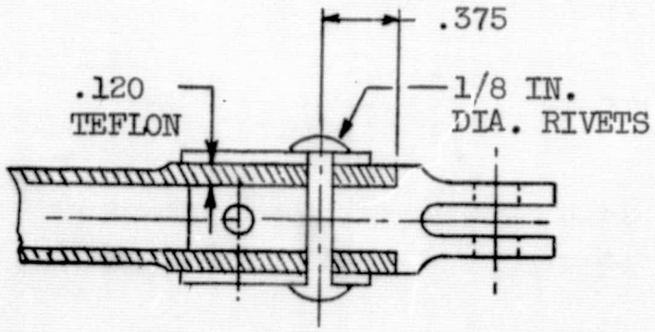


Figure B-11. End Fitting Arrangement

"L" could be increased to 22.4 inches for a P_{CR} = 236 #. The 22.4 inch strut may be sensitive to vibrational modes normal to the axis, therefore, an "L" is limited to 11.0 inches. The 11.0 inch strut reduces θ (which in turn reduces P_S) and increases the heat flow path resistance.

The tension or compression stresses at the minimum area of the tube

$$S = \frac{P_S}{A}$$

where

$$P_S = 120.5\,\#$$

A = cross sectional area of tube

= .0835 in^2 for teflon

= .0236 in^2 for steel

$$S = \frac{120.5}{.0835} = 1,445 \text{ psi for teflon}$$

$$S = \frac{120.5}{.0236} = 5,120 \text{ psi for steel}$$

The stress levels are satisfactory.

Aluminum end fittings are attached to the teflon tubing with rivets. The bearing and tear-out stresses at these rivets are checked as follows:

Bearing stress

$$S_{BR} = \frac{P_S}{\text{Bearing Area}}$$

$$= \frac{120.5}{(.125)(.12)(4)} = 2,000 \text{ psi}$$

Tear-out stress

$$S_S = \frac{(P_S)(.50)}{(\text{Shear Area})}$$

Each rivet is assumed to carry 50% of the load. The outboard rivet which has an edge distance of .375 is checked.

$$S_S = \frac{(120.5)(.50)}{(.375 - .0625)(.120)(4)} = \frac{60.2}{.15} = 400 \text{ psi}$$

The stress levels are satisfactory. For the steel strut, the end fitting are butt welded to the tube per Figure .

Comparing the two strut designs, the heat transferred by conductance

$$Q = \frac{k\,A\,\Delta t}{L}$$

where

k = .125 Btu/hr-ft-°R for teflon

k = 5.0 Btu/hr-ft-°R for 321 steel

L = length of conductive path at the minimum area of the tube

= 2.10 inches for teflon

= 9.00 inches for steel

A = cross sectional area of tube

= .0835 in^2 for teflon

= .0236 in^2 for steel

$$Q_{TEFLON} = \frac{(.125)(.0835/144)}{(2.10/12)} = .000414 \text{ But/hr-°R}$$

$$Q_{STEEL} = \frac{(5.0)(.0236/144)}{(9.00/12)} = .001095 \text{ Btu/hr-°R}$$

The heat transfer rate for the steel strut is approximately 2.6 times greater than that for the teflon design. Where permissable, the steel strut is preferred due to the simplicity and greater reliability.

Part of the retrieving channel support system uses tubular struts as drag links. Tradeoffs exist between the length of these members, the cross sectional areas, type of material and heat transfer rates. The lengths are also controlled by vibrational environments. If the frequency of the driving force is near the natural frequency of the strut, resonance will occur. When no damping is available and when the driving frequency is equal to the strut natural frequency, the amplitude of vibration tends toward infinity. Failure by column action is further augmented if the compressive load should occur when the strut is in a deflected position. If the strut is treated as a simple beam and the damping action of the oxidizer neglected, the natural frequency of the link

$$\omega_N = \left[\frac{48\ EI}{L^3\ (.5\ m_b)}\right]^{1/2}$$

where

E = modulus of elasticity

= 600,000 for teflon

= 29×10^6 for strut

I = moment of inertial of the tube cross section

= .001438 for teflon

= .000414 for steel

L = length of strut measured from pin to pin

= 6.0 inches for the teflon design

= 11.0 inches for the steel design

The 6.0 dimension for the teflon design is conservative since the aluminum end fittings form part of the span.

m_b = mass of strut

= .0001815 lb-sec^2/in for teflon

= .000311 lb-sec^2/in for steel

Using the above values:

$$\omega_n = \left[\frac{(48)(600,000)(.001438)}{(6.0)^3\,(.5)\,(.0001815)}\right]^{1/2}$$

= 1450 cycles per second for teflon

$$\omega_n = \left[\frac{(48)(29)(10)^6\,(.000414)}{(11)^3\,(.5)\,(.000311)}\right]^{1/2}$$

= 1670 cycles per second for steel

From the "AEROSPACE FLUID COMPONENT DESIGNERS' HANDBOOK" Volume II, Rev. B, Report #RPL-TDR-64-25, March 1967 (TRW Systems), page 13.3.5-2, a representative vibrational environment for earth launched space vehicles is 10 g's rms, 600 to 1600 cps.

The above case for steel is outside of this interval. For teflon the cps is slightly within the given range, but can be considered adequate since a conservative length was used. It, therefore, appears reasonable to limit the strut lengths as shown for the assumed cross sections.

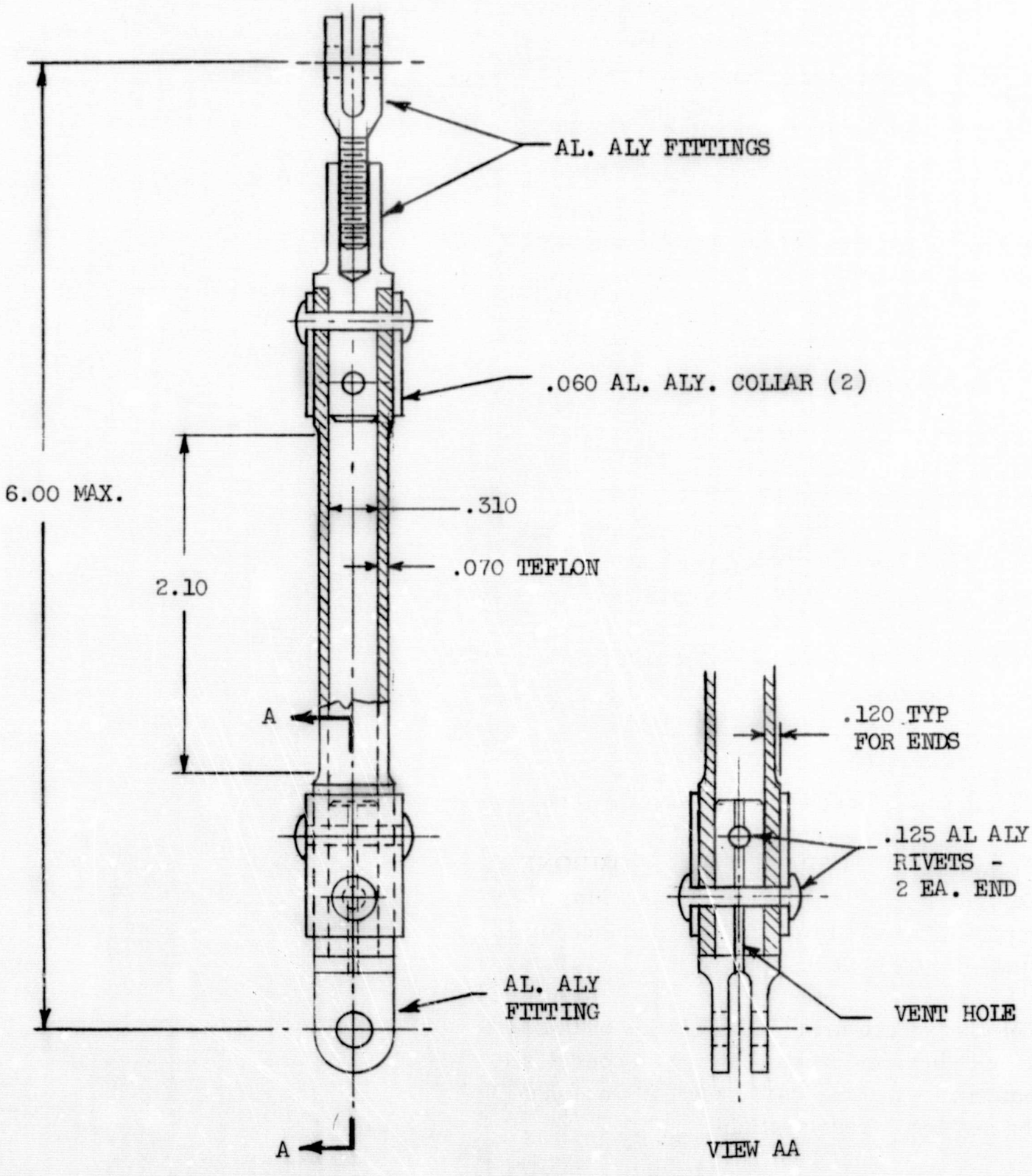


Figure B-12. Teflon Strut Design

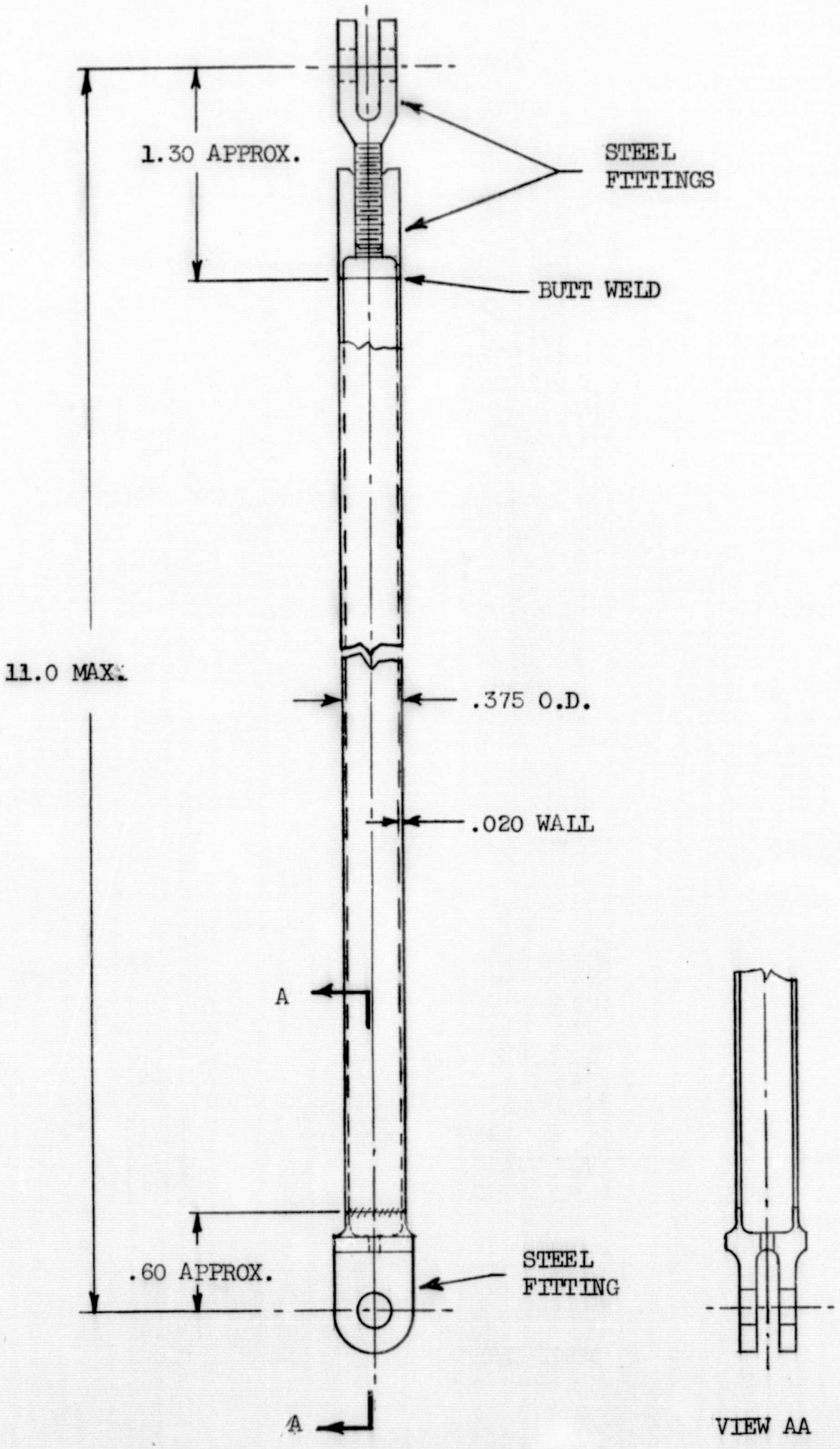


Figure B-13. Steel Strut Design